UNIVERSITY OF OKLAHOMA

GRADUATE COLLEGE

PRODUCTION SUSTAINABILITY OF SHALE PLAYS

A THESIS

SUBMITTED TO THE GRADUATE FACULTY

in partial fulfillment of the requirements for the

Degree of

MASTER OF SCIENCE

By

CHIDOZIE UWAKWE
Norman, Oklahoma
2017

Downloaded from SHAREOK. Persistent Handle URL: https://hdl.handle.net/11244/50865

PRODUCTION SUSTAINABILITY OF SHALE PLAYS

A THESIS APPROVED FOR THE
MEWBOURNE SCHOOL OF PETROLEUM AND GEOLOGICAL ENGINEERING

BY

_____
Dr. Rouzbeh Ghanbarnezhad Moghanloo, Chair

_____
Dr. Deepak Devegowda

_____
Dr. Siddharth Misra

© Copyright by CHIDOZIE UWAKWE 2017
All Rights Reserved.

I dedicate this thesis to God Almighty. He has been the source of strength in my life and has given me the perseverance to make it this far. I also dedicate this work to my parents who have continued to provide me with endless encouragement throughout my life.

Acknowledgements

First and foremost, I give thanks to God for the grace and favor He has put in my life. This work would not have been possible without the knowledge, wisdom, and strength He has provided me.

I would like to acknowledge my advisor, Dr. Moghanloo, for providing me with guidance and support every step of the way in this academic program. Without him, this work would have been enormously more difficult. I would like to acknowledge my committee members, Dr. Misra and Dr. Devegowda, for their support of my research. I would also like to thank my colleagues at the University of Oklahoma for the valuable contributions they made in helping me with this research.

I am especially grateful to my loving parents for always being there for me and supporting me in everything I do. Finally, I would like to thank my family and friends who have kept me going in my life.

Table of Contents

Acknowledgements ..... **iv**

List of Tables ..... **vii**

List of Figures ..... **viii**

Abstract ..... **xiii**

Chapter 1: Introduction **1**

1.1 Problem Statement 4

1.2 Research Objectives 6

1.3 Thesis Organization 7

Chapter 2: Literature Review **8**

Chapter 3: Overview of the Shale Reservoirs **15**

3.1 Overview of the Barnett Shale 16

3.2 Overview of the Hayneville Shale 18

3.3 Overview of the Marcellus Shale 19

Chapter 4: Definitions **20**

4.1 Sustainability 21

4.2 Connectivity 27

Chapter 5: Methodology **30**

5.1 Description of the CMG Simulation Model 34

5.2 Connectivity Evaluation 53

5.3 Sustainability Evaluation 60

Chapter 6: Results and Analysis **61**

6.1 Sustainability Analysis 61

6.2 Connectivity Distributions 70

6.3 Areal Maps 75

6.4 Discussion 81

Chapter 7: Conclusion **83**

Future Work **85**

References **87**

List of Tables

Table 5.1 Properties of the Reservoir Model 42

Table 5.2 Reservoir-Specific Properties of the Reservoir Model 60

List of Figures

Figure 1.1 United States Dry Natural Gas Production in trillion cubic feet (EIA 2013) 3

Figure 1.2 United States Shale gas production in billion cubic feet (EIA 2016). 4

Figure 2.1 Water Imbibition Results for a Barnett Shale in the Analysis Performed by Hu et al. 2015 9

Figure 2.2 Nanopores associated with organic matter in the Barnett Shale (Loucks et al., 2009). 10

Figure 2.3 Overall Pore Network Investigation Workflow in the analysis performed by Goral et al. (2015). 13

Figure 3.1 United States Dry Shale Gas Production (EIA 2017)..... 15

Figure 3.2 Schematic section of the Barnett Shale (Fu et al., 2015) 17

Figure 3.3 Stratigraphic Columns showing the Haynesville Shale in Texas and Louisiana (Thompson et al., 2011) 19

Figure 4.1 Schematic of plot used to evaluate sustainability..... 24

Figure 4.2 Schematic showing an idealized depletion history (Moghanloo 2012) 26

Figure 4.3 Illustration of shale matrix consisting of grains, connected and isolated pores (Moghanloo et al., 2015) 29

Figure 5.1 Backscattered electron image of a Barnett Shale Sample (Davudov and Moghanloo, 2016) 31

Figure 5.2 Backscattered electron image of a Haynesville Shale Sample (Davudov and Moghanloo, 2016) 32

Figure 5.3 Schematic of a Slab Matrix Linear Model of a Hydraulically Fractured Well (Bello and Wattenbarger 2010) 34

Figure 5.4 Slab Matrix Linear Model with Matrix Connected Porosity Flow Path indicated by Red Lines 35

Figure 5.5 Three-dimensional view of the cuboid model constructed in CMG 36

Figure 5.6 Image displaying the Directions the Two-Dimensional Views are taken from 37

Figure 5.7 y-side Two-Dimensional View of the Reservoir Model 38

Figure 5.8 x-side Two-Dimensional View of the Reservoir Model 38

Figure 5.9 Plan View of the Reservoir Model 39

Figure 5.10 Plan View of Reservoir Model with 5% Connectivity 41

Figure 5.12 Plan View of Reservoir Model with 1% Connectivity 43

Figure 5.13 Plan View of Reservoir Model with 8% Connectivity 44

Figure 5.14 Plan View of Reservoir Model with 10% Connectivity 45

Figure 5.15 Plan View of Reservoir Model with 20% Connectivity 46

Figure 5.16 Plan View of Reservoir Model with Configuration 2 of connected Grid Blocks corresponding to 5% Connectivity 47

Figure 5.17 Plan View of Reservoir Model with Configuration 3 of connected Grid Blocks corresponding to 5% Connectivity 48

Figure 5.18 Plan View of Reservoir Model with Configuration 4 of connected Grid Blocks corresponding to 5% Connectivity 49

Figure 5.19 Plan View of Reservoir Model with Configuration 5 of connected Grid Blocks corresponding to 5% Connectivity 50

Figure 5.20 Plan Views of the different Reservoir Model Configurations of connected Grid Blocks corresponding to 1% Connectivity 51

Figure 5.21 Plan Views of the different Reservoir Model Configurations of connected Grid Blocks corresponding to 8% Connectivity 51

Figure 5.22 Plan Views of the different Reservoir Model Configurations of connected Grid Blocks corresponding to 10% Connectivity 52

Figure 5.23 Plan Views of the different Reservoir Model Configurations of connected Grid Blocks corresponding to 20% Connectivity 52

Figure 5.24 Plot showing generated production data for the different Reservoir Configuration Models Corresponding to 5% Connectivity. 54

Figure 5.25 Plot showing generated production data for the different Reservoir Configuration Models Corresponding to 1% Connectivity. 54

Figure 5.26 Plot showing generated production data for the different Reservoir Configuration Models Corresponding to 8% Connectivity. 55

Figure 5.27 Plot showing generated production data for the different Reservoir Configuration Models Corresponding to 10% Connectivity. 55

Figure 5.28 Plot showing generated production data for the different Reservoir Configuration Models Corresponding to 20% Connectivity. 56

Figure 5.29 Average recovery versus normalized time curves for 1%, 5%, 8%, 10%, and 20% connectivity respectively 57

Figure 5.30 Plot for distinguishing between linear flow and boundary-dominated flow (Al Khamees 2015) 58

Figure 5.31 Use of average simulation recovery versus normalized time curves to estimate the connectivity of three Haynesville shale wells. 59

Figure 6.1 Plot of $\frac{q}{qmax}$ versus $\frac{G_p}{EUR}$ for Barnett shale wells 62

Figure 6.2 Plot of $\frac{q}{qmax}$ versus $\frac{G_p}{EUR}$ for Haynesville shale wells 62

Figure 6.3 Plot of $\frac{q}{qmax}$ versus $\frac{G_p}{EUR}$ for Marcellus shale wells 63

Figure 6.4 All $\frac{q}{qmax}$ versus $\frac{G_p}{EUR}$ data for all three shale reservoirs in the same plot 64

Figure 6.5 Divided plot of all $\frac{q}{qmax}$ versus $\frac{G_p}{EUR}$ data for all three shale reservoirs 65

Figure 6.6 Well Distribution showing the proportion of wells from each reservoir in each region 66

Figure 6.7 $\frac{q}{qmax}$ versus $\frac{Gp}{EUR}$ slope distribution for Barnett shale 67

Figure 6.8 $\frac{q}{qmax}$ versus $\frac{Gp}{EUR}$ slope distribution for Haynesville shale 68

Figure 6.9 $\frac{q}{qmax}$ versus $\frac{Gp}{EUR}$ slope distribution for Marcellus shale 69

Figure 6.10 Connectivity Distribution in the Barnett Shale Well Data 71

Figure 6.11 Connectivity Distribution in the Haynesville Shale Well Data 71

Figure 6.12 Connectivity Distribution in Marcellus Shale Well Data 72

Figure 6.13 Connectivity Distribution in Region 1 73

Figure 6.14 Connectivity Distribution in Region 2 73

Figure 6.15 Connectivity Distribution in Region 3 74

Figure 6.16 Connectivity Distribution in Region 4 74

Figure 6.17 Connectivity Areal Map of the Barnett Shale 76

Figure 6.18 Connectivity Areal Map of the Haynesville Shale 77

Figure 6.19 Connectivity Areal Map of the Marcellus Shale 78

Figure 6.20 Sustainability Areal Map of the Barnett Shale 79

Figure 6.21 Sustainability Areal Map of the Haynesville Shale 80

Figure 6.22 Sustainability Areal Map of the Marcellus Shale 81

Abstract

Shale reservoirs are commonly observed to have high initial flow rates followed by the occurrence of rapid declines in these rates early in their productive lives. There is, therefore, a need for terminology which describes not only the declines in these reservoirs but their general production performance. This terminology should be related to the petrophysical properties of shales as well. Numerous studies suggest that the early declines in production rates may be due to the limiting factor of the low pore connectivity of the shale matrix. They reason that pore connectivity impacts production by controlling the dispersion in the shale matrix. Pore connectivity is, therefore, an important parameter in analyzing shale resources.

Sustainability, a new notion is introduced as a means of simultaneously evaluating the production rate declines and the performance of these reservoirs. In this study, it is evaluated using plots of $\frac{q}{qmax}$ versus $\frac{G_p}{EUR}$ derived from the production data of the Barnett, Haynesville, and Marcellus shale reservoirs. Reservoir-scale connectivity is also evaluated for these three reservoirs in this by comparing their well production data to reservoir simulation-generated data from models matching the properties of these reservoirs. Areal maps of sustainability and connectivity are generated to view spatial trends and a possible relationship between these two parameters is investigated.

The estimated reservoir-scale connectivity values were fairly low compared to the results from other studies. This may have been the case because the connectivity

values estimated were not corresponding to values of initial connectivity but rather values which had declined from their initial levels to some extent due to gas production. Sustainability was observed to be proportional to connectivity, confirming the notion that low connectivities in the matrix lead to higher declines in production rate. The Barnett was observed to have the highest connectivity and sustainability while the Marcellus was observed to have the lowest, with the Haynesville estimates falling in the middle.

Chapter 1: Introduction

Conventional reservoirs, by definition, possess conventional features. They are called conventional in the sense that they are very common and are the type of reservoirs that have most regularly been encountered to date. With drive mechanisms that greatly facilitate production, they usually do not involve much further development in addition to the simple drilling of a wellbore through them. The hydrocarbons produced from these reservoirs are mostly recovered by primary recovery mechanisms while secondary and tertiary recovery techniques are either not needed or implemented much later in the lives of these reservoirs. With reasonable values of porosity and permeability, they are essentially the most desirable type of reservoirs.

Unconventional reservoirs, on the other hand, are more uncommon. They possess more unusual and abnormal properties which make it difficult and costly to produce from them. More complex technology and more innovative strategies are needed to produce from these reservoirs. This type of reservoir includes tight gas reservoirs, tight oil reservoirs, shales, heavy oil reservoirs, and others. In the past, it was greatly uneconomical to produce from these reservoirs. However, because of the sheer amount of reserves contained in these unconventional resources, there was a strong determination to find more economical methods of extracting these hydrocarbons. In the present day, it is more economical thanks to the rise of innovative techniques which have made hydrocarbon production more efficient.

Greater amounts of hydrocarbon can be produced at higher rates today at the same cost compared to what could be produced in the past.

Of the several types of unconventional reservoirs, this paper involves gas shales. Shales are fissile, fine-grained sedimentary rocks which are created from the deposition and consolidation of clay and silt-sized particles over prolonged periods of time (Belvalkar and Oyewole, 2010). They possess unfavorable features such very low porosities (< 15%) and very low permeability values (10 nD to 10 mD), paling in comparison to the porosity (15% to 35%) and permeability (10 mD to 10 D) of conventional reservoirs (Ambrose et al., 2010). However, thanks to the development of hydraulic fracturing and horizontal drilling, the unfavorable effects of their low porosity and permeability have been offset. Horizontal drilling provides the advantage of allowing for a higher proportion of the reservoir to be exposed to the wellbore while hydraulic fracturing aids in creating zones of high permeability in these low permeability reservoirs. As a result of the use of these techniques, gas shales now contribute a major proportion of the total hydrocarbon production in the United States. They not only already make up the highest percentage of natural gas production from unconventional reservoirs in the United States but are predicted to contribute an even higher proportion of gas production in future years as shown in Figure 1.1 (EIA 2013).

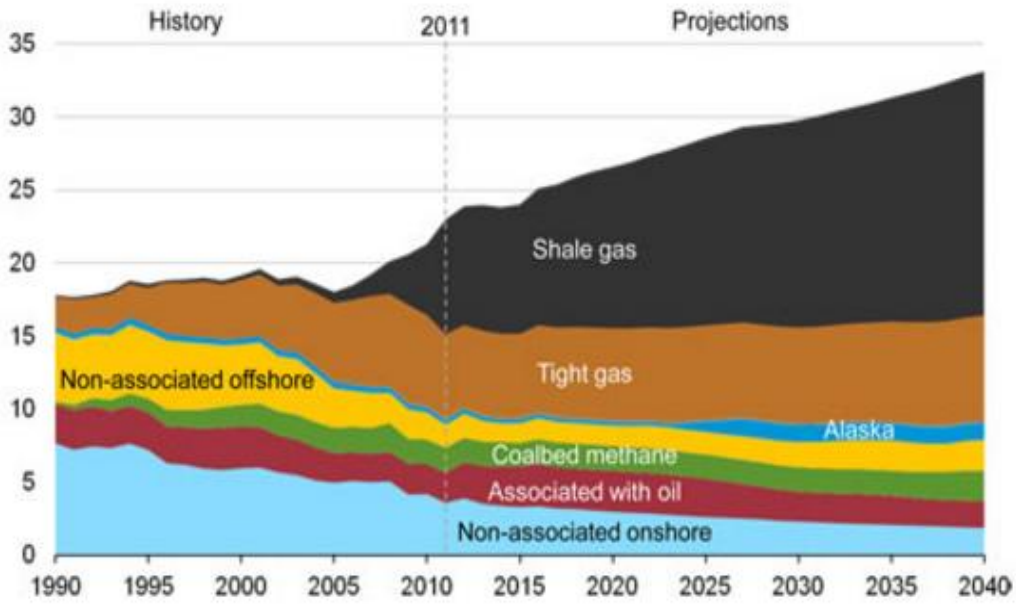


Figure 1.1 United States Dry Natural Gas Production in trillion cubic feet (EIA 2013).

Production from these gas shales continues to rapidly increase with time as more and more of these reservoirs continue to become exploited using horizontal drilling and hydraulic fracturing. The United States shale gas production grew over ten-fold in the span ranging from 2007 to 2015, increasing from 1,293 billion cubic feet to 15,213 billion cubic feet as shown in Figure 1.2 (EIA 2016). This rapid increase in gas production led to the United States becoming the largest natural gas producer in the world in 2012.

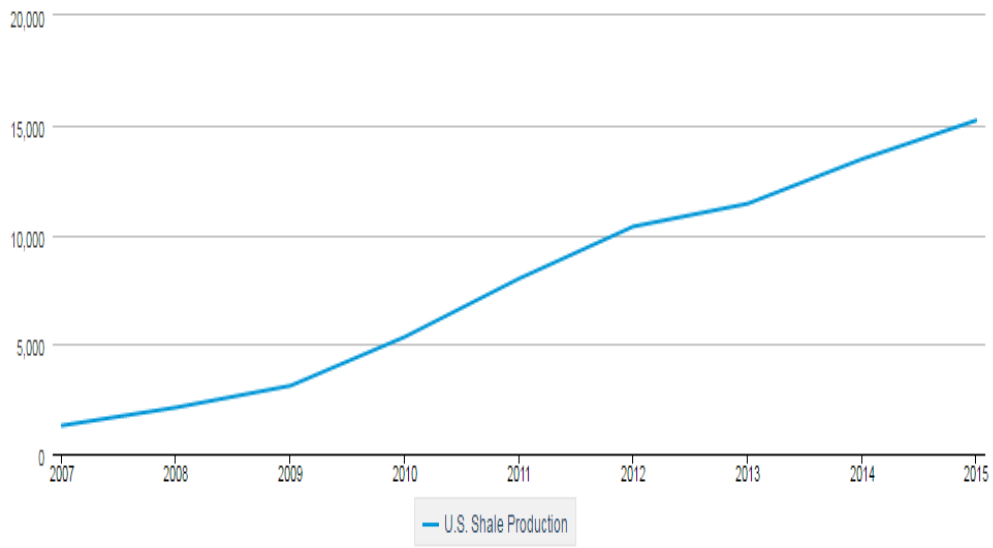


Figure 1.2 United States Shale gas production in billion cubic feet (EIA 2016).

1.1 Problem Statement

While the production from these gas shales has greatly improved recently, these reservoirs are still relatively new and unfamiliar. In order to assess, sustain or possibly improve on the levels and efficiency of production from these reservoirs, it is important to be able to evaluate their production performance. There is a need for new terminology for evaluating not only the declines in production rate but the general production performance in shale reservoirs. It is also important to carry out more studies and obtain more information about the properties of these reservoirs. A substantial number of studies are currently being carried out on numerous aspects of gas shales, for example, oil-in-place estimates (Misra and Han, 2016) and relative permeability (Ojha et al., 2016). However, one area in which more research and understanding is needed is the connectivity of these reservoirs.

Shale reservoirs can be characterized by regions of high permeability, the fractures, and regions of low permeability, its matrix. The matrix section of a shale reservoir refers to the section that has largely been unaffected by the fractures and contains the characteristic low porosity and permeability expected of shale reservoirs. In these reservoirs, fractures are the main source of permeability while majority of the gas storage is provided by the reservoir matrix (Bello and Wattenbarger, 2010). The permeability in the fractures can be up to eight orders of magnitude higher than that of the matrix (Gutierrez et al. 2000). The production mechanism in fractured shales is initially gas decompression in the fractures close to the wellbore (Davudov and Moghanloo, 2016). However, once the gas in these fractures has been exhausted, the fractures must then draw on the gas stored in the matrix of the reservoir. At this point, production is then controlled by flow from the matrix to the fracture, which in turn is controlled by dispersive flux in the matrix. This switch in production mechanism may be responsible for the sharp declines in shale gas reservoir production rates occurring early in their production lives. Hu et al. (2015) suggest that the source of production declines in shale is the limiting factor of the rate of diffusion of gas from the matrix to the fracture network, which itself is controlled by the low connectivity of shale reservoirs. Connectivity has a direct impact on the dispersive flux in the matrix of shale reservoirs and therefore has a profound effect on the long-term productivity of gas wells (Davudov and Moghanloo, 2016). Amann-Hildenbrand et al. (2011) make a similar suggestion, stating that matrix flow directly impacts the long-term productivity of fractured gas shale reservoirs due to its transport properties, such as pore

connectivity, limiting the flow of gas towards fractures. Knowledge of the connectivity in the matrix of shale reservoirs is therefore very important with respect to production performance. This importance fuels the need for this study on the production performance of shales and its possible relationship with connectivity.

1.2 Research Objectives

This study aims at introducing a new terminology, called sustainability, for evaluating production performance in shale reservoirs. It uses this term as a means of evaluating the production rate declines in shale reservoirs and aims at investigating the relationship between these declines and the petrophysical aspect of shale reservoirs through the estimation of pore connectivity. In doing this, this study aims to give an insight on what levels of declines in the production rate could be expected based on knowledge of the connectivity of a reservoir.

This study also aims at enhancing our knowledge of shale reservoirs through its evaluation of the reservoir-scale connectivity of some of the highest producing shale reservoirs in the United States. It aims to not only quantify estimations of the connectivity in these reservoirs but also to use these estimations to analyze spatial reservoir-scale connectivity trends in certain regions through the creation of connectivity areal maps as well compare them with areal trends observed in sustainability areal maps.

1.3 Thesis Organization

Chapter 2 provides a detailed literature review for the study. It gives an overview on studies that have previously been carried out relating to the pore connectivity and petrophysical properties of the reservoirs in this study. It also looks at the different approaches that have been utilized in obtaining pore connectivity and the varying results and conclusions that these approaches led to.

Chapter 3 gives an overview of the shale reservoirs involved in this study. It provides background information on these reservoirs and gives a summary of some of their important properties.

Chapter 4 gives in-depth definitions of the two important terms in this study. These terms are sustainability, the newly introduced terminology in this study, and connectivity, a more widely known term. It explains their relevance and importance to shale reservoirs and explores how they may be related.

Chapter 5 features a description of the methodology used to carry out the analysis performed in this study. It explains how the connectivity and sustainability are evaluated and details the steps taken in going about this. The study involves the use of a simulation model in evaluating the reservoir-scale connectivity of shale reservoirs. A detailed description of this constructed simulation model and its properties is provided in this section along with an explanation of how it is used to evaluate connectivity. This section also describes the plots used in making evaluations of the connectivity and sustainability of the reservoirs.

In Chapter 6, the results of the analysis performed in the study are shown. The evident trends are discussed and analyzed.

Chapter 7 is the conclusion this study. It summarizes what was done and the contribution that was made in carrying out this study. It also looks at the possibility of future work in this research area, exploring how this study could be built upon to increase its effectiveness or applied to other areas.

Chapter 2: Literature Review

In performing the study done in this paper, it was important to view other studies that had previously been done on pore connectivity in shales. While this area is relatively lacking in understanding, there are numerous studies that have been done on it. Hu et al. (2012) assessed the pore connectivity of different rocks samples using various approaches. Some of these approaches involved water imbibition, Wood's metal injection, and tracer concentration profile analysis, with some of the samples used originating from the Barnett shale and the Berea sandstone. Hu et al. (2012) concluded that the pore spaces in the Barnett shale were poorly connected with the Barnett sample resulting in an imbibition slope of 0.26, characteristic of sparsely connected rocks, in contrast to the slope of 0.5, characteristic of well-connected rocks, obtained in the well-connected Berea sandstone sample. Hu et al. (2015) analyzed more Barnett shale samples from different depths, observing a short intermediate-time slope of 0.52 followed by the expected imbibition slope value of 0.25 from the Barnett samples as shown in Figure 2.1. Hu et al. (2015) reasoned that the

intermediate-time slope of 0.5 occurred as a result of the exterior surface of the rock samples not being completely wet, and unlike the slope value of 0.25, was therefore not indicative of the true connectivity of the rock samples. Ojha et al. (2016) obtained the pore connectivity of shale samples from Eagle Ford and Wolfcamp shale formations by processing low-pressure nitrogen adsorption-desorption measurement. They reported pore connectivity, in terms of average coordination number, that decreases by 33% with the increase in TOC from 0.02 to 0.06.

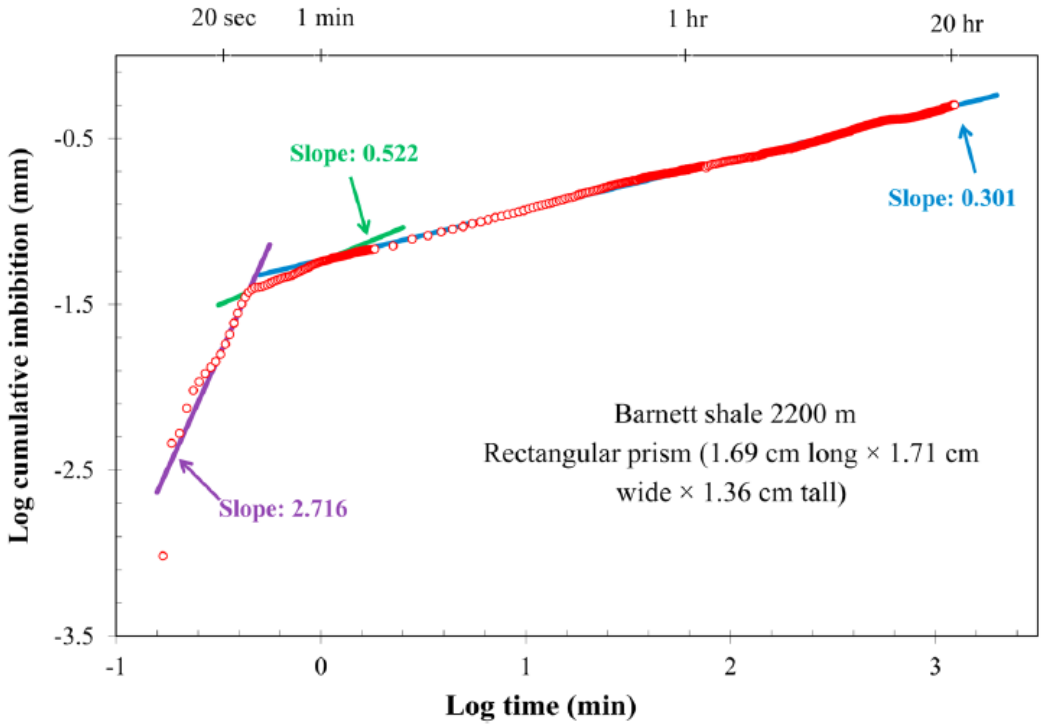


Figure 2.1 Water Imbibition Results for a Barnett Shale in the Analysis Performed by Hu et al. 2015.

Loucks et al. (2009) observed three general modes in which nanopores occur: inside grains of organic matter as intraparticle pores, between kerogen patches as

interparticle pores, and in fine-grained matrix unassociated with organic matter. Interparticle pores lie between grains and crystals while intraparticle pores are found within particles (Loucks et al., 2010). Nonorganic matter interparticle and intraparticle pores are greatly influenced by mechanical and chemical diagenesis while organic matter intraparticle pores are affected by the thermal maturation of organic matter (Curtis et al., 2011). It was determined that the pores in the Barnett are predominantly nanometer in scale (Hu et al., 2014) and occur mostly in the form of intraparticle nanopores found in the grains of organic matter (Loucks et al., 2009). Some of the nanopores observed by Loucks et al. (2009) are shown in Figure 5.

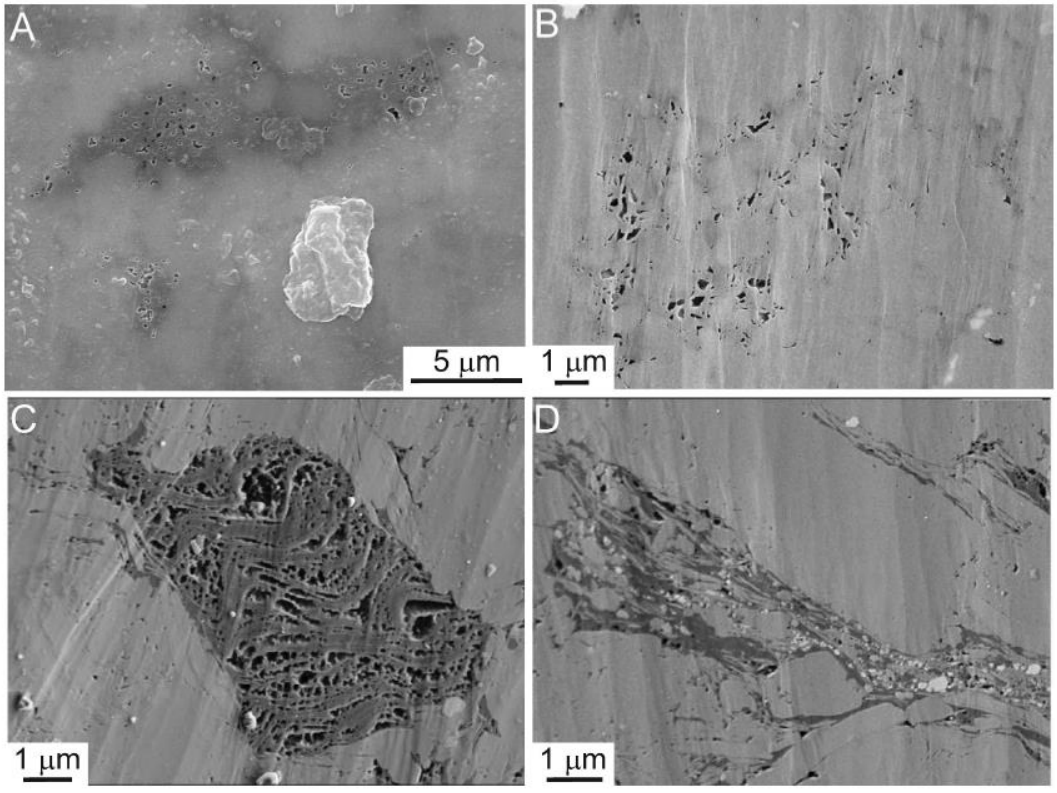


Figure 2.2 Nanopores associated with organic matter in the Barnett Shale (Loucks et al., 2009).

From their mercury injection experiment, Hu et al. (2015) observed their Barnett samples to have matrix permeabilities ranging from 2-5 nanodarcy. They believed that the low connectivity in their samples caused a high tortuosity which in turn decreased the rate of diffusion in the rock matrix (Hu et al., 2015). They concluded that once the hydrocarbon in the fracture network is exhausted, production in then limited by the slow rate of diffusion in the shale matrix, leading to steep declines in production rates (Hu et al., 2015). Fluid flow in a rock matrix is affected by the geometry of its pores (Bear 1972) and their connectivity (Dullien 1992). However when the pore connectivity of a rock is low, as is the case in shales, the connectivity exerts a higher dominance on fluid flow than pore geometry (Hunt et al., 2014).

It was determined that the porosity in the Haynesville shale is predominantly found in its inorganic part (Curtis et al., 2012; Chalmers et al., 2012). With the lenticular geometry of this kind of porosity, Curtis et al. (2012) suggested that the structural integrity of inorganic pores may be questionable as a result of the presence of overburden pressure with gas flowing out of the pores. This could mean that the Haynesville could have more of an issue with production declines because its decrease in connectivity with time would have a greater negative impact on its production rates. Kuila (2013) observed that the presence of a secondary calcite appeared to decrease the porosity and connectivity in the Haynesville.

Montgomery et al. (2005) stated that, in shale gas reservoirs, gas is stored in the form of adsorbed as well as nonadsorbed gas. Adsorbed gas is attached to the surfaces of organic matter and mineral material while nonadsorbed gas is found in the

pore space as solution gas in liquid or as free gas (Loucks et al., 2009). In organic porosity such as in the Barnett, there is the occurrence of gas storage and release through sorption processes (Amann-Hildenbrand et al., 2011). A study performed by Zhang and Krooss (2001) suggests that sorption on organic matter decreases the mobility of hydrocarbon gases and subsequently their effective diffusion coefficients. Loucks et al. (2012) show that organic matter and interparticle pores have higher connectivity and contribute more to the effective pore network than intraparticle pores. This suggests that the Barnett should have a higher pore connectivity than the Haynesville shale. The types of pores in the pore network also have a great effect on storage, permeability, and wettability of rocks (Loucks et al., 2012).

Goral et al. (2015) analyzed Marcellus shale samples by using 3D image processing software and image analysis techniques to reconstruct 3D digital pore structures from which pore properties were derived.

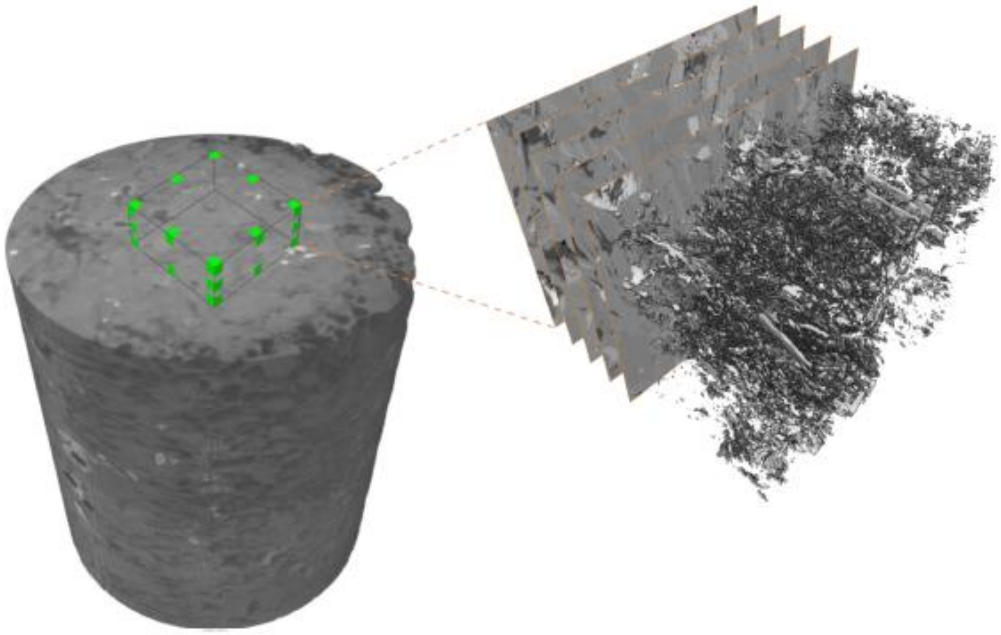


Figure 2.3 Overall Pore Network Investigation Workflow in the analysis performed by Goral et al. (2015).

Through their analysis, they determined that the sample had a porosity of 2.44% with 1.12% of the sample being connected (about 46% of the porosity of the sample), and a predominance of porosity associated with nonorganic matter as compared to that associated with organic matter (Goral et al., 2015). They also observed that the porosity in the nonorganic matter was more connected than the porosity in the organic matter for the Marcellus shale sample (Goral et al., 2015), contrary to the suggestion by Loucks et al. (2012) that organic porosity is more likely to be connected than inorganic porosity. This emphasizes just how heterogenous shale reservoirs can be.

Davudov et al. (2016) evaluated the pore connectivity of Barnett and Haynesville shale samples in the lab scale before evaluating the connectivity at a larger scale by comparing well data to reservoir simulation-generated data. Using MICP experimental data, they found that their Barnett samples had a connectivity of around 34% and their Haynesville sample had a connectivity of around 22% (Davudov et al., 2016). After evaluation with simulation models, similar results were observed (Davudov et al., 2016). Their findings in the lab scale and in the larger scale generally corresponded to each other and also suggest that the Barnett shale has a higher connectivity than Haynesville shale (Davudov et al., 2016). They reasoned that this may be the case due to the shapes and distribution of the pores from these reservoirs, stating that the porosity in the Barnett was more radially shaped as it was mainly located in the organic section of the samples, while the pores in Haynesville were more of a slit shape (Davudov et al., 2016). They also observed that the connectivity of both shale samples increased with sample size. (Davudov et al., 2016)

These studies suggest that some considerable progress has been made in understanding shale reservoirs and significant advances have been made in obtaining their petrophysical properties as well as grasping what roles these properties may play in their production. In addition to introducing new terminology for evaluating production performance, this study aims at contributing to the research that has already been done concerning the connectivity of these shale reservoirs and generally bettering our understanding of these reservoirs and their petrophysical properties.

Chapter 3: Overview of the Shale Reservoirs

In this paper, the Barnett, Haynesville, and Marcellus shale reservoirs are analyzed. These reservoirs are three of the "magnificent seven" along with Fayetteville, Woodford, Horn River, and Montney, and are thus important hydrocarbon reservoirs in the United States today (Goral et al., 2015). Their production over time is displayed in Figure 3.1 (EIA 2017).

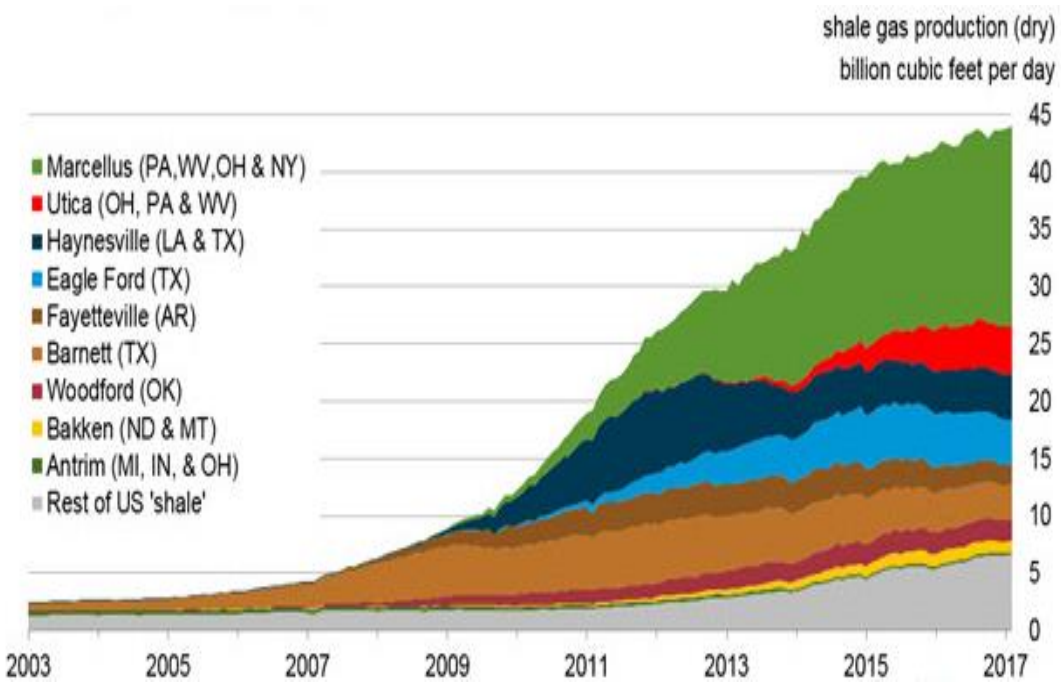


Figure 3.1 United States Dry Shale Gas Production (EIA 2017).

The Marcellus shale has had the most drastic increase in production levels and currently produces the most natural gas out of all the gas shales. The Barnett, on the other hand, has been a major natural gas producer for the longest period. The Haynesville had its prominence around the same time as the Marcellus however its increase in gas production has been fairly less drastic.

These reservoirs are analyzed because knowledge of their production performance and connectivity would be beneficial to the prediction of future production levels of wells producing from them. This section serves as an overview in which general information about each shale reservoir is provided. It provides background information on these reservoirs and material that may relate to their production levels. It is important because it gives insights on the kind of properties and results that could be expected from this study for each reservoir.

3.1 Overview of the Barnett Shale

The Barnett shale is an organic-rich shale reservoir deposited in the Mississippian period which is found in the Fort Worth Basin. It was first discovered in the 1950s but did not become commercial until the 1980s. Lying under at least 18 counties in the Fort Worth Basin, this relatively thin reservoir stretches over a large area of 13,000 km^2 (Hu et al., 2015), warranting the need for the use of horizontal drilling in extracting its reserves. Majority of the area it encompasses is located under the Dallas-Fort Worth Metroplex. As indicated in Figure 3.1, it was responsible for majority of the shale gas production in the United States from 2003 till 2009, when the production from the other shale plays started to become significant. It is divided in some areas into the Upper and Lower Barnett by an intrusion of a laminated, argillaceous lime mudstone known as the Forestburg limestone as shown in Figure 3.2 (Loucks and Ruppel, 2007; Montgomery et al., 2005). The Forestburg limestone is a dense and relatively impermeable limestone, enabling it to act as an effective hydraulic fracture barrier (Pollastro et al., 2007). The Barnett is overlain by the Marble

Falls Limestone and sits atop the Ellenburger limestone. The Upper and Lower Barnett formations (in areas where the Forestburg is present) consist of siliceous mudstones with less abundant interbedded lime mudstones and skeletal packstones (Loucks and Ruppel, 2007).

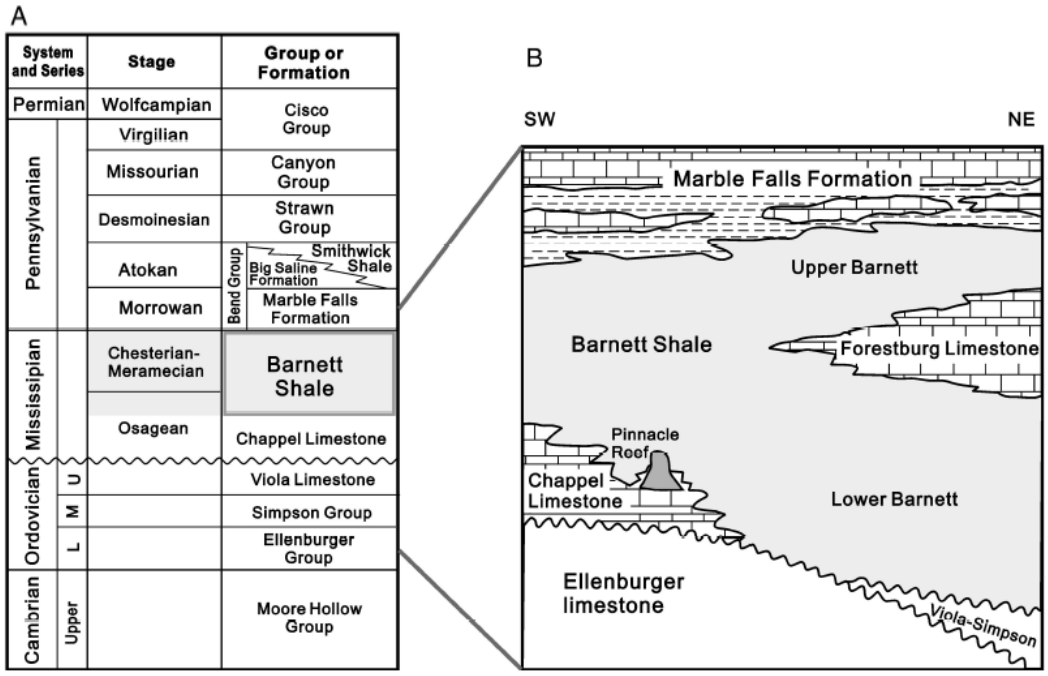


Figure 3.2 Schematic section of the Barnett Shale (Fu et al., 2015).

By the end of 2015, the Barnett had a proved reserves estimate of 17 trillion cubic feet of gas (EIA 2016). In 2014, the Barnett was the most developed and most extensively studied shale play with almost 18,000 active wells (Nicot et al., 2014; Fu et al., 2015). Curtis (2002) estimated its recovery to range from 8 to 15%, before this estimate was later increased to a range from 12% to 30% by King (2012). Wells producing from the Barnett show a steep decline from their initial production rates (Hu et al., 2015) which is typical of shale reservoirs. With about 45% of the gas found

in the Barnett sorbed onto the shale matrix (Hill et al., 2007), adsorption and desorption processes may play a significant role in the production from this reservoir. Its permeability ranges from 1 to 10 nanodarcy (Heller and Zoback, 2013; Sigal 2013) while its depth ranges from less than 4000 ft to over 8500 ft (Fu et al., 2015).

3.2 Overview of the Haynesville Shale

Named after the town of Haynesville located in Claiborne Parish, Louisiana, the Haynesville shale is a carbonate-rich, siliceous, and organic shale formation which was deposited in the Upper Jurassic Period (Hammes et al., 2011). It is located in Northwestern Louisiana and Eastern Texas. Extensive calcite cementation in the Haynesville shale negatively impacts the connectivity of its pores by creating sections of closed off ineffective porosity (Kulia 2013). It underlies an area of about 23,000 km^2 and its thickness ranges from 200 ft to 300 ft while its depth ranges from 10,300 ft to 14,000 ft (Parker et al., 2009). It is overlain by the Cotton Valley Group formations and underlain by the Smackover formation as shown in the stratigraphic columns displayed in Figure 3.3 (Thompson et al., 2011). It has temperatures exceeding 300°F and abnormally high reservoir pressures with pressure gradients of up to 0.9 psi/ft (Thompson et al., 2011). For a brief period between the dominance of the Barnett and that of Marcellus, the Haynesville was the highest producing shale in the United States. This period was from about 2011 to 2012 as shown in Figure 3.1. By the end of 2015, the Haynesville had a proved reserves estimate of 12.8 trillion cubic feet of gas (EIA 2016).

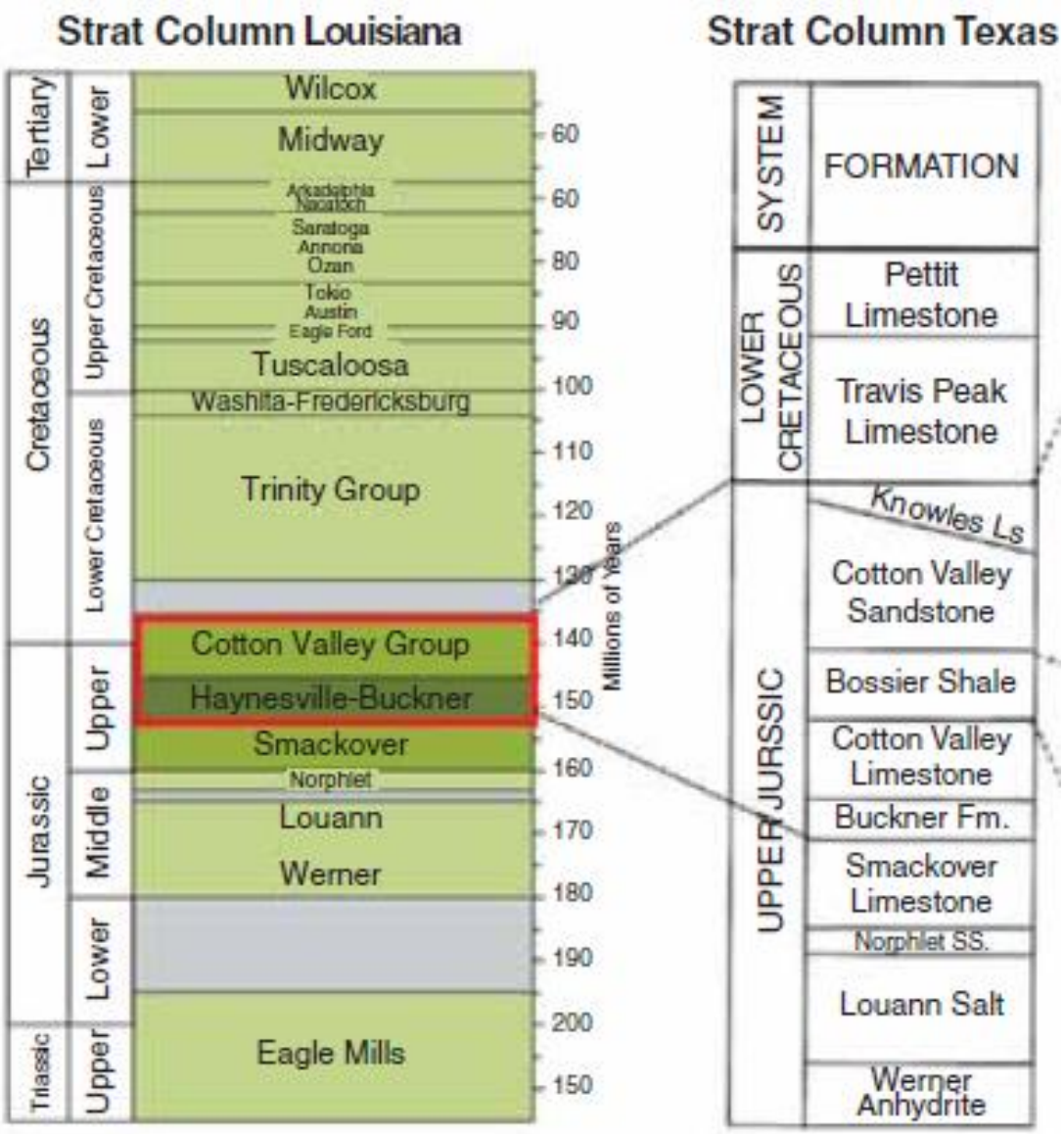


Figure 3.3 Stratigraphic Columns showing the Haynesville Shale in Texas and Louisiana (Thompson et al., 2011).

3.3 Overview of the Marcellus Shale

The Marcellus shale is a shale reservoir located in the Appalachian basin, specifically in the states of New York, Ohio, West Virginia, and Pennsylvania (Belvalkar and Oyewole, 2010). It is rich in organic matter and in carbonates. Production from the

Marcellus is impacted by gas desorption (Belvalkar and Oyewole, 2010; Zamirian et al., 2016). The Marcellus is responsible for the entire growth in natural gas production in the United States between 2011 and 2013 (Yu et al., 2014), also evident in Figure 3.1. It covers an area of over 250,000 km^2, reaches depths ranging from 4,000 ft to 8,500 ft, and has thicknesses varying from 50 ft to 200 ft (U.S Department of Energy, 2013). It has a reservoir temperature of about 140°F and the bottomhole pressure for its wells can reach up to 6,000 psi (Williams et al., 2011).

Overtaking the Haynesville shale in 2012, it became the largest contributor to total shale gas production in the United States and still retains that position today as shown in Figure 3.1. By the end of 2015, the Marcellus had a proved reserves estimate of 72.7 trillion cubic feet of gas (EIA 2016), easily making it the reservoir with the largest amount of recoverable gas amongst all the shale plays in the United States. Prior to 2000, most of the wells in the Marcellus were low production rate wells with very long productive lives. However, following the introduction of horizontal drilling and hydraulic fracturing and their subsequent perfection in the Barnett shale, these principles were later applied in the Marcellus leading to its current high production volumes.

Chapter 4: Definitions

In this analysis, two important terms are evaluated. These terms are connectivity and sustainability. Definitions and explanations of these terms are provided in the section as they would be helpful in improving our understanding of the

trends and insights shown in the results of this study. This section not only describes these terms but also explains what make them important in this study and in producing from these shale reservoirs.

4.1 Sustainability

The word, sustainability, is most commonly used in the renewables industry and in discussions pertaining to the environment. It generally refers to the ability to maintain a process, parameter, or balance at a certain rate or level. It defines rates or levels of the process, parameter, or balance that can be continued indefinitely. If these rates or levels cannot be continued indefinitely, then they are not sustainable. Sustainability usually involves the occurrence of an equilibrium and is applied in different subject areas such as in environmental sustainability, the ability to maintain an ecological balance in an environment indefinitely, and economics, the ability of an economy to remain at a relatively stable size indefinitely. If the ecological balance in a certain environment cannot be maintained indefinitely, then that environment has a low level of environmental sustainability. This description is similar to definitions in which the properties of a system are observed not to change or vary with time. However, the definition of sustainability is used, it always points to capability of something to remain the same with time.

In this study, sustainability, is introduced as a term describing the ability of a reservoir to maintain reasonable levels of production rates for extended periods of time. Following this raw definition of sustainability however, one would be drawn to the conclusion that all reservoirs are fundamentally unsustainable. This is because

reservoirs are essentially highly pressured systems in which the mere presence of hydrocarbons inside these reservoirs is the source of this high pressure. The hydrocarbons in these reservoirs are extracted through the utilization of the pressure difference between the reservoir and the wells being used. The rates at which they produced are, therefore, functions of this pressure difference as shown in equation (4-1). (Economides et al., 2013).

$$q = \frac{kh(p_r - p_{wf})}{141.2B\mu\left(ln\left[\frac{r_e}{r_w}\right] + s\right)}, \quad \text{(4-1)}$$

where k is permeability, h is reservoir thickness, p_r, is average reservoir pressure, p_{wf}, is well bottomhole flowing pressure, B is formation volume factor, μ is fluid viscosity, r_e is effective drainage radius, r_w is wellbore radius, and s is skin factor. Out of these parameters, p_r, p_{wf}, and B could be functions of time.

However, by extracting the hydrocarbons from these reservoirs, the reservoirs lose their source of high pressure and this results in pressure depletion. And with pressure depletion, comes decreases in flow out from these reservoirs and therefore declines in production rates. As a result of this, reservoirs are unsustainable as their production rates eventually always decline with time. Because of this fact, sustainability is not evaluated as a term in which there can only be two outcomes, being sustainable and being unsustainable. It is rather evaluated as a qualitative term with levels associated with it. In this sense, reservoirs may be fundamentally unsustainable however, their sustainability can be compared to one another. High levels and low levels of

sustainability can be distinguished and a spectrum can essentially be created in evaluating it.

In this way, sustainability is used as a means of evaluating the declines in production rates and the performance of wells from the reservoirs in this study. Production rate declines are commonly represented in the form of the Arps decline exponent, b, used in decline curve analysis. This value ranges from 0 to 1 and based on what its value is, the production rate declines in reservoirs can be evaluated. Declines can be evaluated based on the decline exponent as exponential if b is equal to 0, hyperbolic if b is neither 0 nor 1, or harmonic if b is equal to 1 (Arps 1945). In evaluating reservoir performance on the other hand, the productivity index (PI) of a reservoir is used instead. This value is the slope of a plot of bottomhole pressure versus production rate. It is described in equation (4-2) (Economides et al., 2013).

$$PI = \frac{q}{p_r - p_{wf}} = \frac{kh}{141.2B\mu\left(ln\left[\frac{r_e}{r_w}\right]+s\right)} \quad \text{..... (4-2)}$$

It is a function of reservoir properties, fluid properties, formation damage in the reservoir. The productivity index essentially evaluates performance by quantifying the amount of hydrocarbon that can be produced using a certain pressure difference. A reservoir with a high productivity index will be able produce hydrocarbons at higher rates than other reservoirs using the same pressure drop, and would be therefore more profitable as it has a better performance.

Sustainability is similar to the Arps decline exponent and the productivity index in that it is used as a means of evaluating the declines in production rates and

reservoir performance. The manner in which it goes about evaluating these, however, is slightly different to those used by the Arps decline exponent and the productivity index. The depletion history of a reservoir ideally consists of two sections namely the constant rate section and the depletion flow section as shown in Figure 4.1 (Moghanloo 2015). This is normally the case for conventional reservoirs. However, for unconventional reservoirs, the constant rate section either occurs for a very short period of time or is nonexistent. Unlike the Arps b exponent which can only be used on the depletion flow section, sustainability can be applied to both the constant rate section and the depletion flow section of the production history of a reservoir.

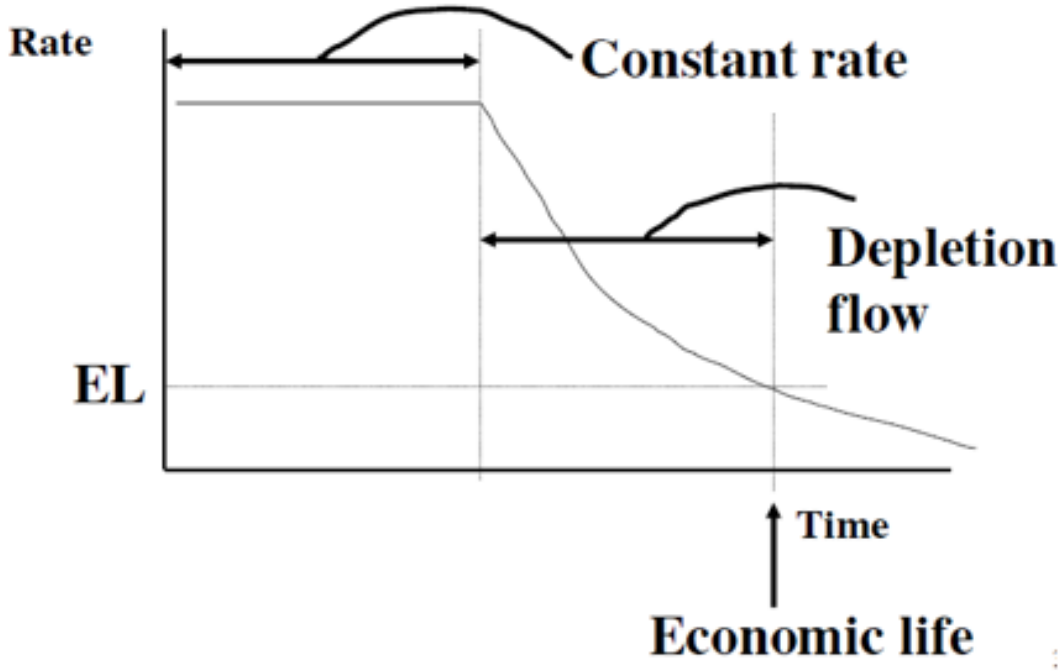


Figure 4.1 Schematic showing an idealized depletion history (Moghanloo 2012).

The terms, q, production rate, q_{max}, the maximum production rate, G_p, the cumulative gas production, and estimated ultimate recovery (EUR), the maximum amount of

cumulative gas production that is estimated for a reservoir, are used in evaluating sustainability in this study. Unlike the productivity index, sustainability does not involve the use of pressure data in being evaluated. Also, the productivity index evaluates performance relating to the movement of hydrocarbons from a reservoir into a wellbore. Sustainability, on the other hand, evaluates performance relating to the replacement of hydrocarbons that have flowed into the wellbore by the reservoir matrix. Using these terms, plots of $\frac{q}{q_{max}}$ versus $\frac{G_p}{EUR}$ are made. Sustainability of different reservoirs can be evaluated relative to each other by comparing their $\frac{q}{q_{max}}$ versus $\frac{G_p}{EUR}$ curves. The reservoir with a steeper decline in its $\frac{q}{q_{max}}$ versus $\frac{G_p}{EUR}$ curve has a lower sustainability compared to a curve with a less steep decline in its $\frac{q}{q_{max}}$ versus $\frac{G_p}{EUR}$ curve. Figure 4.2 displays a schematic of this plot used to determine sustainability. In the figure, the curve with a convex shape is one of a high sustainability while the curve with a concave shape is a curve representative of low permeability. The straight-line curve found between the high sustainability and low sustainability curves is a curve with slope equal to -1. It can be used as a general marker to distinguish between good levels and poor levels of sustainability. In conventional reservoirs, it is common to have curves resembling the high sustainability curve in the schematic. For shales however, low sustainability concave curves are observed to be the more dominan t.

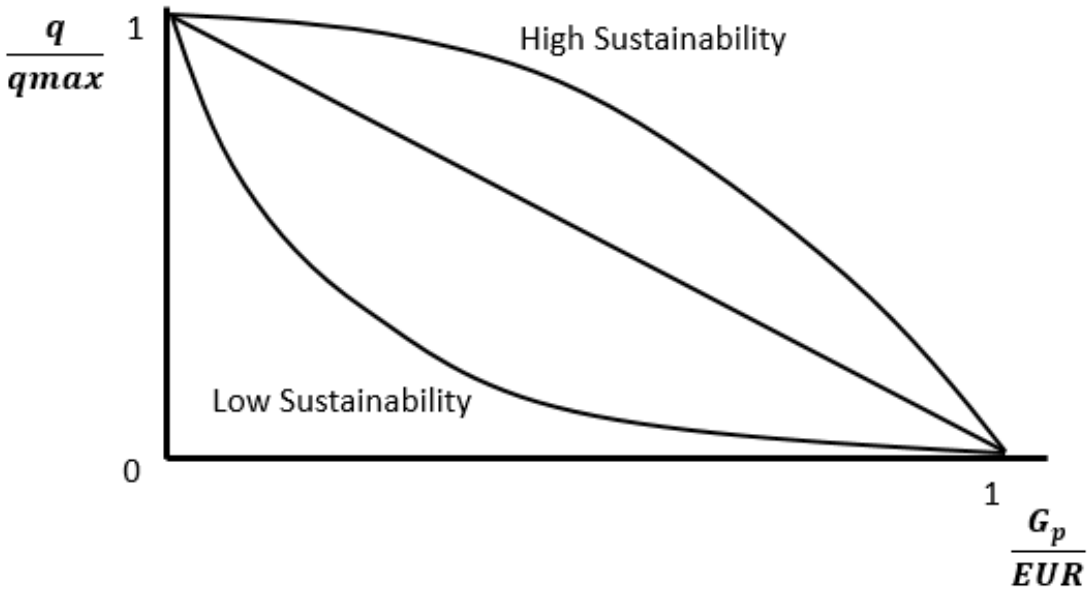


Figure 4.2 Schematic of plot used to evaluate sustainability.

Also, by calculating the values of the slope in these $\frac{q}{q_{max}}$ versus $\frac{G_p}{EUR}$ curves, the sustainability of reservoirs can be quantified. The slopes for each individual point on the $\frac{q}{q_{max}}$ versus $\frac{G_p}{EUR}$ curve can be calculated using a method of choice between forward finite difference, backward finite difference, and central divided finite difference techniques described by equation (4-3), equation (4-4) and equation (4-5) respectively (Chapra and Canale, 2010).

$$f'(x_i) = \frac{f(x_{i+1}) - f(x_i)}{x_{i+1} - x_i} \quad \text{(4-3)}$$

$$f'(x_i) = \frac{f(x_i) - f(x_{i-1})}{x_i - x_{i-1}} \quad \text{(4-4)}$$

$$f'(x_i) = \frac{f(x_{i+1}) - f(x_{i-1})}{x_{i+1} - x_{i-1}} \quad \text{(4-5)}$$

These slopes are mostly negative because production rates generally decrease with time or cumulative production. Any positive slopes occur as a result of fluctuations in the production rates of the wells. Because the sustainability of the reservoir can be quantified by the slope of this curve, the sustainability can be evaluated based on the distribution of the slopes obtained. A reservoir with an average slope value that has a higher magnitude (is more negative) will have a lower sustainability while one with an average slope value that has a lower magnitude (is less negative) will have a higher sustainability.

It is already known that wells in shale reservoirs start off with very high production rates with these rates experiencing rapid declines early in the lives of the wells. This phenomenon is very important as it has an effect on the economics for the well or reservoir. It affects not only the estimated ultimate recovery of the well but also how quickly it can be attained. It is therefore important to study this phenomenon in order to better understand it and its nature in different shale reservoirs so as more economically and efficiently produce from these reservoirs. By analyzing or quantifying this phenomenon in the form of the term, sustainability, it is possible to obtain a better understanding of these reservoirs.

4.2 Connectivity

Goral et al. (2015) define porosity as a measure of how much void space there is contained in a rock. It is a function of rock parameters such as grain size, shape, sorting, rock compaction, and cementation. Each of these parameters play unique roles in determining the porosity of rocks. Variations in these parameters cause

significant heterogeneity in rocks and reservoirs and their properties. As a result of this, samples collected from different regions could have significantly different values of porosity as well as other rock properties.

Because the hydrocarbons found in a rock is stored in its pore space, porosity is a very important parameter when it comes to hydrocarbon exploration and production. It quantifies the storage ability of a rock, and thus its ability to hold hydrocarbons. It has become customary to determine the porosity for a reservoir before developing or producing from it, as it gives important insight on the amount of hydrocarbon that is contained by the reservoir. A smaller reservoir could contain a higher amount of hydrocarbon than a larger reservoir simply due to the fact that it contains a larger amount of pore space compared to the larger one. While porosity can be determined using numerous well logs, it is usually determined in the lab using techniques such as helium injection, nitrogen injection, mercury injection, imbibition, thin section analysis, and by measurement of bulk and grain volumes.

There are two types of porosity, namely total porosity and effective porosity. Total porosity refers to the total pore space in a rock while effective porosity refers to the accessible pore space. Most measurement techniques tend to measure the latter. By comparing these two types of porosity, the pore connectivity of a rock can be determined. Pore connectivity refers to the percentage or proportion of pore space in a reservoir that is connected. Davudov and Moghaloo (2016) define it as the ratio of accessible pore volume to total pore volume. This is illustrated in Figure 4.1 (Moghanloo et al., 2015).

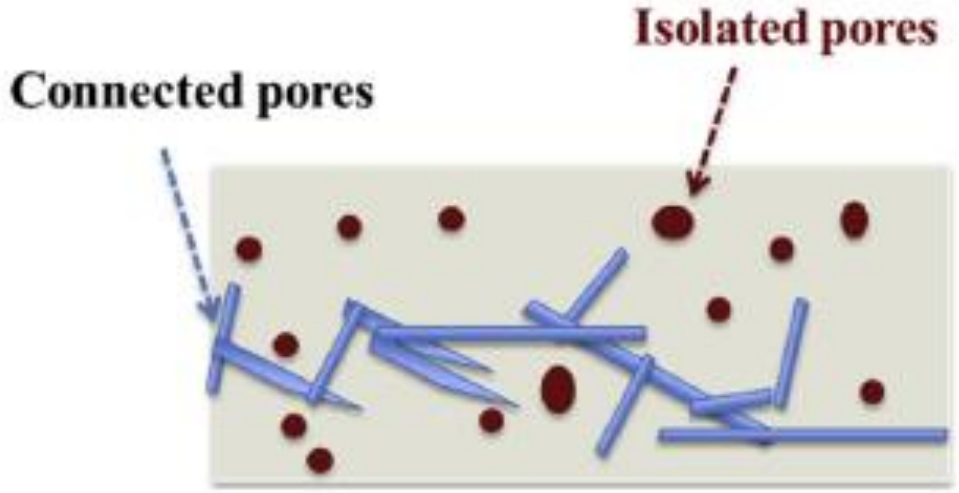


Figure 4.3 Illustration of shale matrix consisting of grains, connected and isolated pores (Moghanloo et al., 2015).

This is an important term because it relates directly to the flow paths taken by hyrdrocarbons as they flow from the matrix of a reservoir to the wellbore of a well producing from it. Not only does it provide information on the amount of hydrocarbon that can be extracted from a rock (recovery factor) but it also has an impact on the rate at which the rate at which this amount of hydrocarbon can be extracted. How connected the porosity is in a rock affects the ability of a fluid to flow through it and based on this, it becomes conceivable that connectivity could have an impact on production. Pore connectivity impacts flow rates by affecting the main transport mechanism controlling late time production rates in shale matrices, dispersive flux. With everything else being equal, higher pore connectivity provides greater flux (Davudov and Moghanloo, 2016). Shales tend to have low levels of pore connectivity

as a result of their small grain sizes. These low levels of connectivity in shales may be the reason for their steep decline in production rates and low levels of production.

Chapter 5: Methodology

Until recently, connectivity information has been mostly obtained at the lab scale. It is usually determined using methods involved in porosity and pore size distribution analysis such as water imbibition, imaging techniques, tracer concentration analysis, MICP analysis, low-pressure nitrogen adsoprtion-desorption measurement, and Wood's metal injection. While the information obtained using these methods is very valuable, it is obtained by analyzing core samples. Core samples are obtained from specific parts of a reservoir and, while information derived from them is commonly used to represent the whole reservoir, this information is actually only localized to the region of the reservoir from which the core sample is obtained from. As a result of this, the information obtained from core samples in the lab may not generally be representative of the whole reservoir of interest. In very heterogenous reservoirs, this information may have little value and could even be misleading. In this kind of scenario, the costs incurred in obtaining and analyzing a core could make it a fruitless investment, a situation operators strive to avoid. The source of this risk is the small scale of the of the analysis performed on the core samples in the lab. If performed at a larger scale, a study can result in information that is more representative of the reservoir, thus reducing this risk. Therefore increasing the scale of an analysis may have beneficial effects on its effectiveness.

There have not been many connectivity analyses performed on a large scale. However a method of upscaling connectivity analysis from the lab scale to the well scale was introduced by Davudov and Moghanloo (2016). In their study, the pore connectivity of Barnett and Haynesville shale samples are determined at lab-scale before being upscaled to well-scale using production data. At lab scale, a scanning electron microscope (SEM) analysis was used to analyze the shale samples in the study (Davudov and Moghanloo, 2016). The images of their Barnett shale sample and Haynesville shale sample are shown in Figures 5.1 and 5.2 respectively, with the darker shaded material representing organic matter and the lighter shaded material corresponding to quartz and clays (Davudov and Moghanloo, 2016).

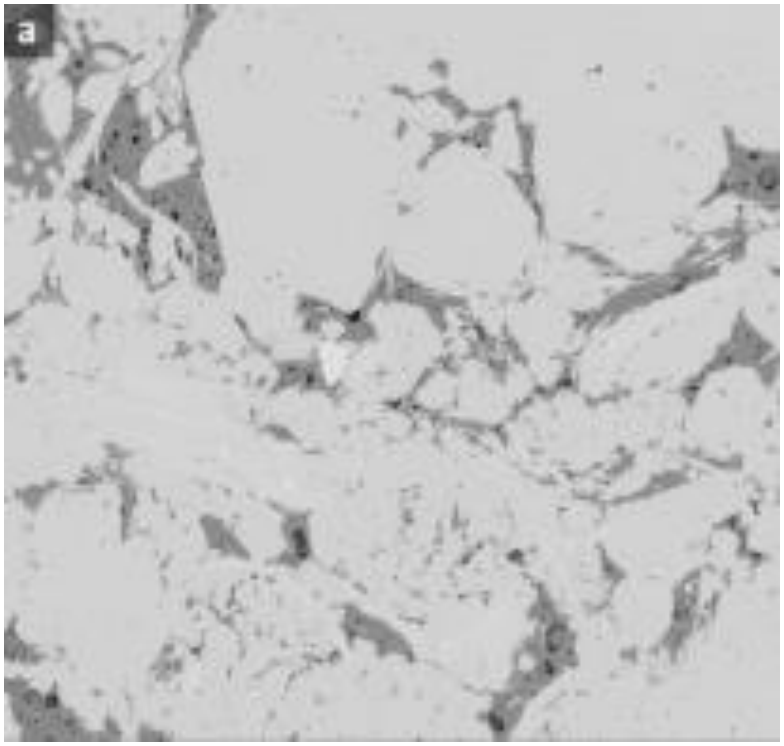


Figure 5.1 Backscattered electron image of a Barnett Shale Sample (Davudov and Moghanloo, 2016).

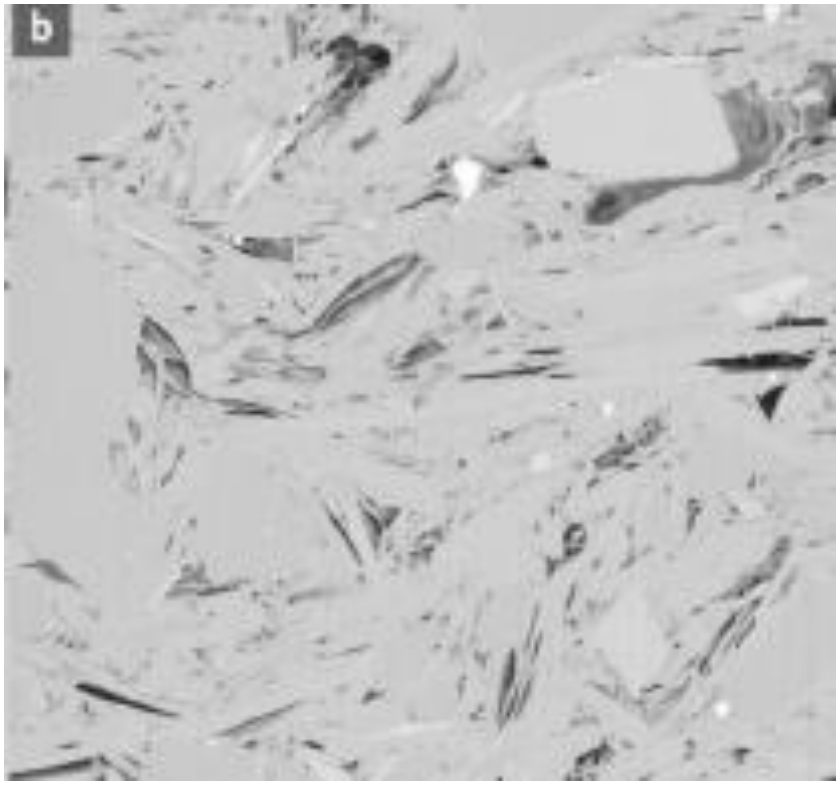


Figure 5.2 Backscattered electron image of a Haynesville Shale Sample (Davudov and Moghanloo, 2016).

It was observed in the Barnett shale sample that majority of the porosity resided in the organic matter-containing section of the sample, in agreement with the the findings made by Loucks et al. (2009), while majority of the porosity in the Haynesville shale sample was located in its inorganic matrix (Davudov and Moghanloo, 2016). In addition to the SEM analysis, a mercury injection capillary pressure (MICP) experimental analysis was performed and laser-produced plasma (LPP) helium measurements were taken on the shale samples in their analysis in order to determine their porosities (Davudov and Moghanloo, 2016). Defining connectivity as the ratio of accessible pore volume to total pore volume, they evaluated the pore connectivity of the samples as

the ratio of their MICP-determined porosity to their LPP-determined porosity values (Davudov and Moghanloo, 2016). From their lab-scale analysis, they concluded that the Barnett shale had a higher pore connectivity than the Haynesville shale, attributing this to the fact that majority of the porosity in the Barnet shale is found in its organic matter while majority of the porosity in the Haynesville shale is found in its inorganic matrix (Davudov and Moghanloo, 2016). In the second part of their study, a simulation approach using GEM, CMG's advanced general equation-of-state compositional reservoir simulator, was used to evaluate the connectivity for the shale plays. Using late time production data from a few selected Barnett and Haynesville wells, recovery factor data was evaluated and compared with simulation-generated data to determine the connectivity for the different fields. Their connectivity results were consistent with the pore connectivity they observed at lab-scale, with the Barnett connectivity being evaluated to be around 20% higher than that of the Haynesville shale (Davudov and Moghanloo, 2016).

A similar approach is taken in this study to that used in the second part of the study performed by Davudov and Moghanloo (2016). The analysis involves the use of an analogous simulation model to evaluate pore connectivity at the well scale using production data. As it is evaluated on a large scale, the connectivity determined in this study is therefore referred to as reservoir-scale connectivity. A simulation model is constructed in a manner in which a dual-permeability model representing both matrix and fracture permeability, is simulated. The model is described in the section below.

5.1 Description of the CMG Simulation Model

Most of the wells producing from shale reservoirs today incorporate the use of horizontal drilling and hydraulic fracturing. In other words, they mostly consist of wells with horizontal wellbores situated in fracture-matrix systems. Bello and Wattenbarger (2010) assumed a model involving a horizontal well draining a rectangular reservoir containing a matrix blocks separated by a network of fractures, in their work. This model is displayed in Figure 5.3. A similar assumption is made in the model used in this study.

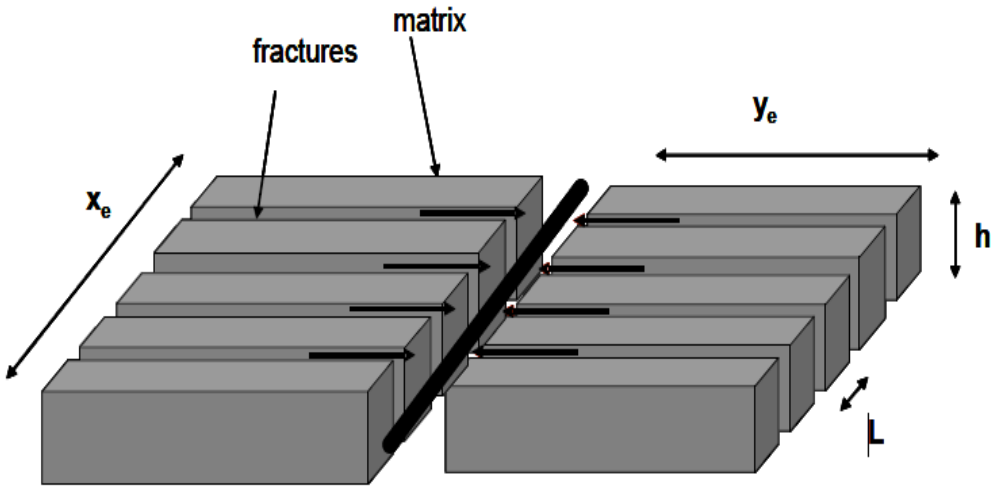


Figure 5.3 Schematic of a Slab Matrix Linear Model of a Hydraulically Fractured Well (Bello and Wattenbarger 2010).

These blocks representing the matrix of the reservoir each contain a certain measure of porosity. They also each contain a proportion of the porosity that forms a connected

flow path linking the gas they store to the fractures adjacent to them. These connected porosity flow paths are represented as the red lines in Figure 5.4.

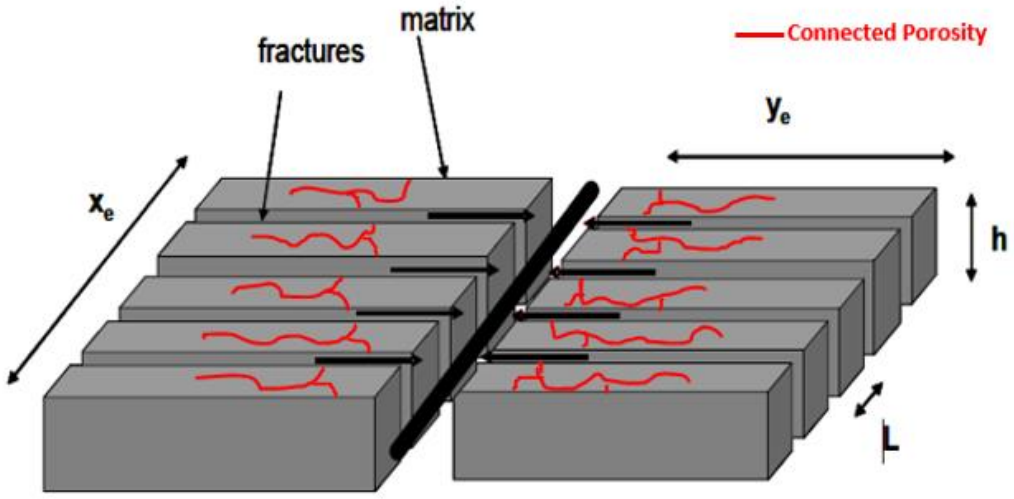


Figure 5.4 Slab Matrix Linear Model with Matrix Connected Porosity Flow Path indicated by Red Lines.

The gas that is initially stored in the matrix blocks flows through these paths formed by the connected matrix pore spaces into the fracture network, from which it flows into the horizontal wellbore located at the center of image in Figure 5.4, and then up the vertical section of the wellbore to the surface. While actual fracture-matrix networks in shale reservoirs are more complex than the model assumed in this study, this model represents a reasonable approximation of the system. In the constructed model used in this study, half of one of the matrix blocks in Figure 5.4 is taken along with a one of the fractures separating it from a matrix block adjacent to it. Using CMG, a cuboid reservoir model incorporating a matrix block and an adjacent fracture, is constructed

to model desribed system. A three-dimensional view of the construted model is shown in Figure 5.5.

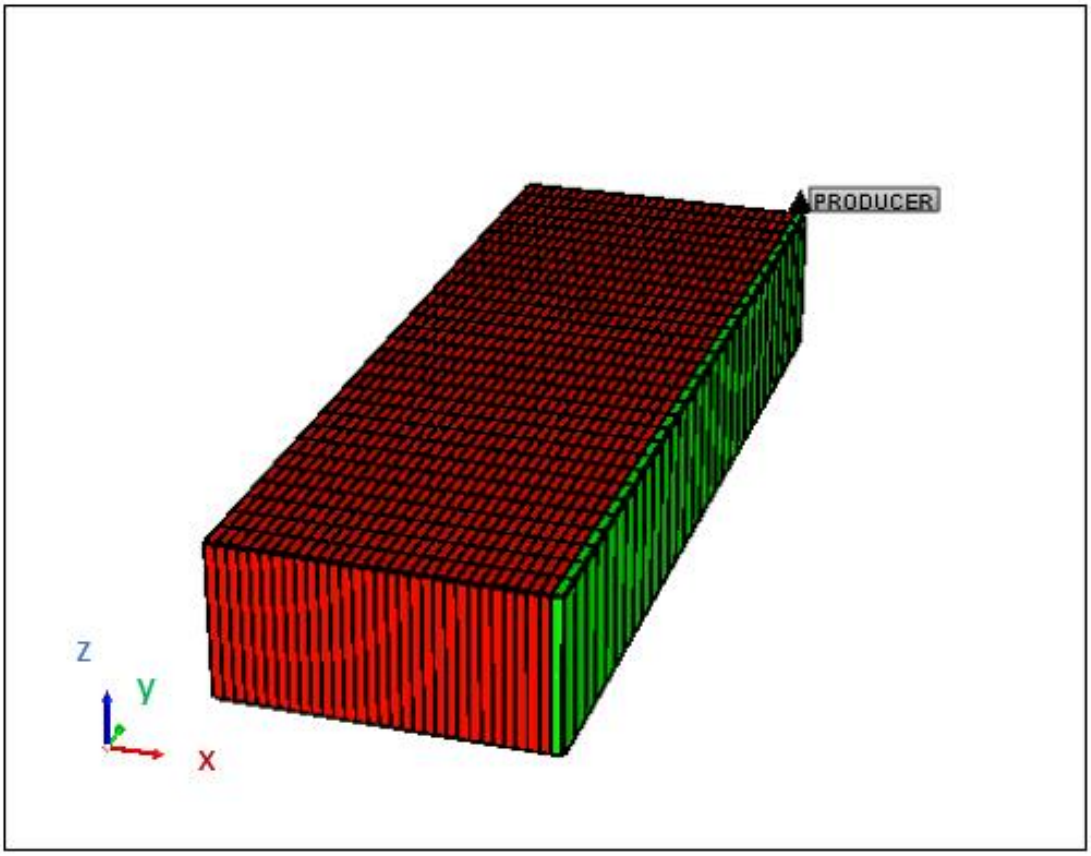


Figure 5.5 Three-dimensional view of the cuboid model constructed in CMG.

The model is features a reservoir consisting of 930 grid blocks in total. More precisely, it consists of 30 grid blocks in the x direction, 30 grid blocks in the y direction and 1 block in the z direction. The matrix is represented by the grid blocks shown in red and consists of 900 grid blocks. The fracture in this model, on the other hand, is represented by the string of green grid blocks located on the far right of the figure, consisting of the remaining 30 grid blocks. The model contains one producing well located in the North-Eastern corner reservoir. In order to give a better depiction of the

constructed model, two dimensional views of it are provided. Figure 5.6 displays the directions these views are taken from while Figures 5.7 and 5.8 display actual two-dimensional views.

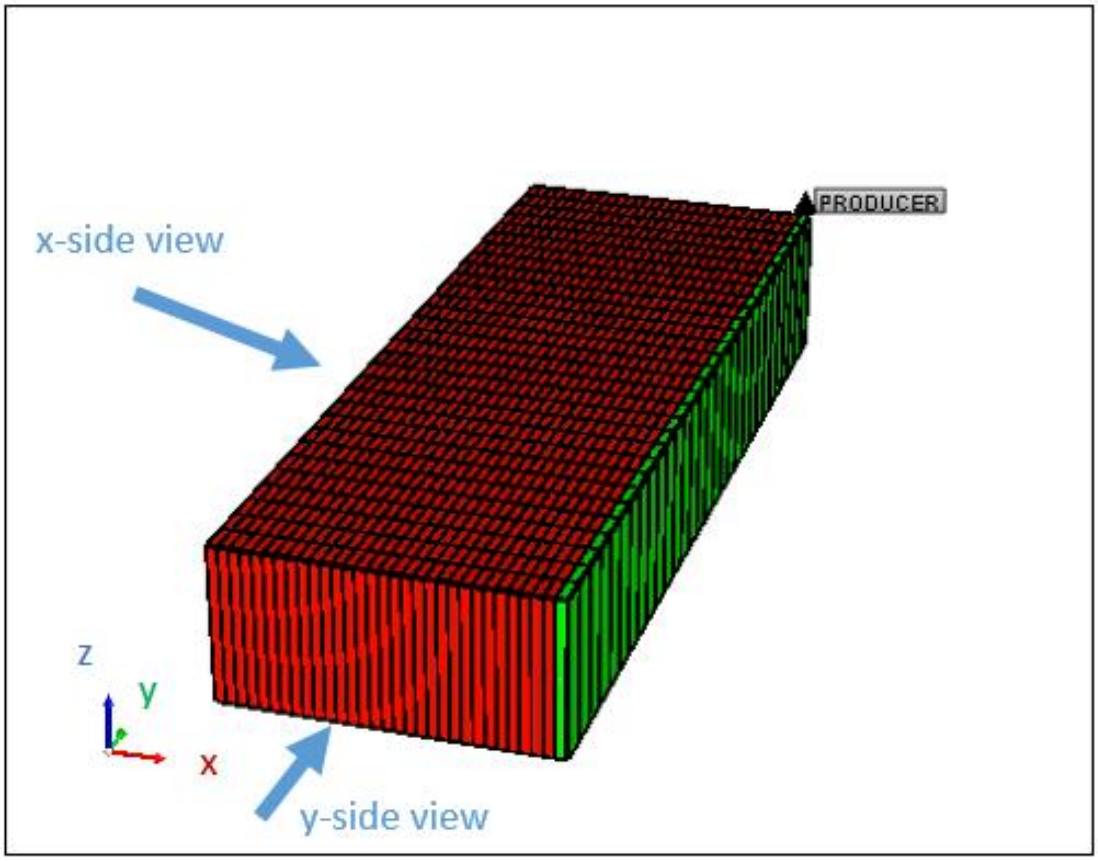


Figure 5.6 Image displaying the Directions the Two-Dimensional Views are taken from.

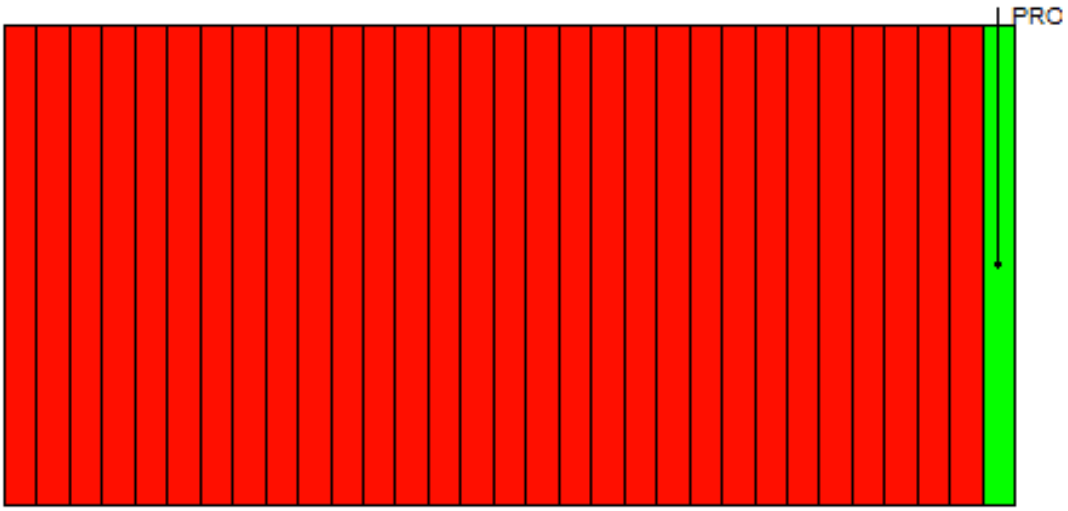


Figure 5.7 y-side Two-Dimensional View of the Reservoir Model

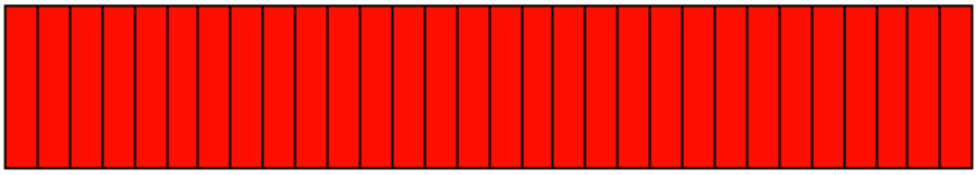


Figure 5.8 x-side Two-Dimensional View of the Reservoir Model

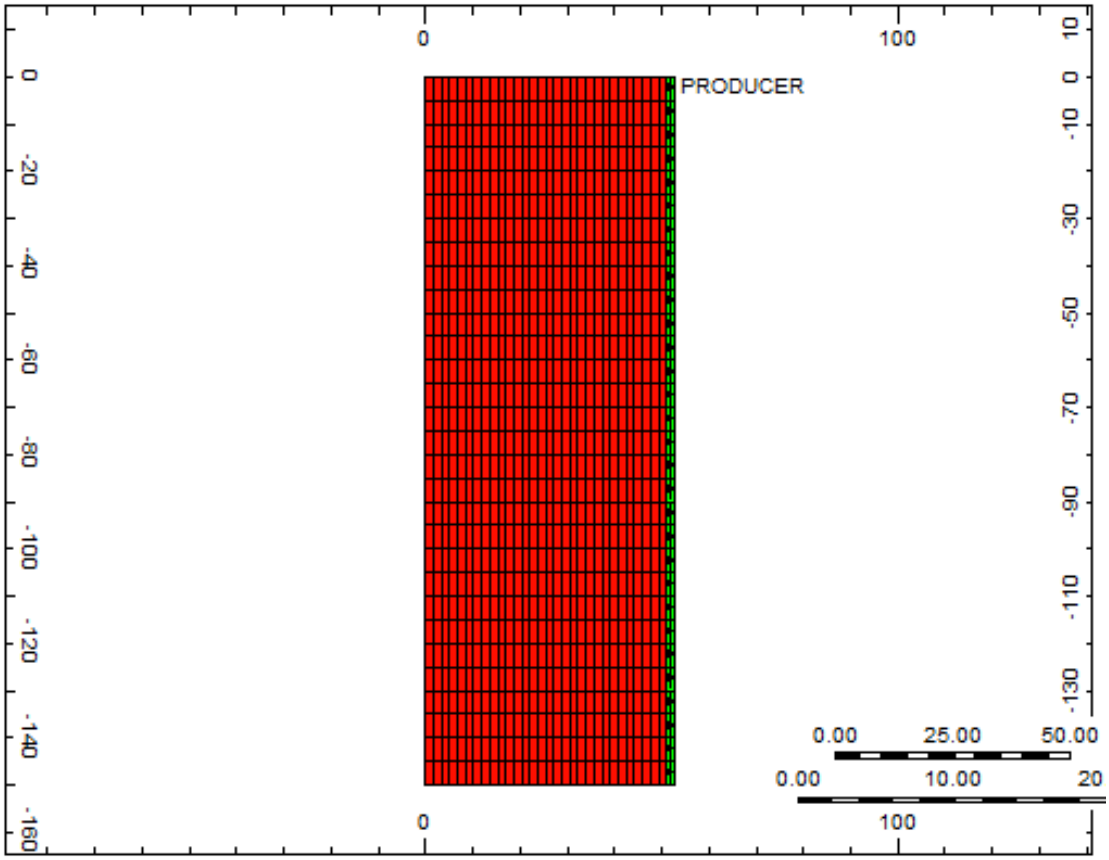


Figure 5.9 Plan View of the Reservoir Model.

A plan view is of the reservoir model is also displayed in Figure 5.9. In these figures, while the red and green grid blocks represent the matrix and fracture zones respectively, they also represent grid blocks with low and high transmissibility values respectively. Transmissibility is a special type of conductance used in reservoir simulators to quantify flow allowance between grid blocks. It is a function of permeability and block geometry. More precisely it is proportional to a cross-sectional inter-block flow area, an averaged permeability value, and a divisor equal to the inter-block distance (Computer Modelling Group Ltd 2015). For two adjacent grid blocks, *i* and *j*, it is given by equation (5-1) (Cordazzo et al., 2002).

$$T_{ij} = k_{ij} \frac{A_{ij}}{h_{ij}} \quad \text{(5-1)}$$

where A_{ij} is the cross-sectional area of flow and h_{ij} is the length across which flow is taking place. Being the inverse of resistivity to flow, its properties were taken advantage of in this study. By strategically assigning transmissibility values to certain grid blocks in the matrix section of the reservoir model, a connected pore network can be created in the reservoir to imitate than of an actual shale reservoir matrix.

In the matrix section of this model, an arbitrarily chosen set of grid blocks are chosen and assigned high transmissibility values. These grid blocks are chosen in a manner in which they are all connected to each other and connected to the grid block intersected by the well or the string of grid blocks on the far right of the model representing the fracture. Also, the number of grid blocks chosen are such that they contain 5% of the total number of grid blocks in the matrix section of the model. As there are 900 grid blocks in the matrix section of this model, 45 of the grid blocks are chosen. Having done this, the model now represents a fracture-matrix system in which the reservoir matrix possessing a reservoir-scale connectivity of 5%. The plan view of the model with 45 arbitrarily chosen grid blocks with high transmissibility values is shown in Figure 5.10.

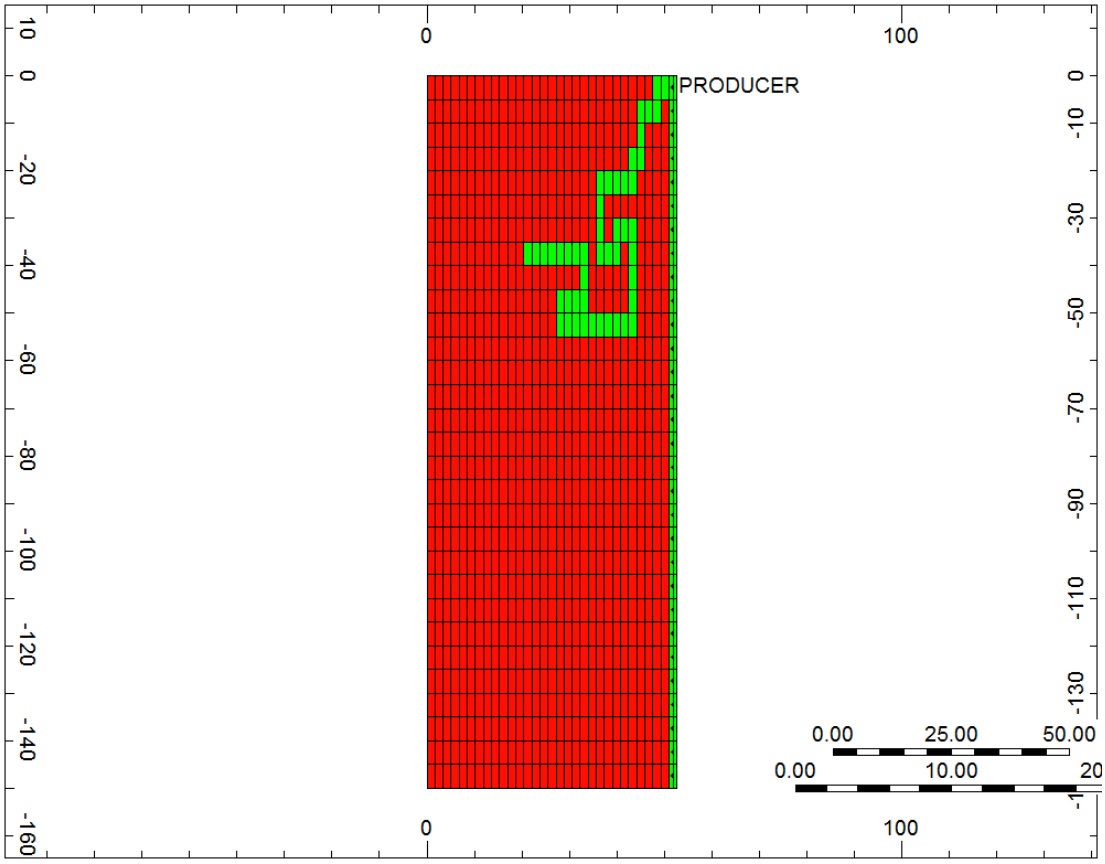


Figure 5.10 Plan View of Reservoir Model with 5% Connectivity

The simulation model is then run and production rate and cumulative production data are generated for the producing well as functions of time. The well producing from the reservoir model is given a constraint on its bottomhole pressure such that this value cannot fall below a minimum value of 1000 psi. The properties of the model are summarized in Table 5.1.

Table 5.1 Properties of the Simulation Model.

Original gas in Place (OGIP)	733098 SCF
Minimum Producer Bottom hole pressure	1000 psi
Total pore volume	2870.3 ft^3

Following this, duplicates of the reservoir are created for 1%, 8%, 10%, and 20% connectivity matrix reservoirs respectively. In each reservoir, a number of grid blocks corresponding to the respective connectivity of the reservoir, is chosen. Therefore, 9, 72, 90, and 180 grid blocks are chosen for the 1%, 8%, 10%, and 20% connectivity matrix reservoirs respectively. Plan views showing the models with the arbitrarily chosen high transmissibility-valued grid blocks are shown in Figures 5.12, 5.13, 5.14, 5.15, and 5.16.

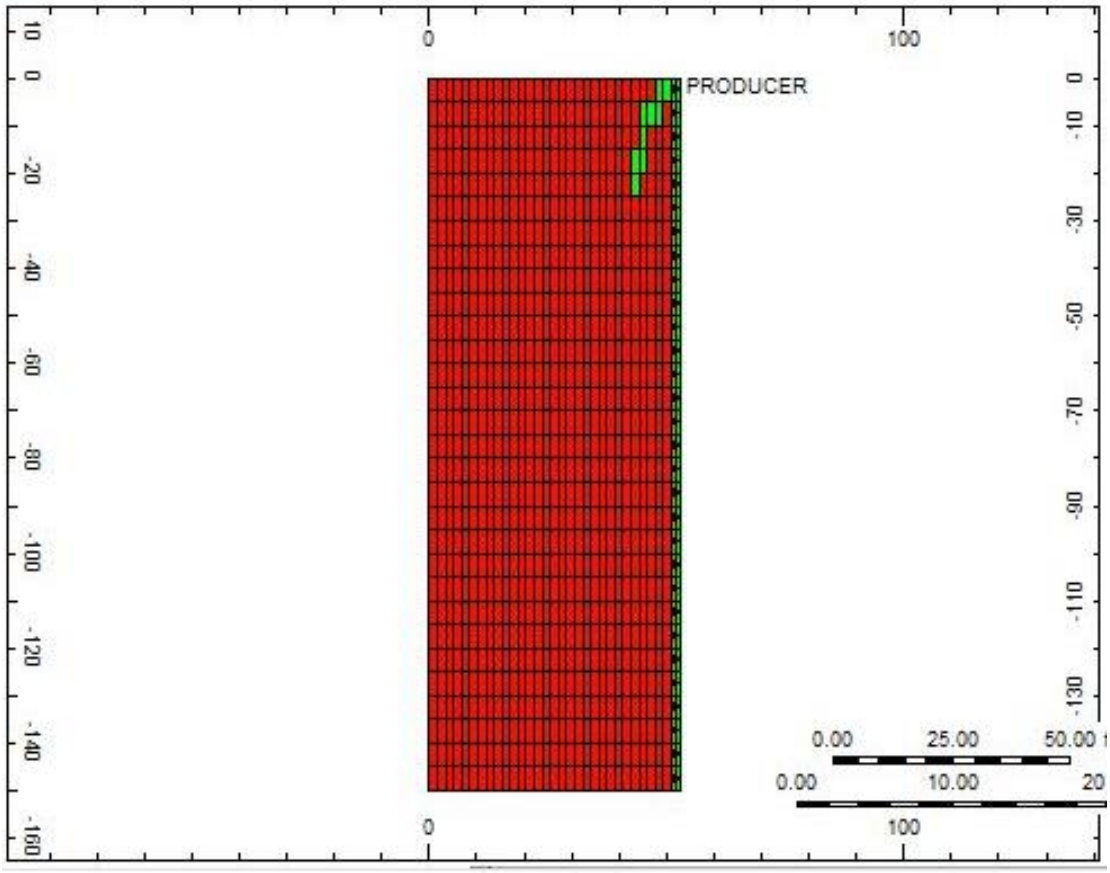


Figure 5.12 Plan View of Reservoir Model with 1% Connectivity.

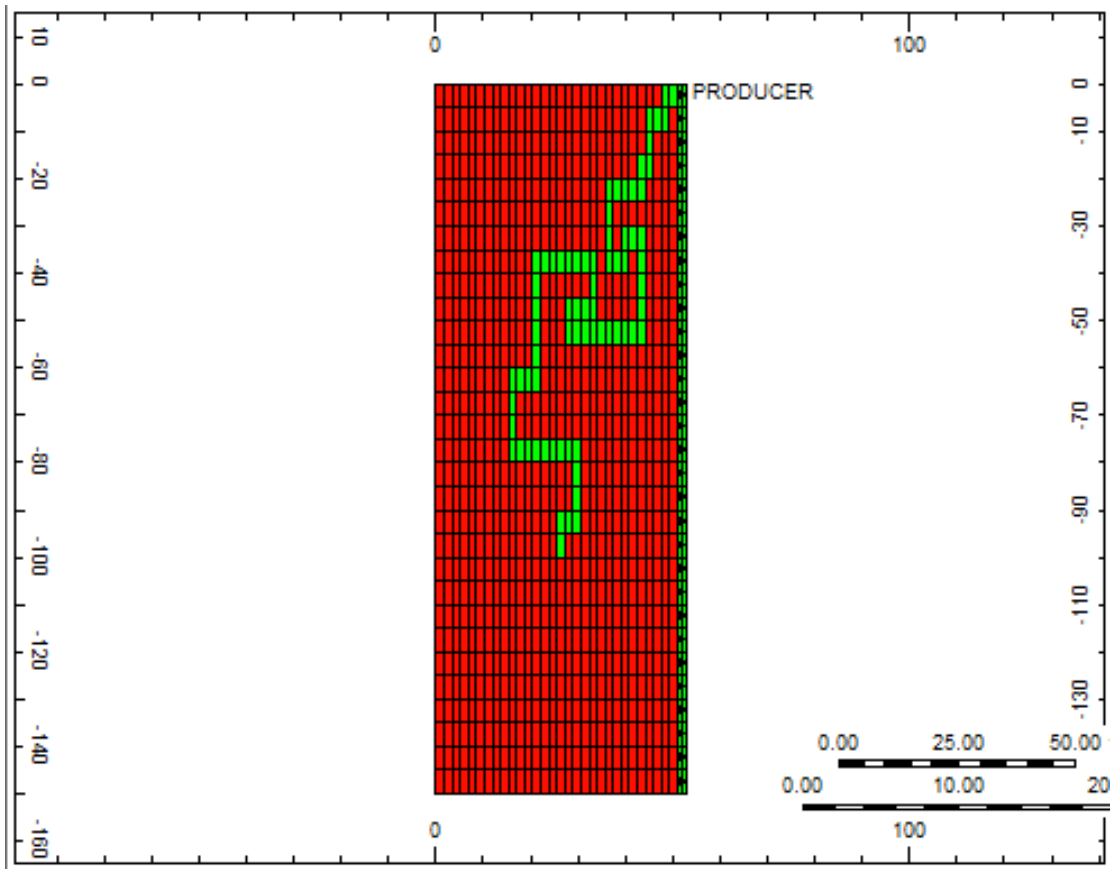


Figure 5.13 Plan View of Reservoir Model with 8% Connectivity.

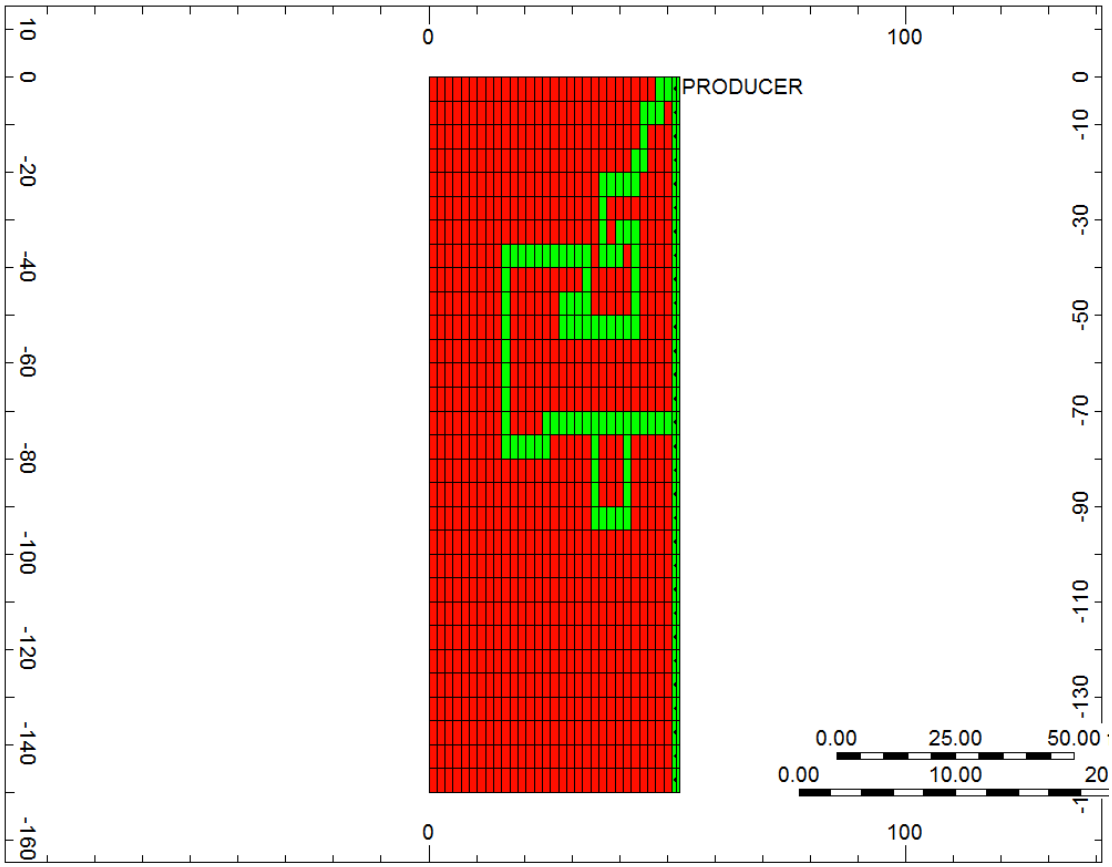


Figure 5.14 Plan View of Reservoir Model with 10% Connectivity.

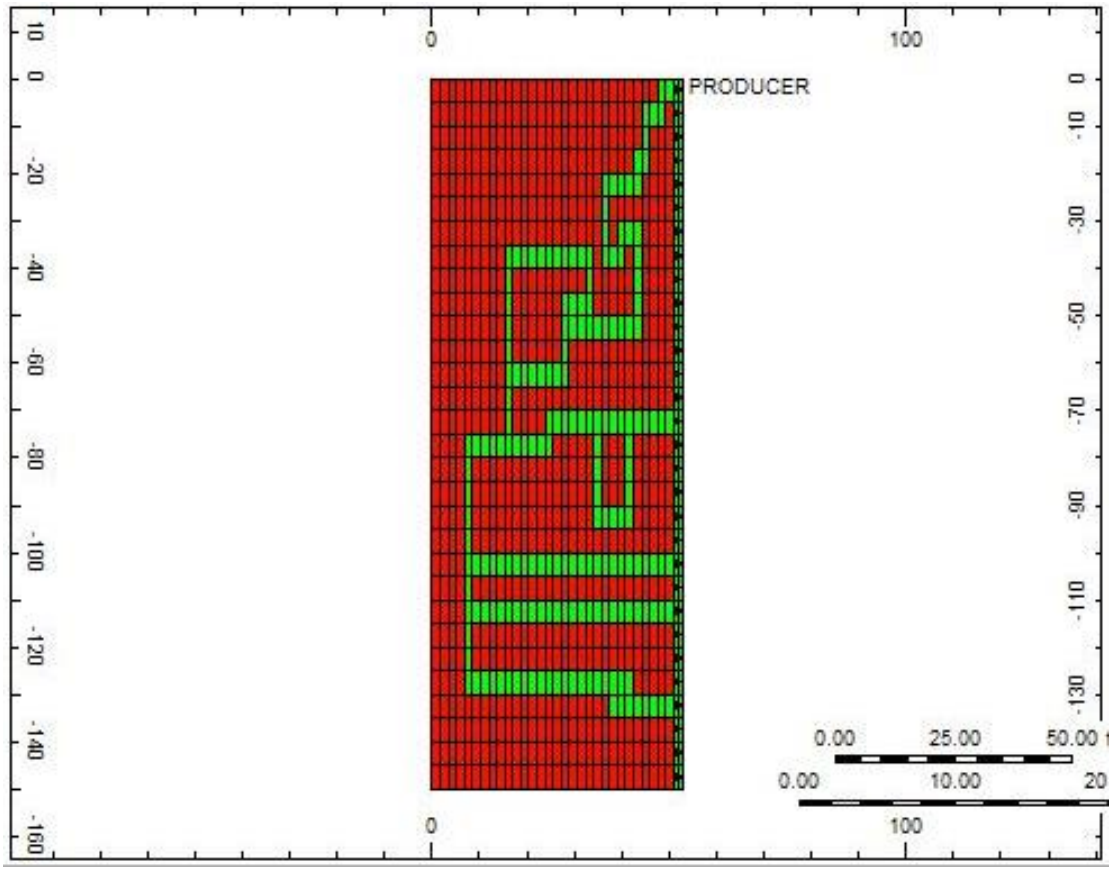


Figure 5.15 Plan View of Reservoir Model with 20% Connectivity.

Because the connected grid blocks have been arbitrarily chosen, there is a fair level uncertainty associated with the results generated from this model. In order to address this source of uncertainty, four additional copies of the reservoir model for each connectivity are created in which the configuration of chosen connected grid blocks is chosen differently. This is done with the aim of subsequently averaging all the data generated from these models, thereby reducing this uncertainty. Plan views showing the different configurations of chosen grid blocks of the additional reservoir models that were created corresponding to 5% connectivity are shown in Figures 5.16, 5.17,

5.18, and 5.19 (Configuration 1 of connected grid blocks corresponding to 5% connectivity was displayed in Figure 5.10).

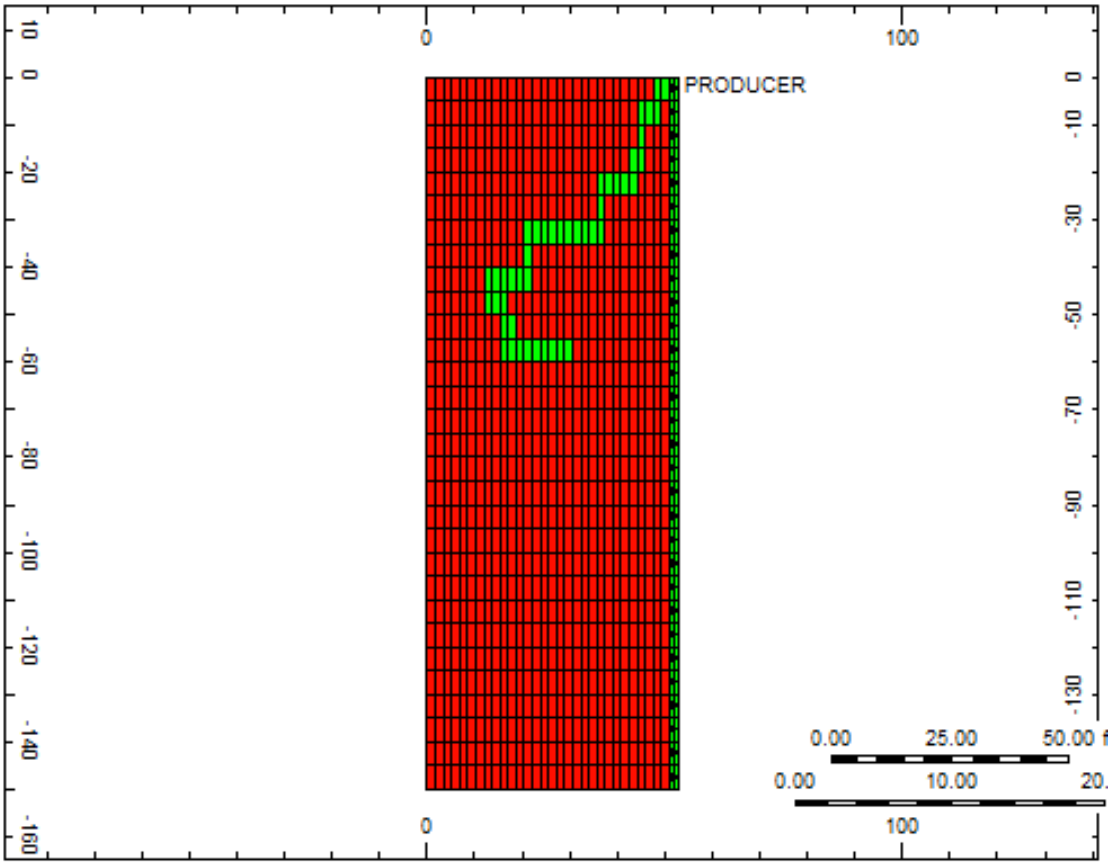


Figure 5.16 Plan View of Reservoir Model with Configuration 2 of connected Grid Blocks corresponding to 5% Connectivity.

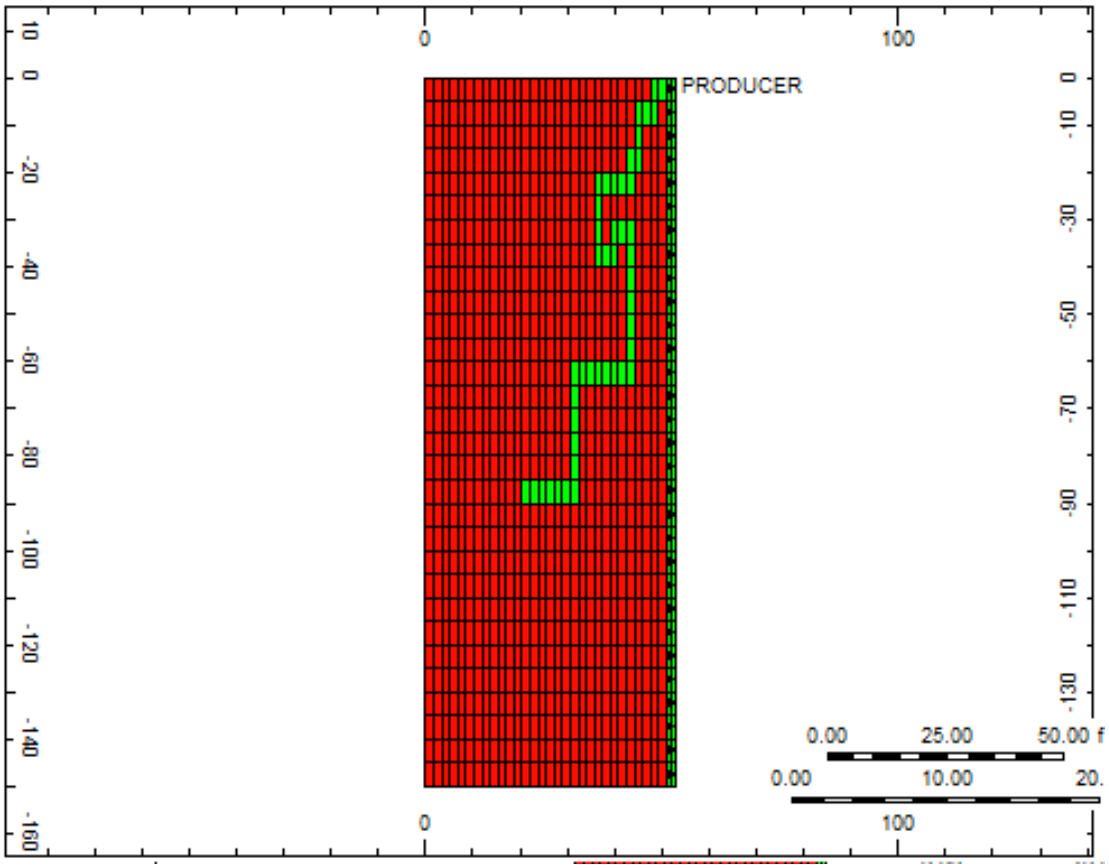


Figure 5.17 Plan View of Reservoir Model with Configuration 3 of connected Grid Blocks corresponding to 5% Connectivity.

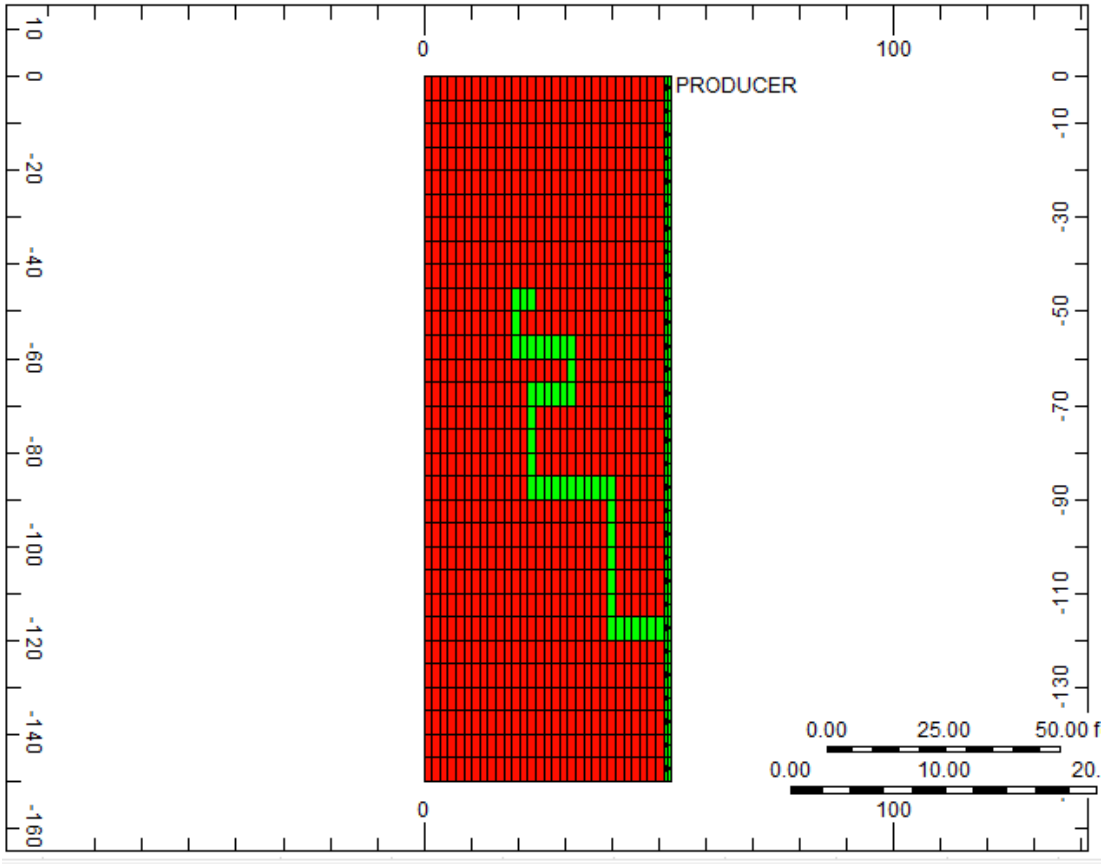


Figure 5.18 Plan View of Reservoir Model with Configuration 4 of connected Grid Blocks corresponding to 5% Connectivity.

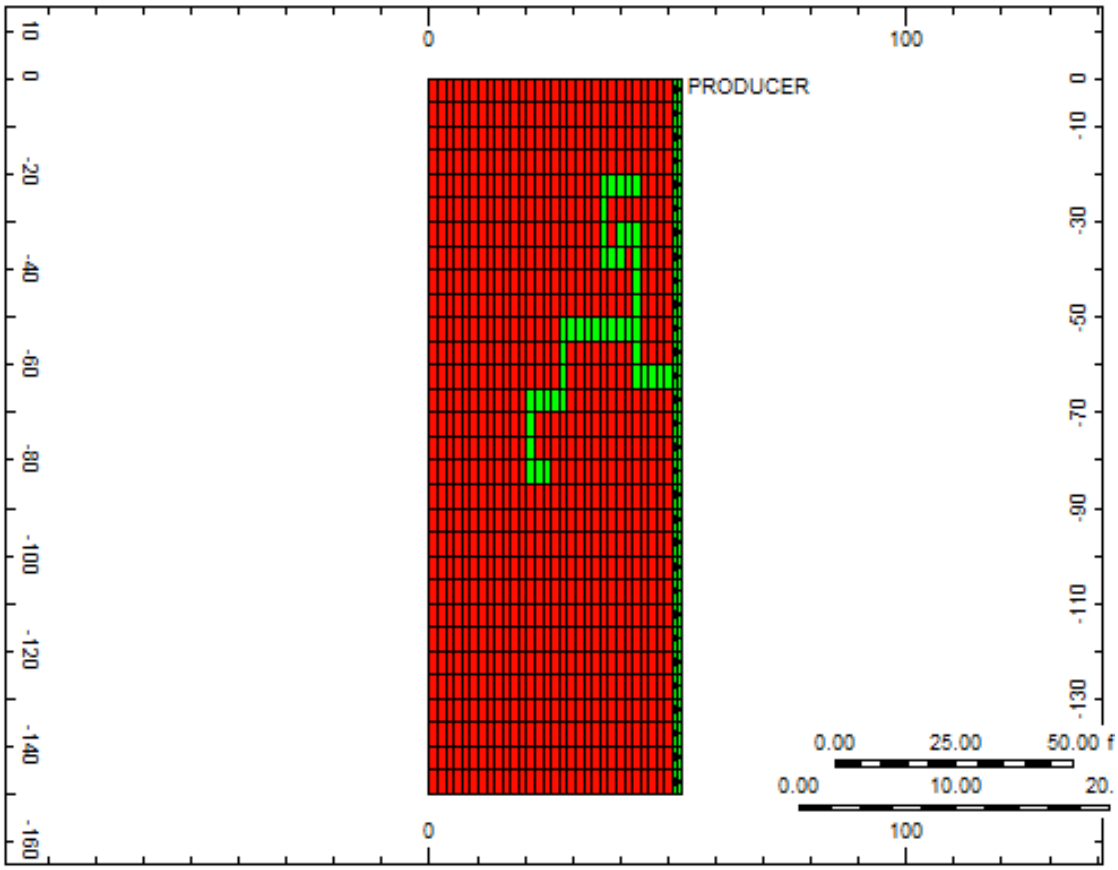


Figure 5.19 Plan View of Reservoir Model with Configuration 5 of connected Grid Blocks corresponding to 5% Connectivity.

Similar variations in chosen connected grid block configurations are made for the 1%, 8%, 10%, and 20% connectivity reservoir models. These additional variations are displayed in Figures 5.20, 5.21, 5.22, and 5.23.

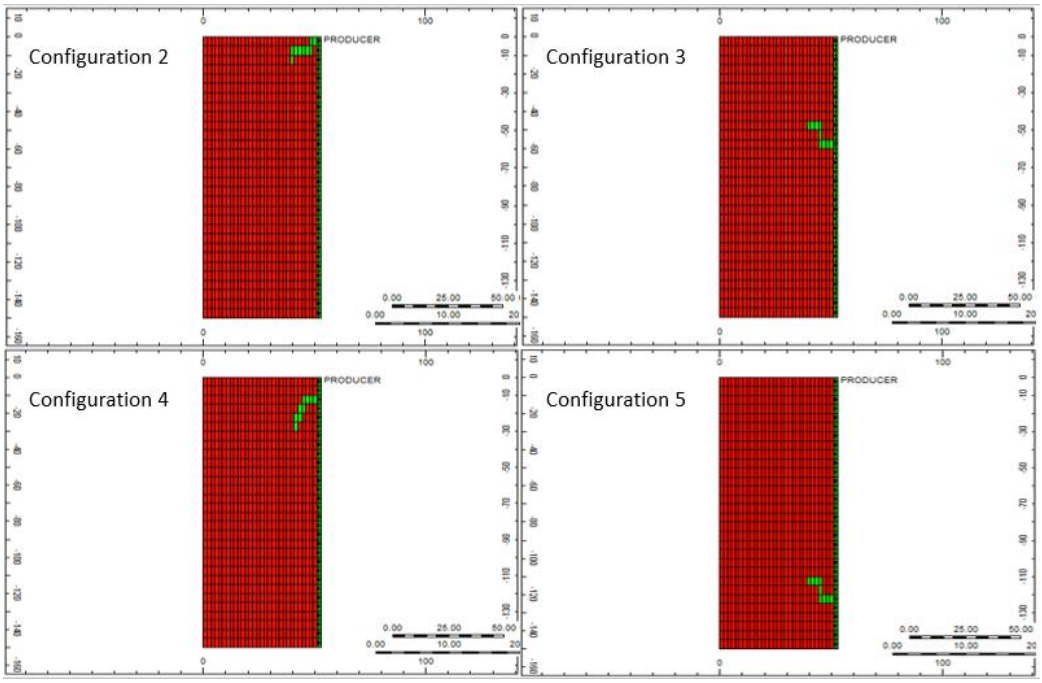


Figure 5.20 Plan Views of the different Reservoir Model Configurations of connected Grid Blocks corresponding to 1% Connectivity.

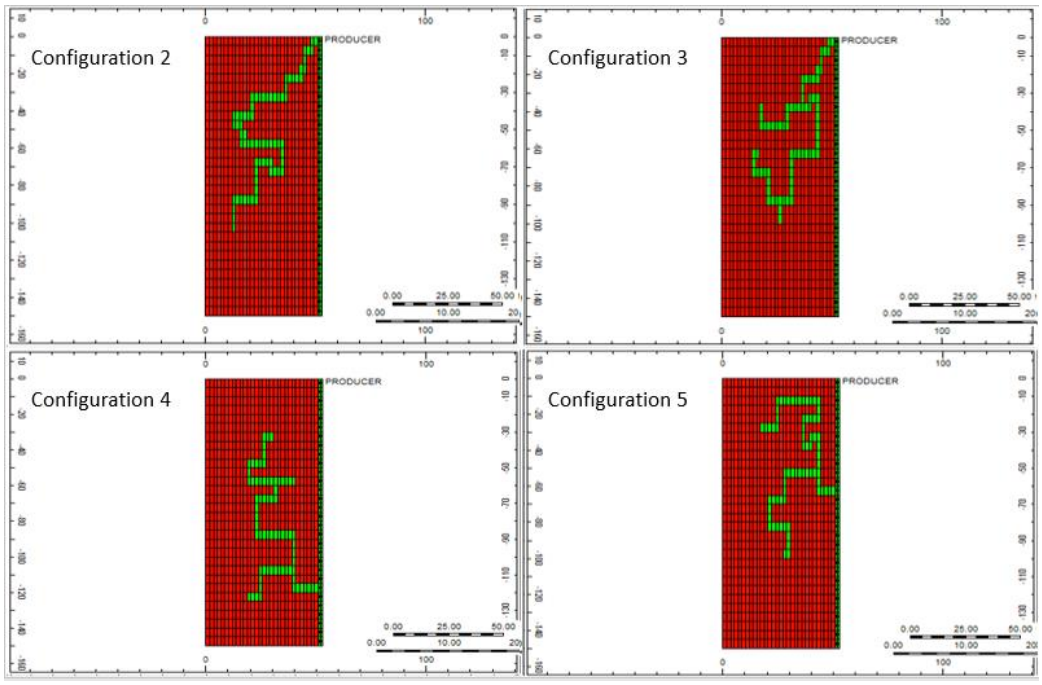


Figure 5.21 Plan Views of the different Reservoir Model Configurations of connected Grid Blocks corresponding to 8% Connectivity.

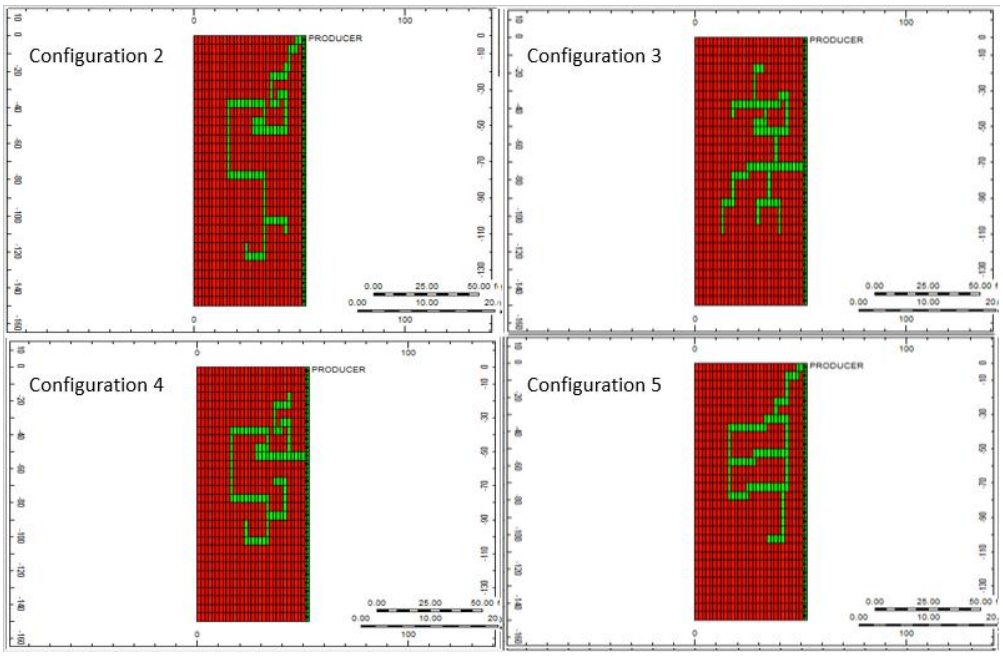


Figure 5.22 Plan Views of the different Reservoir Model Configurations of connected Grid Blocks corresponding to 10% Connectivity.

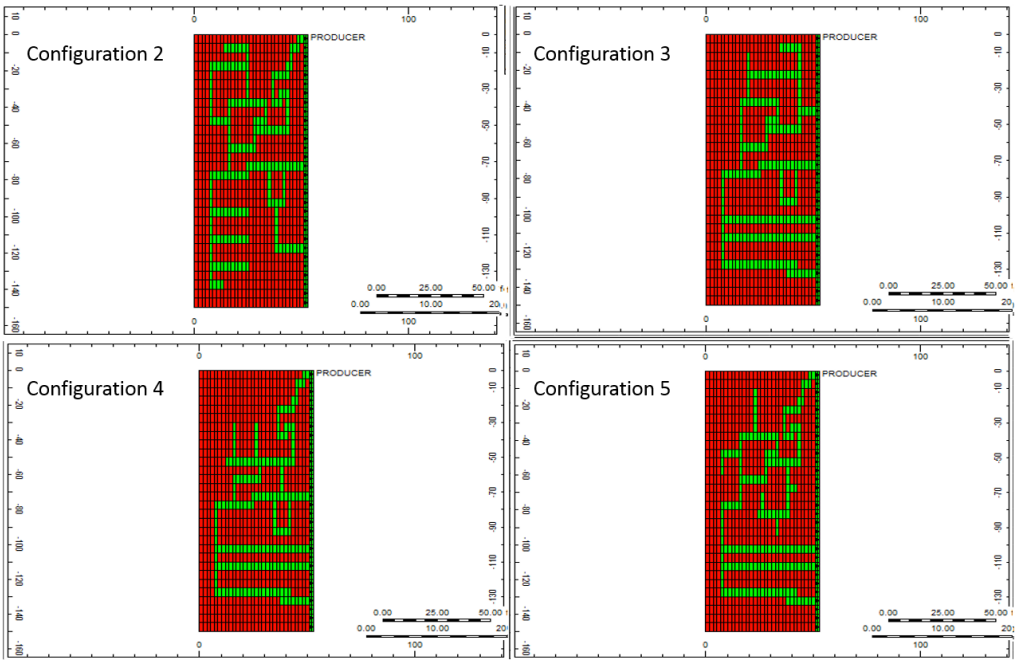


Figure 5.23 Plan Views of the different Reservoir Model Configurations of connected Grid Blocks corresponding to 20% Connectivity.

In each connectivity scenario, the manner in which the connected grid blocks are chosen is different. This is done in order to make this analysis using simulation models more robust.

5.2 Connectivity Evaluation

All twenty-five reservoir models (five models with differing connected grid block configurations for 1%, 5%, 8%, 10%, and 20%, connectivities) are run and production data is generated from them. More specifically plots of recovery versus normalized time are made. Recovery and normalized time referred to in this study are described by equation (5-2) and equation (5-3).

$$Recovery = \frac{Cumulative\ Gas\ Production}{Original\ Gas\ in\ Place\ (OGIP)} \quad \text{(5-2)}$$

$$Normalized\ Time = \frac{Time}{Total\ Production\ Time} \quad \text{(5-3)}$$

Figure 5.24 shows a plot of recovery vs normalized time in which data generated by all five of connected grid block configurations for a connectivity of 5% are plotted.

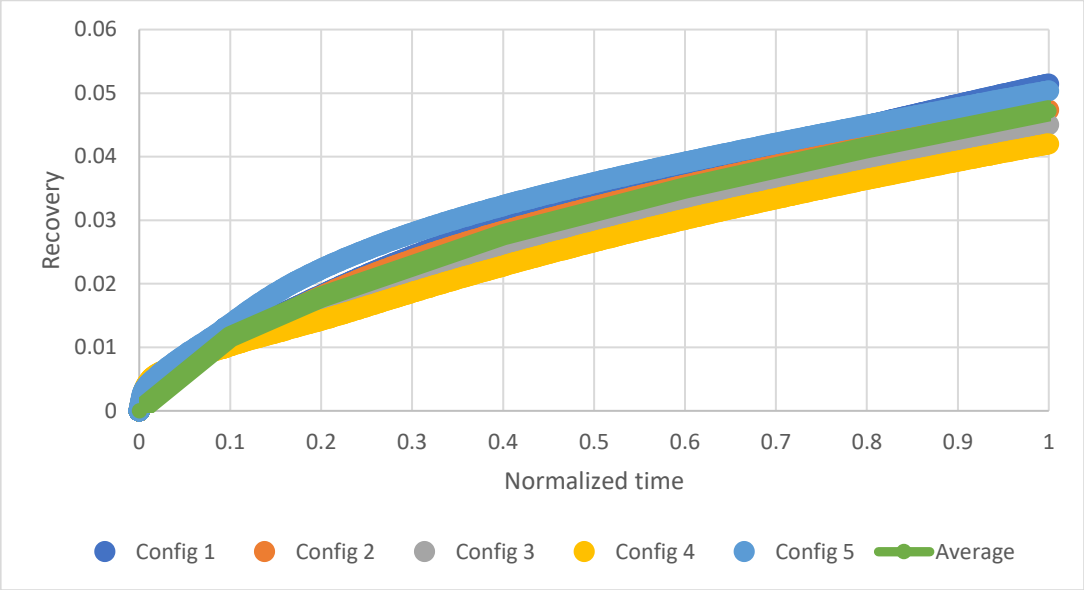


Figure 5.24 Plot showing generated production data for the different Reservoir Configuration Models Corresponding to 5% Connectivity.

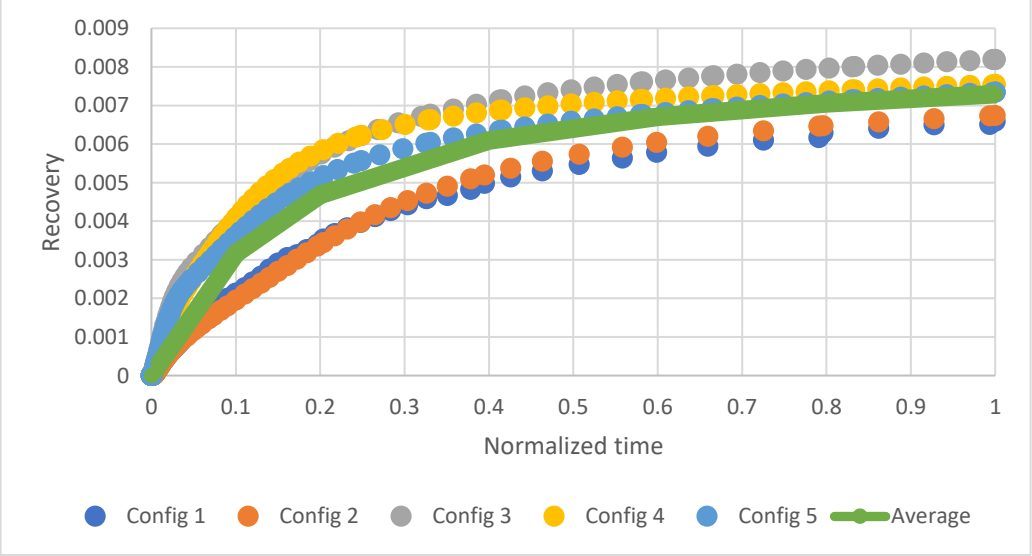


Figure 5.25 Plot showing generated production data for the different Reservoir Configuration Models Corresponding to 1% Connectivity.

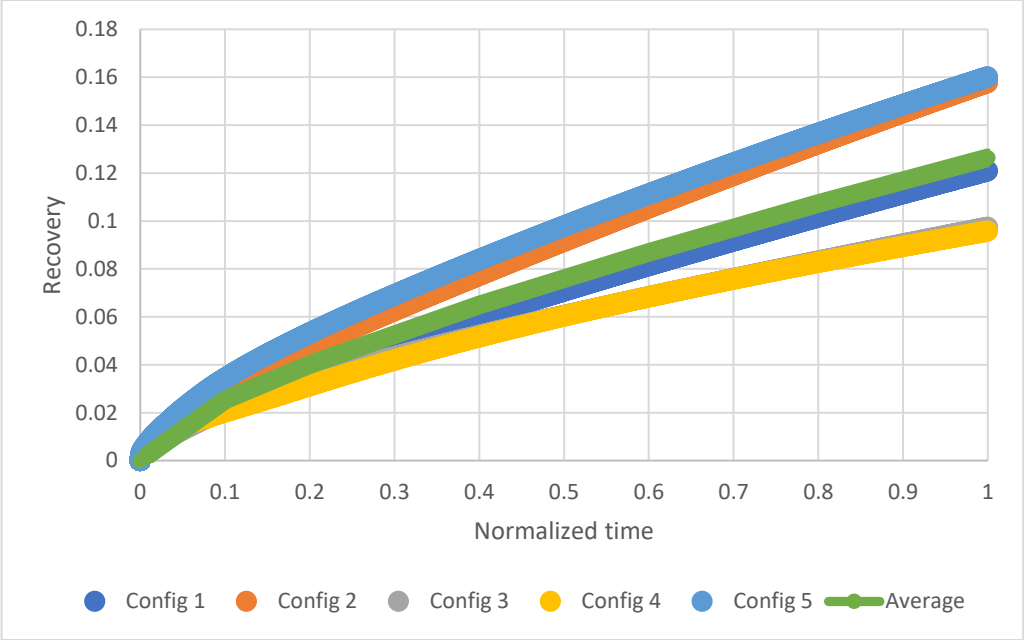


Figure 5.26 Plot showing generated production data for the different Reservoir Configuration Models Corresponding to 8% Connectivity.

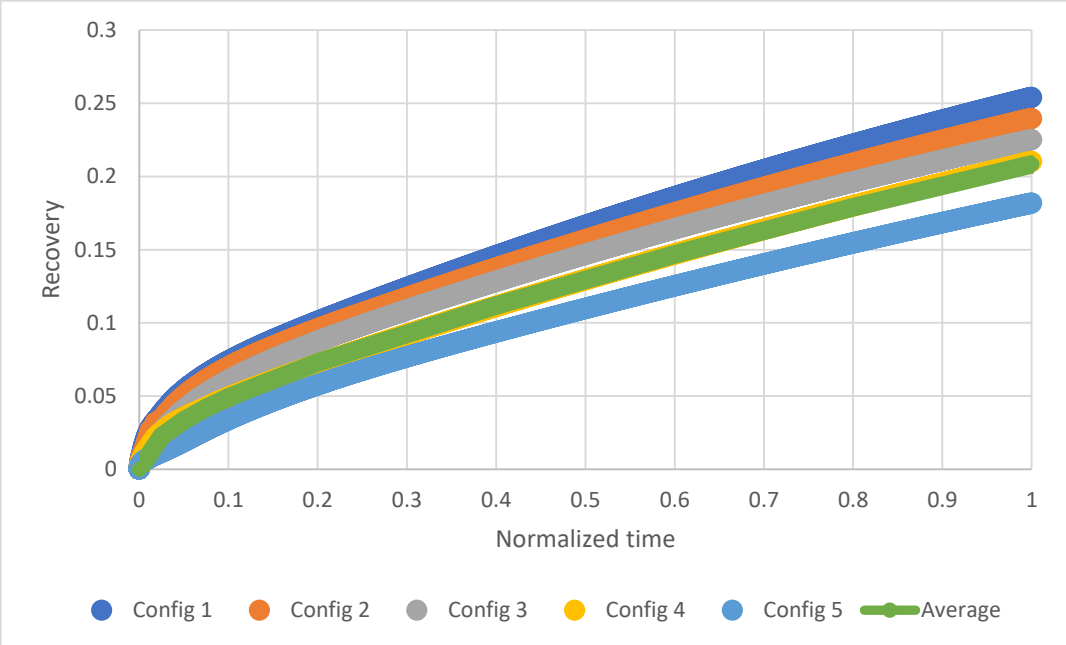


Figure 5.27 Plot showing generated production data for the different Reservoir Configuration Models Corresponding to 10% Connectivity.

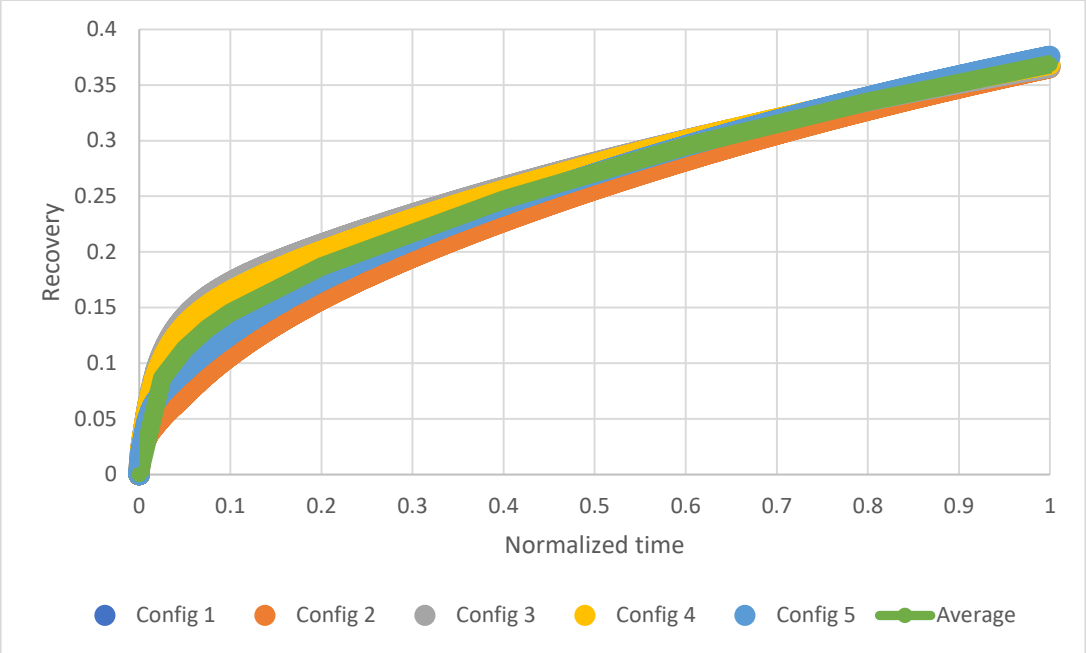


Figure 5.28 Plot showing generated production data for the different Reservoir Configuration Models Corresponding to 20% Connectivity.

The curves are all relatively close to each other. The production data from these different curves are averaged to form one general recovery versus normalized time curve representative of 5% connectivity. The same is done for the other connectivity models. The average recovery versus normalized time curves for each modeled connectivity value are shown in Figure 5.29.

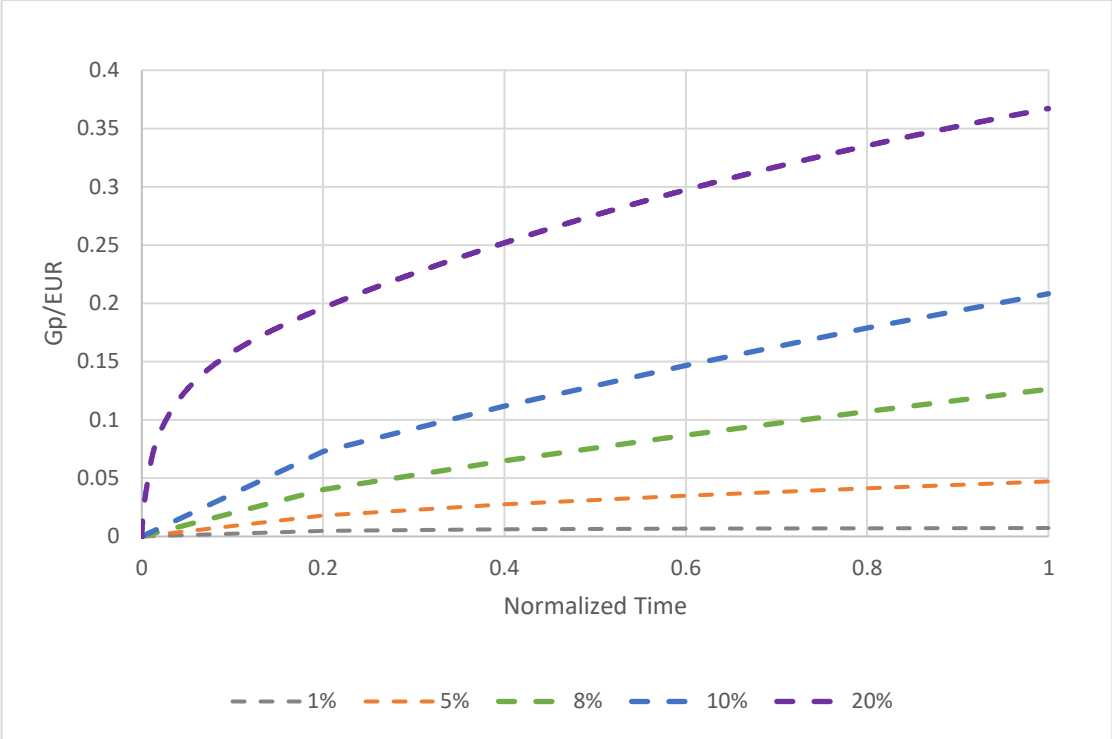


Figure 5.29 Average recovery versus normalized time curves for 1%, 5%, 8%, 10%, and 20% connectivity respectively.

These average curves serve as type curves in this study and are used to evaluate the reservoir-scale connectivity of reservoirs using their production data. Following the generation of these average curves, well production data is obtained for 53 Barnett wells, 51 Haynesville wells and 25 Marcellus wells. According to Al Khamees (2015), two distinct sections can be distinguished in the production data of a fractured well using a plot of reciprocal rate (1/q) versus cumulative production (G_p), namely the linear flow period and the boundary dominated flow period. This plot is shown in Figure 5.30 (Al Khamees 2015). The linear flow section is mainly dominated by the effect of fractures while the boundary dominated flow is the flow observed once the pressure transients reach the boundary of the reservoir.

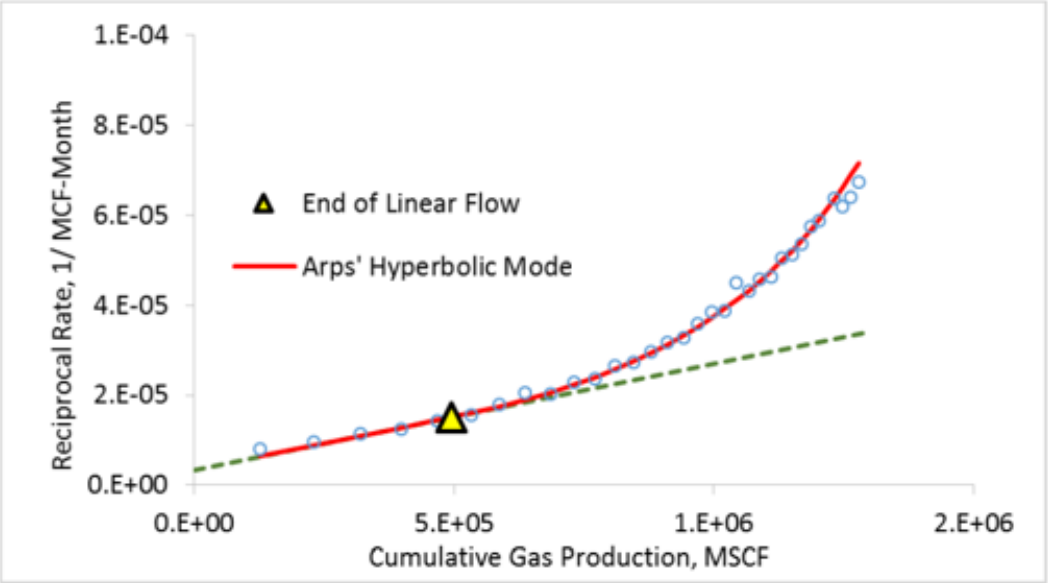


Figure 5.30 Plot for distinguishing between linear flow and boundary-dominated flow (Al Khamees 2015).

This plot is used to perform this separation on all the wells analyzed in this study and all their boundary dominated time period data is isolated from the infinite acting time period data. The motive for doing this is to make this analysis independent of fracturing, stimulation and early time data effects. The estimated ultimate recoveries (EURs) are calculated for each well using the Arps hyperbolic decline equation by using equation (5-4) and equation (5-5) below (Arps 1945).

$$q = \frac{q_i}{(1+bD_i t)^{\frac{1}{b}}} \quad \text{(5-4)}$$

$$EUR = Q_f + \frac{q_f}{(1-b)D_f}\left({q_i}^{1-b}\left(1 + bD_i t_f\right)^{1-\frac{1}{b}} - {q_{ab}}^{1-b}\right) \quad \text{(5-5)}$$

Where q_i is the initial rate, q_{ab} is the abandonment rate, q_f is the rate at the beginning of the forecast period, Q_f, the cumulative production at the beginning of the forecast

period, D_i is the initial decline rate, D_f is the decline rate at the beginning of the forecast period, and b is the decline exponent.

A curve following equation (5-4) is fitted onto the production data for each well. Based on the fitted curve, equation (5-5) is used to calculate the EUR for each well. The G_p from the boundary dominated section of each well is then divided by the respective EUR for each well. The resulting value is used to compare well data to the reservoir simulation-generated data. These values are plotted against normalized time and curves are generated for each well. The curves are then compared to the reservoir simulation-generated recovery factor versus normalized time data by being placed in the same plot as the simulation-generated data and the connectivity is estimated based on where the well data curves lie relative to the simulation-generated data curves. Figure 5.30 displays an example for three Barnett wells whose data is used alongside the simulation data to determine their connectivity values.

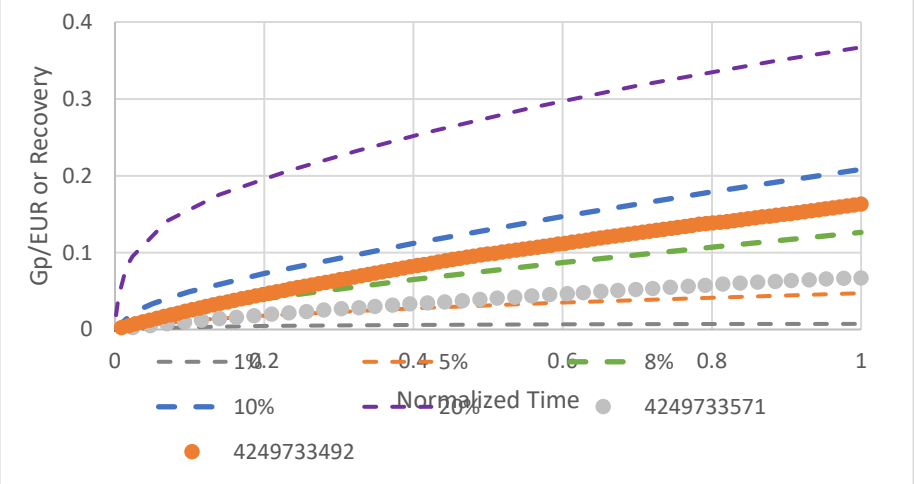


Figure 5.31 Use of average simulation recovery versus normalized time curves estimate the connectivity of three Barnett shale wells.

Well 4249733492 is observed to have a connectivity of 9% while well 4249733571 is observed to have one of 6%. The entire set of reservoir models used to go about this connectivity evaluation are made separately for each reservoir, each time using properties corresponding to the specific reservoir they are modelling (such as porosity and permeability). Table 5.2 shows the different porosity and permeability used for each reservoir.

Table 5.2 Reservoir-Specific Properties of the Reservoir Model.

Reservoir	Porosity	Matrix Permeability
Barnett	5% (Hu et al., 2015)	2.3 nanodarcy (Polito et al., 2014)
Haynesville	8% (Gilbert 2009)	5.6 nanodarcy (Parker et al., 2009)
Marcellus	3.7% (Verba et al., 2016)	3.5 nanodarcy (Heller et al., 2014)

Through this means, connectivity is estimated for all the wells from the three shale reservoirs using their production data.

5.2 Sustainability Evaluation

The same production data obtained for the 53 Barnett, 51 Haynesville, and 25 Marcellus shales, is used to evaluate the sustainability in these reservoirs. Plots of $\frac{q}{qmax}$

versus $\frac{G_p}{EUR}$ are created in order to evaluate this. The slopes of these $\frac{q}{qmax}$ versus $\frac{G_p}{EUR}$ curves are calculated using the forward finite difference equation and distributions of the slope values are generated.

Chapter 6: Results and Analysis

After the procedures described in Chapter 5 were implemented, certain results were obtained. They involve some fairly significant trends as well as some rather more subtle observations. These results are described and analyzed in this Chapter.

6.1 Sustainability Analysis

The plots of $\frac{q}{qmax}$ versus $\frac{G_p}{EUR}$ created from the well data are displayed in the next three figures. Figure 6.1 displays the $\frac{q}{qmax}$ versus $\frac{G_p}{EUR}$ plot created using all the well data from the Barnett shale. Figure 6.2 displays the $\frac{q}{qmax}$ versus $\frac{G_p}{EUR}$ plot created using all the well data from the Haynesville shale. Figure 6.3 displays the $\frac{q}{qmax}$ versus $\frac{G_p}{EUR}$ plot created using all the well data from the Marcellus shale.

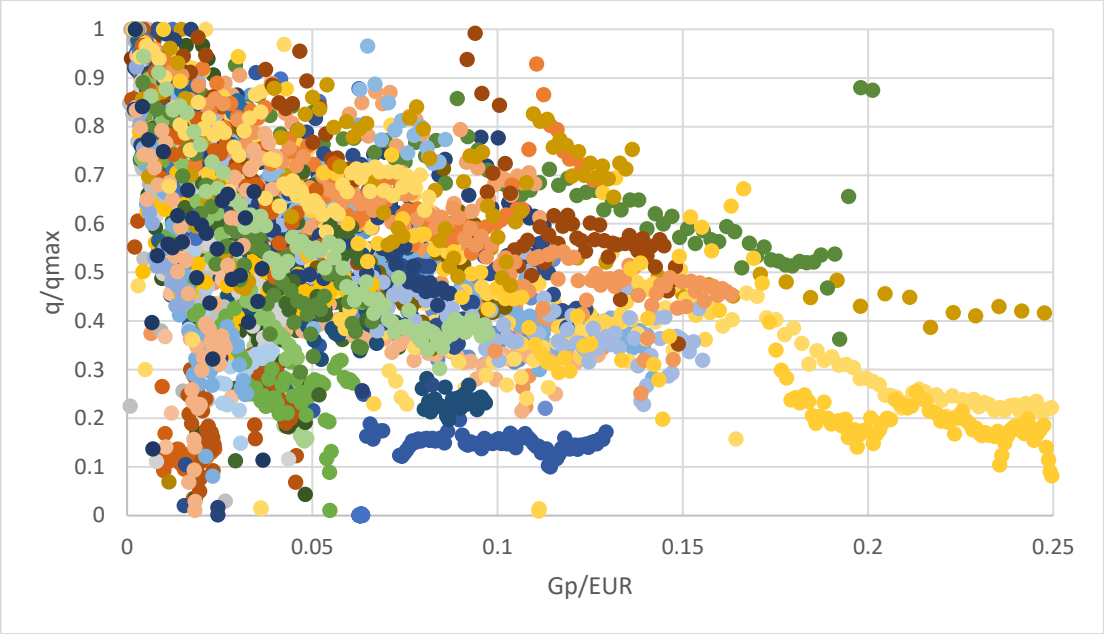


Figure 6.1 Plot of $\frac{q}{qmax}$ versus $\frac{G_p}{EUR}$ for Barnett shale wells.

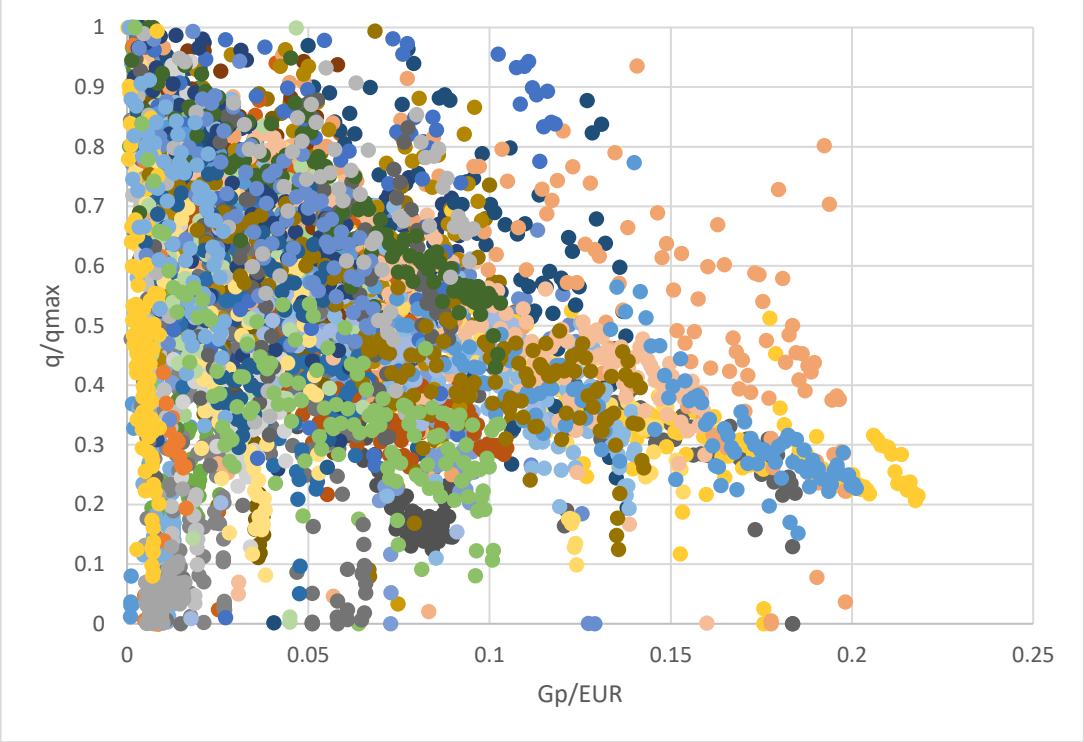


Figure 6.2 Plot of $\frac{q}{qmax}$ versus $\frac{G_p}{EUR}$ for Haynesville shale wells.

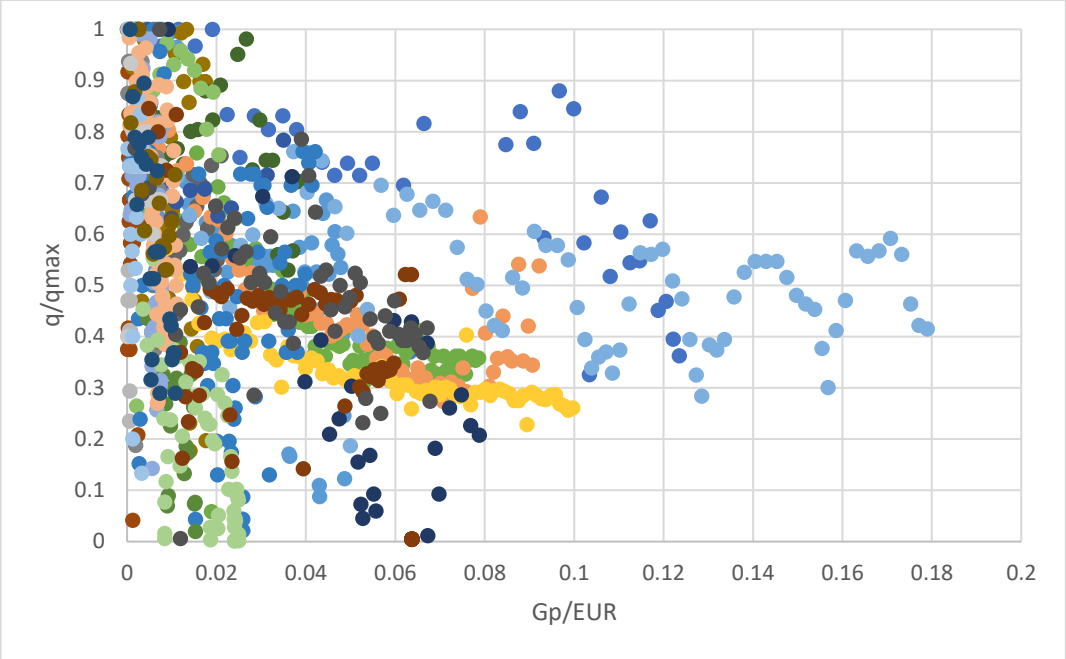


Figure 6.3 Plot of $\frac{q}{qmax}$ versus $\frac{G_p}{EUR}$ for Marcellus shale wells.

These plots all generally display data that is sporadic. They do not convey significant information regarding the sustainability of these reservoirs. From these plots, the slopes do appear to gradually become less steep over long periods of time. However, they appear to be relatively constant for a short period of time. In all three reservoirs, all the data curves are significantly lower than the line of -1 slope shown in the schematic in Figure 4.2, meaning that they generally have poor sustainabilities. This is expected as all three reservoirs are shales. It is notable that the Marcellus may have a significantly lower sustainability compared to the other two reservoirs as the range of its $\frac{G_p}{EUR}$ data does not reach as far as that of the Barnett and Haynesville data, yet its $\frac{q}{qmax}$ data declines to similar extents as the data from the other two reservoirs. To

better compare their sustainability, all the data from these three reservoirs are placed in the same plot. This plot is displayed in Figure 6.4.

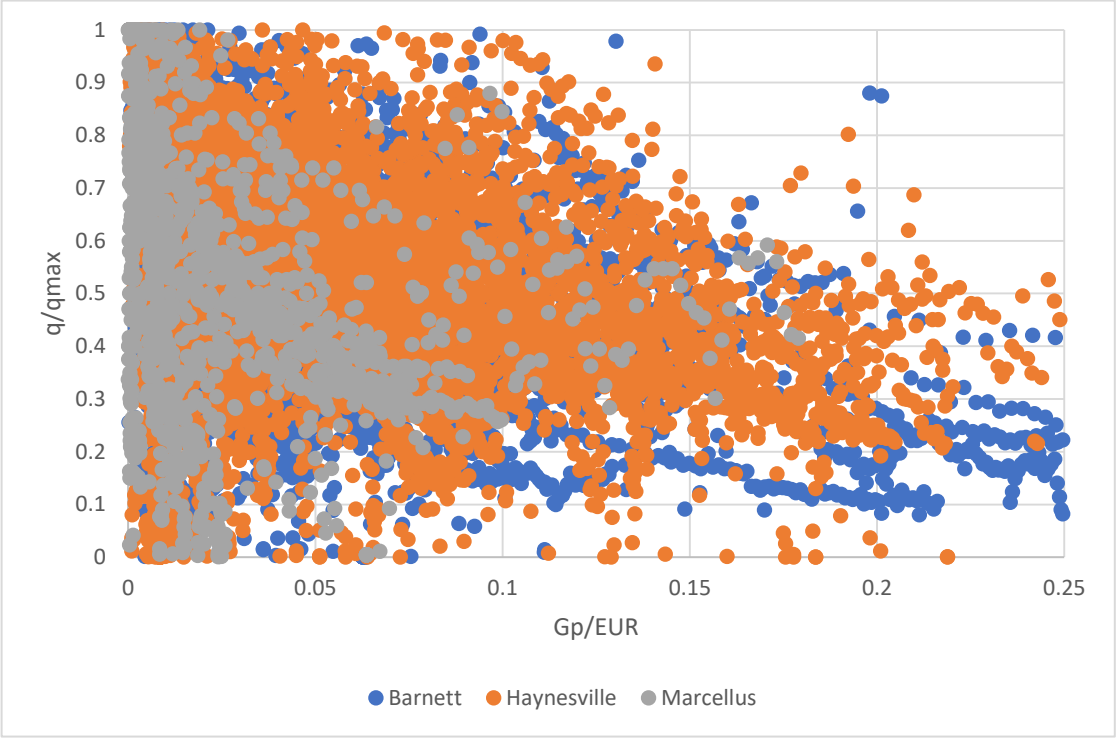


Figure 6.4 All $\frac{q}{qmax}$ versus $\frac{G_p}{EUR}$ data for all three shale reservoirs in the same plot

Again, the data is observed to be fairly noisy and sporadic. However, the observation that the Marcellus shale well data has a lower sustainability than the Barnett and Haynesville becomes more pronounced in Figure 6.4. It is evident that the Marcellus shale wells in this study have higher declines in their production rates than those of the Barnett and Haynesville shales. As a result of these plots, it is concluded that the Marcellus appears to have a lower sustainability than the Barnett and Haynesville. With regard to the Barnett and Haynesville shales, Figure 6.4 is not very informative. It does not give any significant insight as to which of these reservoirs has a higher

sustainability. As a result of this, the plot is segmented into different regions as shown in Figure 6.5. This is done in order to refine the analysis.

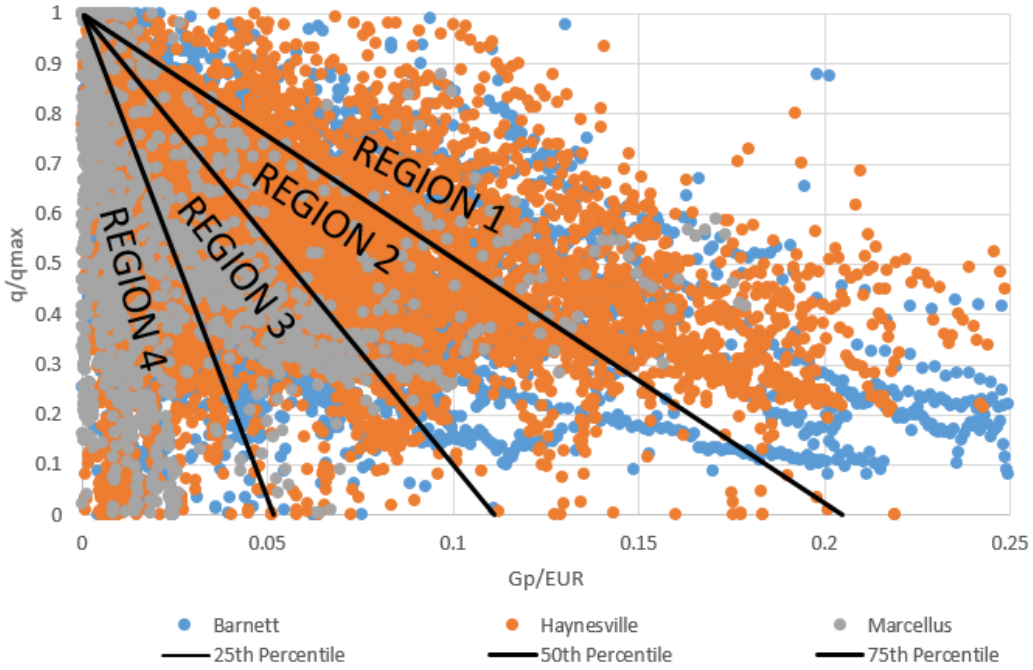


Figure 6.5 Divided plot of all $\frac{q}{qmax}$ versus $\frac{G_p}{EUR}$ data for all three shale reservoirs.

The lines dividing up the plot area correspond to the 25th, 50th, and 75th percentiles. In other words, they represent lines which perfectly divide all the data points into the ratios 1:3, 1:1, and 3:1 respectively. These lines separate the plot area into four sections, namely Region 1, Region 2, Region 3, and Region 4. These regions are named in decreasing levels of sustainability. This means the data in Region 1 has the highest level of sustainability while the data in Region 4 has the lowest level of sustainability. The distributions of the well data in the different regions are analyzed. Figure 6.6 shows the proportion of well data that fell in each region. For example, 25% of the

Barnett well data fell in Region 1. This distribution plot shows that majority of the Marcellus data fell within Region 4, cementing the conclusion that the Marcellus has the lowest sustainability of the three reservoirs.

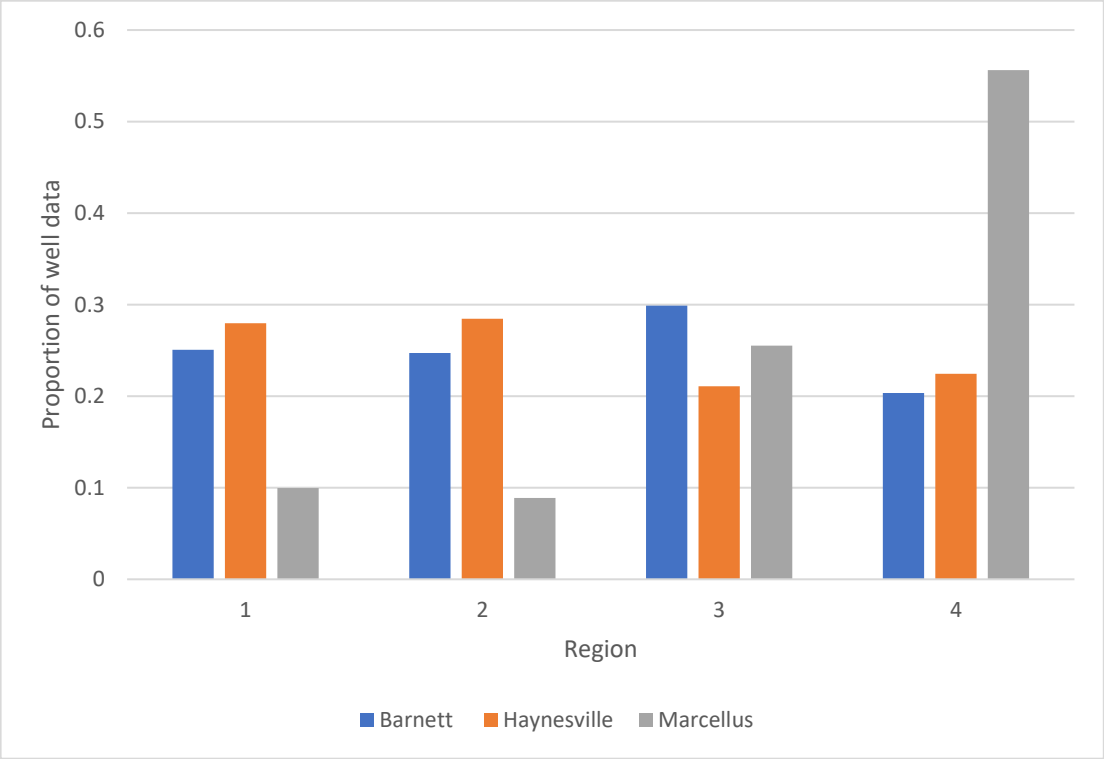


Figure 6.6 Well Distribution showing the proportion of wells from each reservoir in each region

The Barnett and Haynesville shales had more relatively uniform distributions. The Barnett had majority of its data lying in Region 3, however considerable amounts of its data was in Regions 1 and 2. Haynesville, on the other hand, had most of its data split equally between Regions 1 and 2. The distributions suggest that Barnett and Haynesville had significant amounts of their data in all the regions. These distributions were too uniform to obtain a significant insight as to which reservoir may have the

higher sustainability. Following this, the slopes of the $\frac{q}{qmax}$ versus $\frac{Gp}{EUR}$ curves were calculated for each reservoir using the forward finite difference were used to create distributions. The distributions of these slope values for each reservoir were analyzed. This is done with the aim of using the apparent averages of the slopes obtained from the distributions to determine the sustainability variations between the reservoirs. These distributions are shown in Figures 6.7, 6.8, and 6.9.

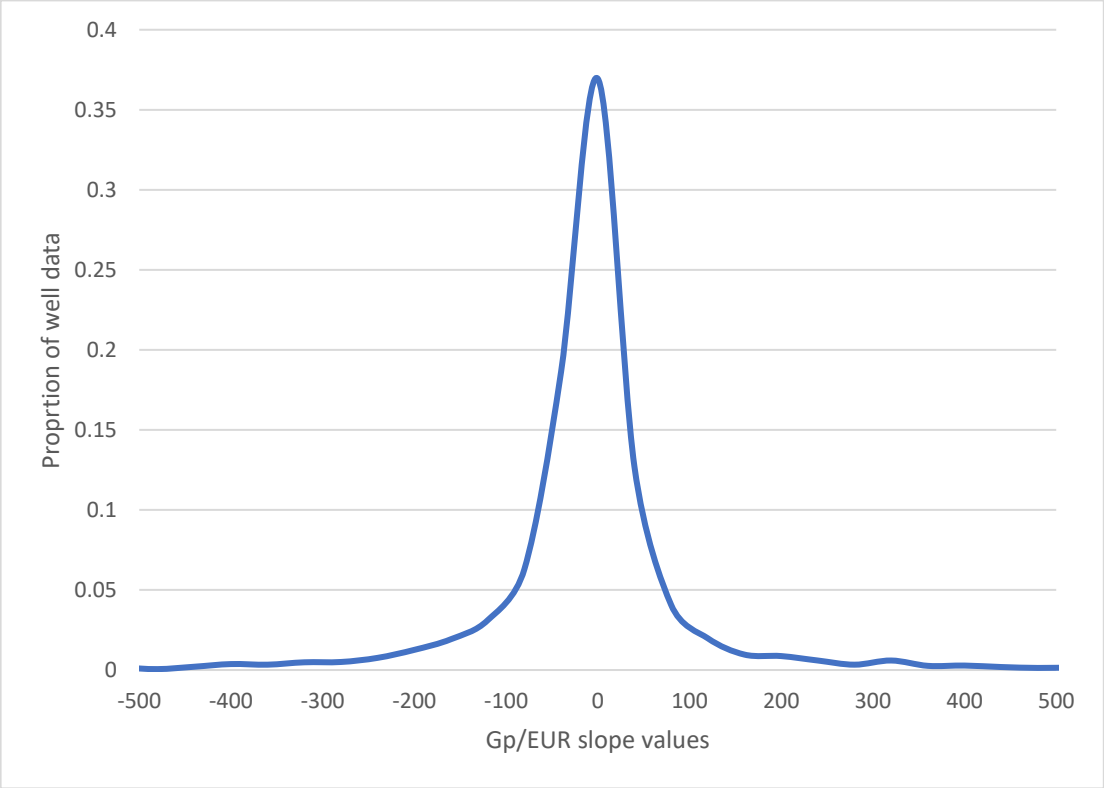


Figure 6.7 $\frac{q}{qmax}$ versus $\frac{Gp}{EUR}$ slope distribution for Barnett shale.

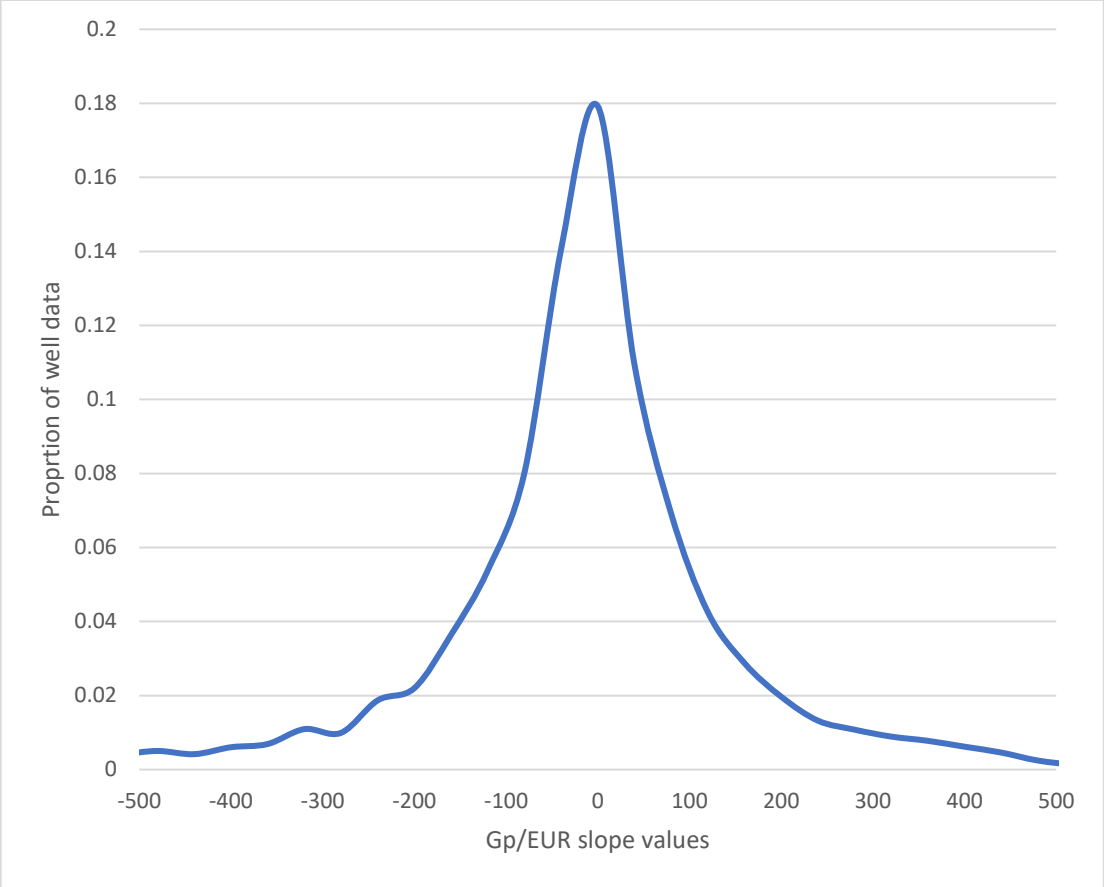


Figure 6.8 $\frac{q}{qmax}$ versus $\frac{Gp}{EUR}$ slope distribution for Haynesville shale.

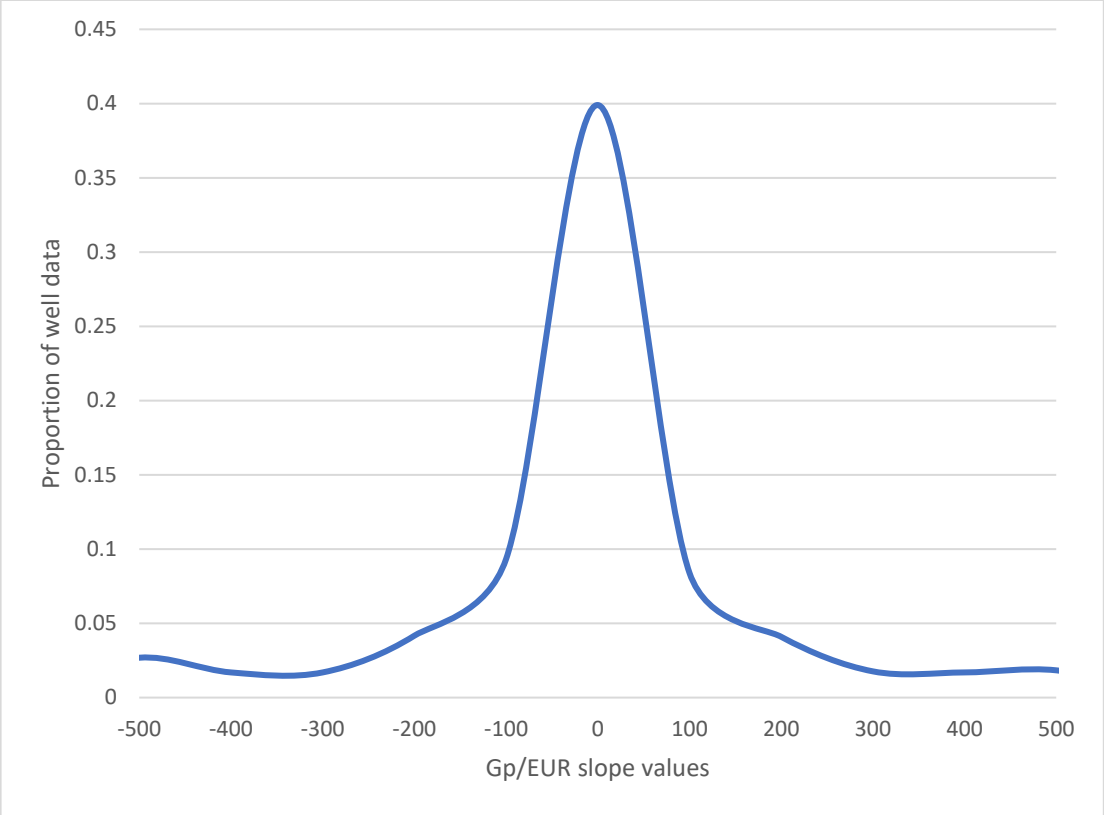


Figure 6.9 $\frac{q}{qmax}$ versus $\frac{Gp}{EUR}$ slope distribution for Marcellus shale.

As the slope values essentially quantify the levels of sustainability in each reservoir, they form an effective means of evaluating sustainability. The slope values are generally supposed to be negative due to the declines in the flow rates. However, in all the distributions, the range of values extends well past the value of 0 and involves a significant amount of positive values. These positive-valued slopes represent fluctuations in production rate from these reservoirs. The distributions for the three reservoirs look very similar. They all appear to have normal distributions with peaks close to 0. However, the proportions of well data at their peaks are slightly different with this value being equal to 0.37 for Barnett, 0.18 for Haynesville, and 0.4 for

Marcellus. Their peaks all fall to the negative side of the 0 (the left side), with Barnett having an average slope value of -11.11, Haynesville having an average slope of -13.35, and the Marcellus having an average slope value of -19.69. These average slope values again confirm Marcellus having the lowest sustainability. However they also succeed where the previous sustainability analysis steps failed, they distinguish the sustainability of Barnett and that of Haynesville. Based on the determined average slope values, the Barnett appears to have a higher sustainability than the Haynesville shale.

6.2 Connectivity Distributions

Using the simulation data generated from the constructed reservoir simulation models, the connectivity for all the wells were estimated. The connectivity distributions of the well data for each shale reservoir are created. These are shown in Figures 6.10, 6.11, and 6.12.

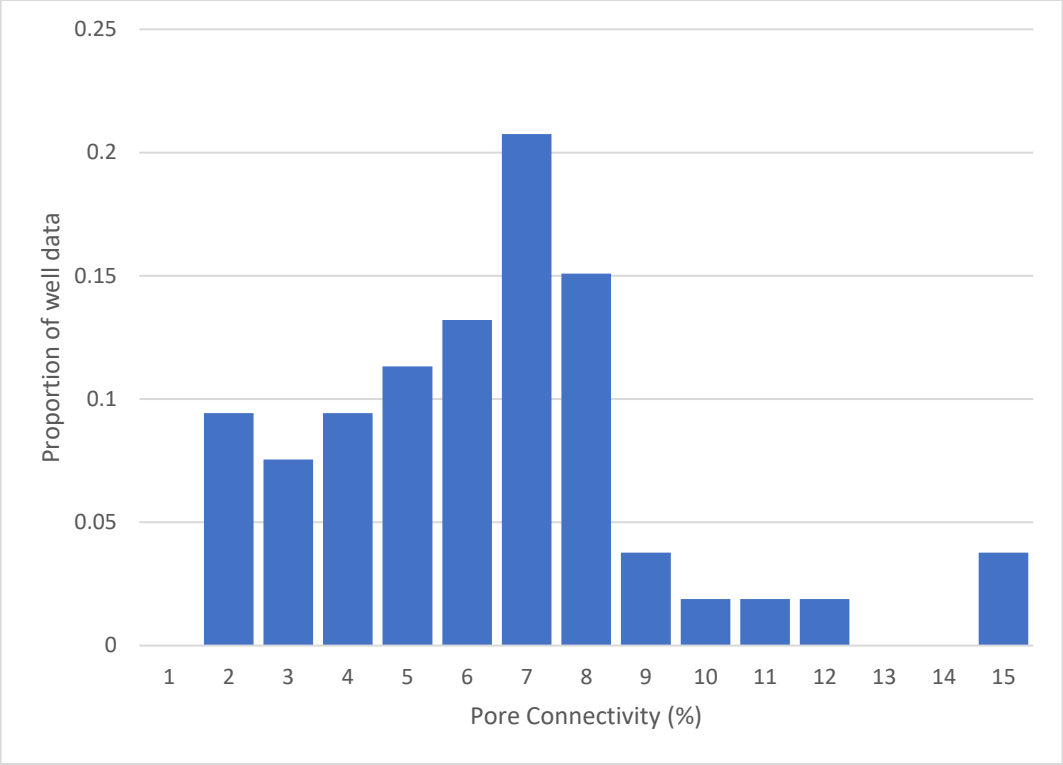


Figure 6.10 Connectivity Distribution in the Barnett Shale Well Data

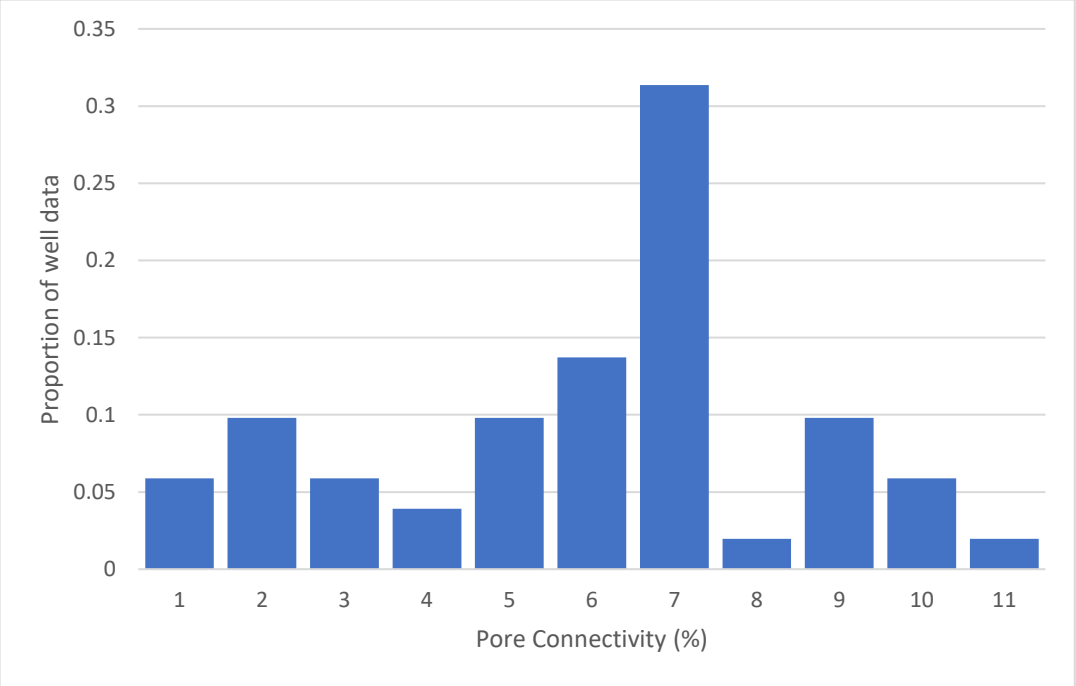


Figure 6.11 Connectivity Distribution in the Haynesville Shale Well Data

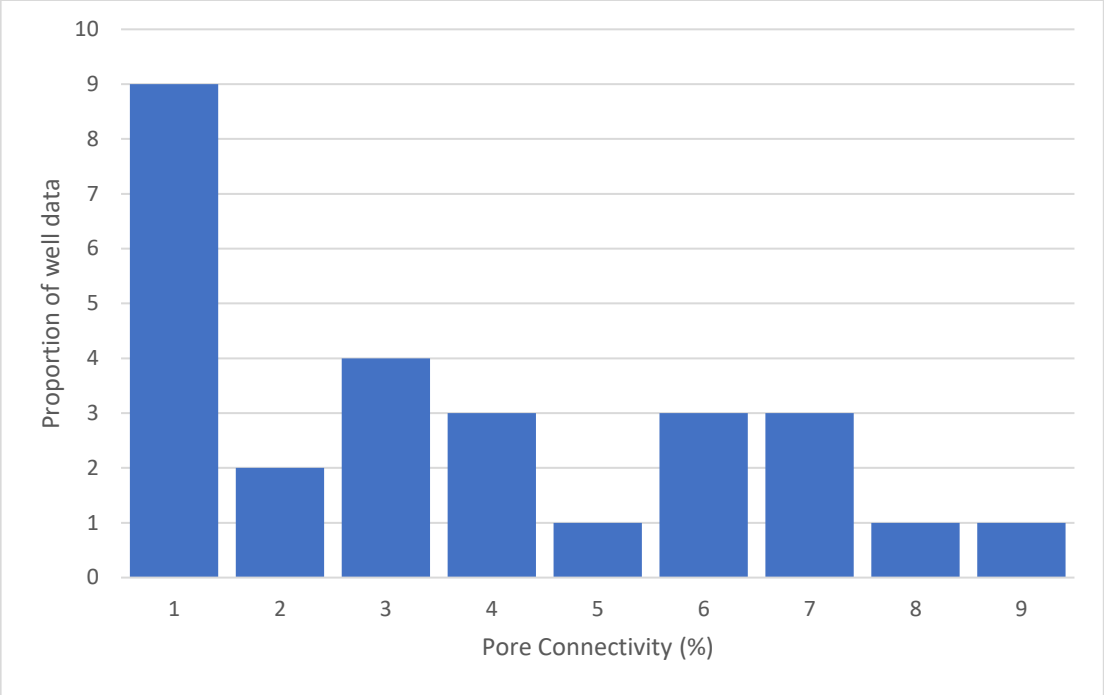


Figure 6.12 Connectivity Distribution in Marcellus Shale Well Data

The Barnett, Haynesville, and Marcellus shale data had average connectivities of 6.2%, 5.8%, and 3.5% respectively. Following this, connectivity distributions for the well data in each sustainability region are created. These are shown in Figures 6.13, 6.14, 6.15, and 6.16.

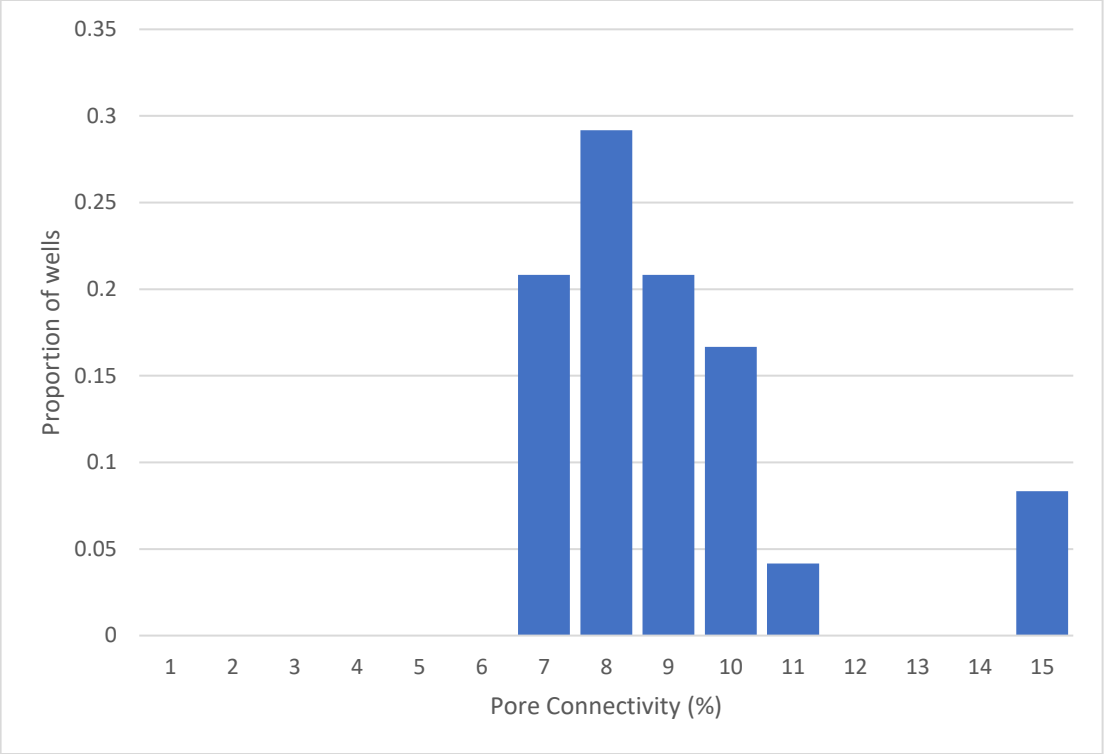


Figure 6.13 Connectivity Distribution in Region 1.

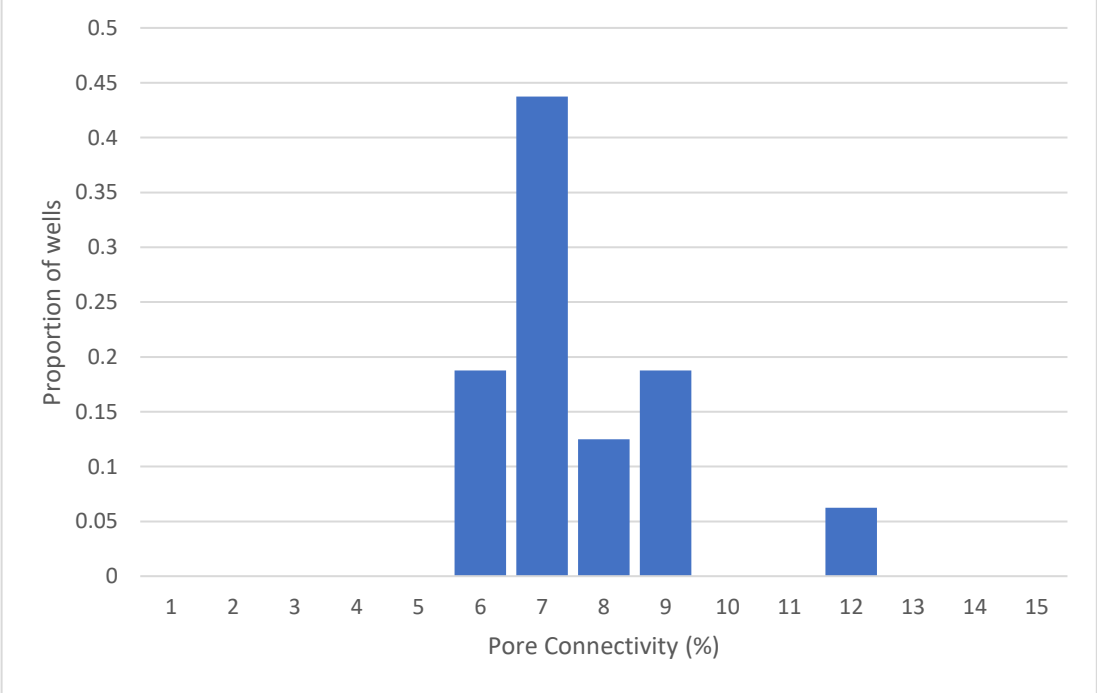


Figure 6.14 Connectivity Distribution in Region 2.

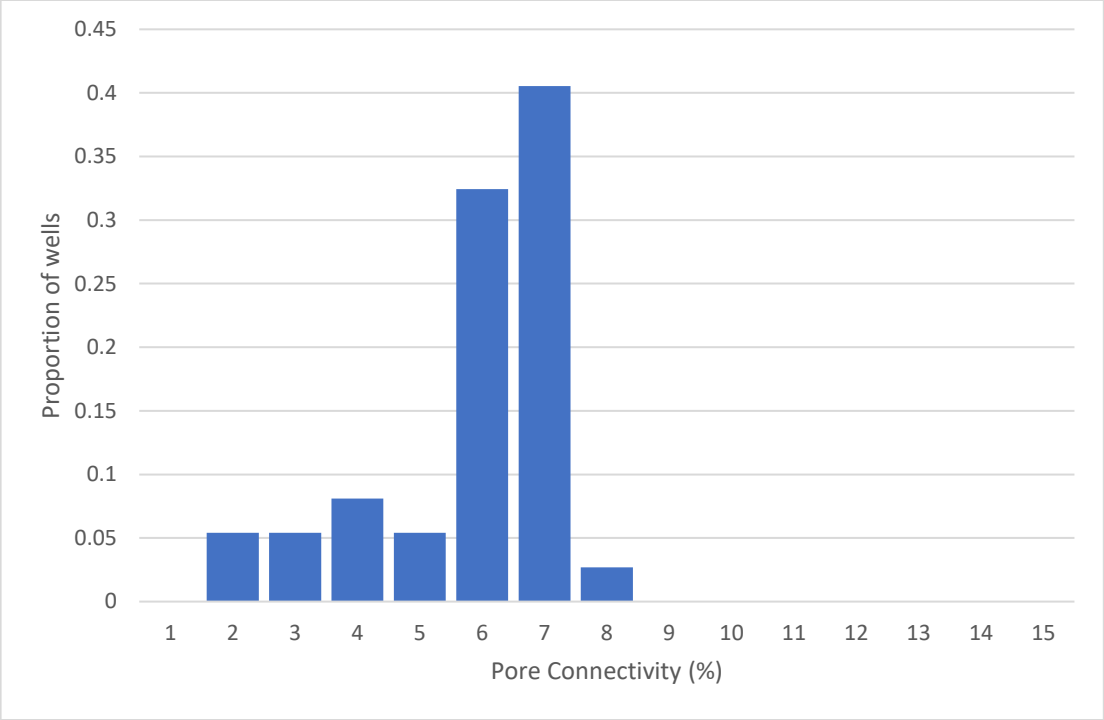


Figure 6.15 Connectivity Distribution in Region 3.

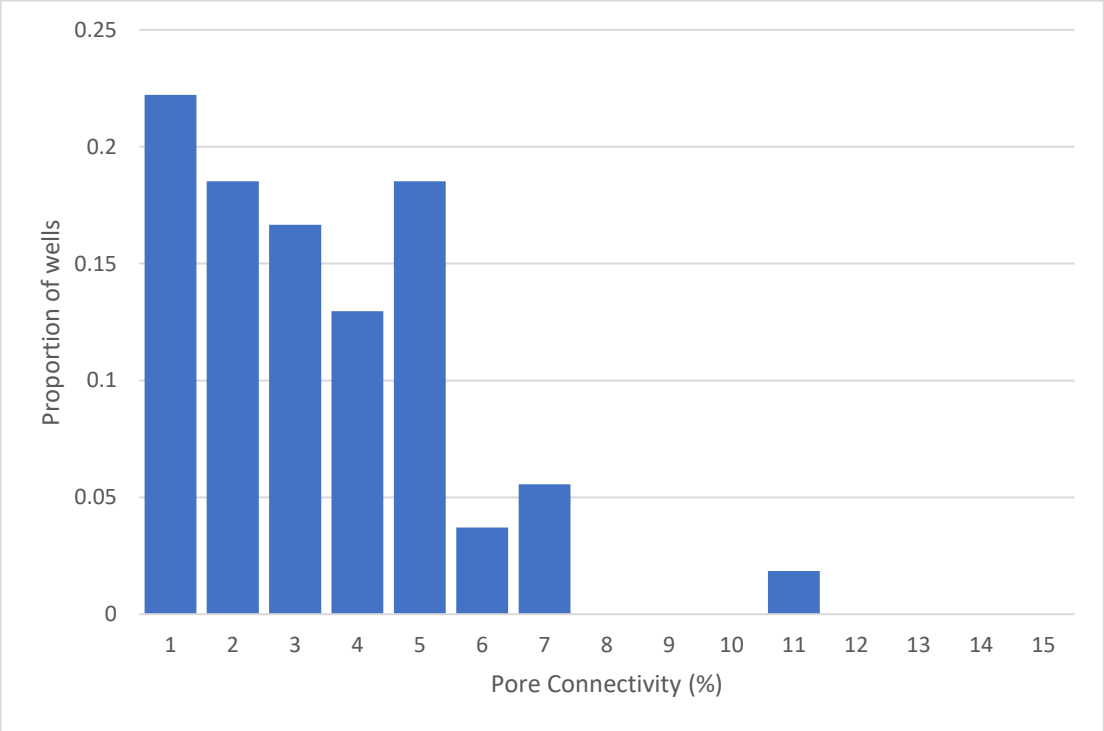


Figure 6.16 Connectivity Distribution in Region 4.

From these figures, there appears to be a trend of connectivity increasing with sustainability. In other words, Region 1 data had the highest connectivity while Region 4 data had the lowest connectivity. This was validated by the average connectivities of these distributions. Region 1, Region 2, Region 3, and Region 4, had average connectivity values of 9%, 7.6%, 5%, and 3.5% respectively. This was expected as a higher connectivity results in a higher rate of gas transport in the shale matrix by diffusion, leading to more sustainable rates of production.

6.3 Areal Maps

Areal maps of the estimated reservoir-scale connectivity in each reservoir were created. This was done using PETRA mapping software. It was done in order to view how the estimated connectivity varied spatially and compare the connectivity in different regions within those reservoirs. By doing this, regional trends in the areas encompassed by these reservoirs could be observed. The physical locations of the wells were imported using their API numbers and, by assigning each estimated connectivity value to its respective well location in the imported file operated on by the software, areal connectivity maps were generated. These maps are displayed in Figures 6.17, 6.18, and 6.19.

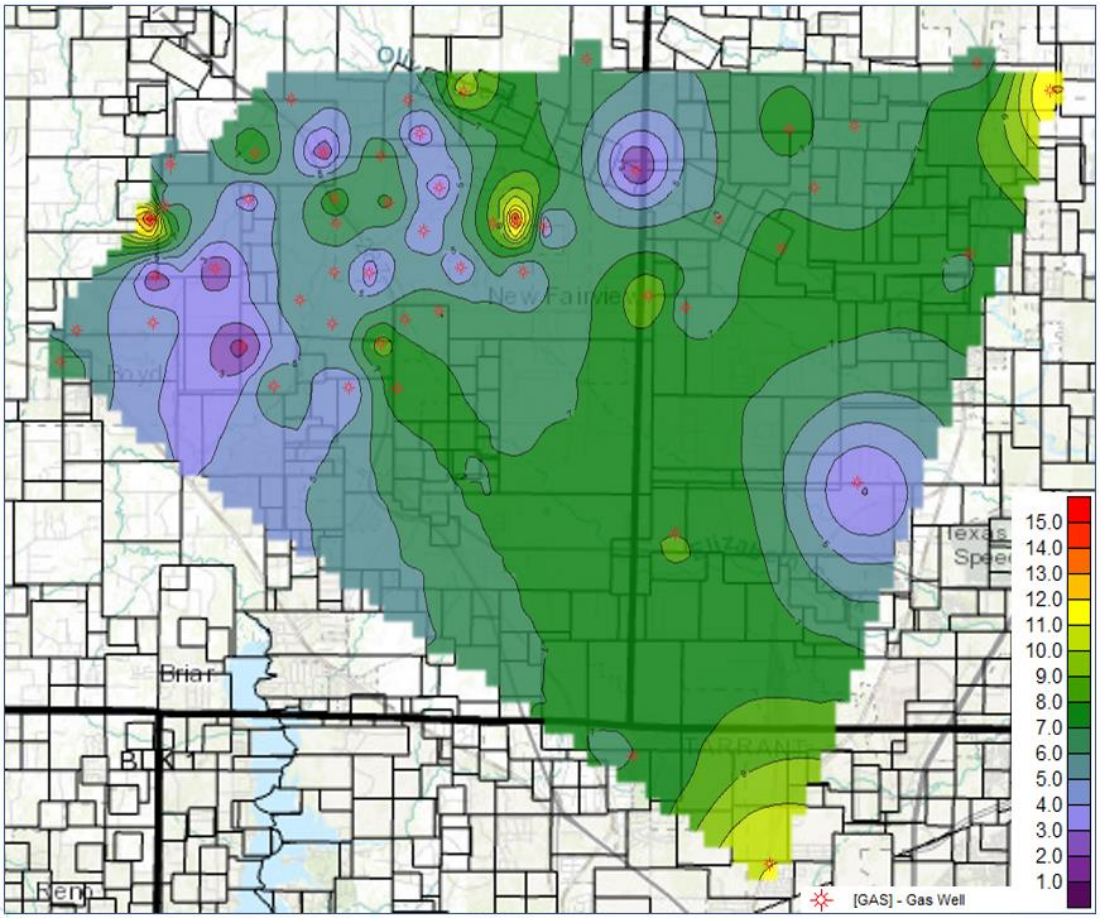


Figure 6.17 Connectivity Areal Map of the Barnett Shale.

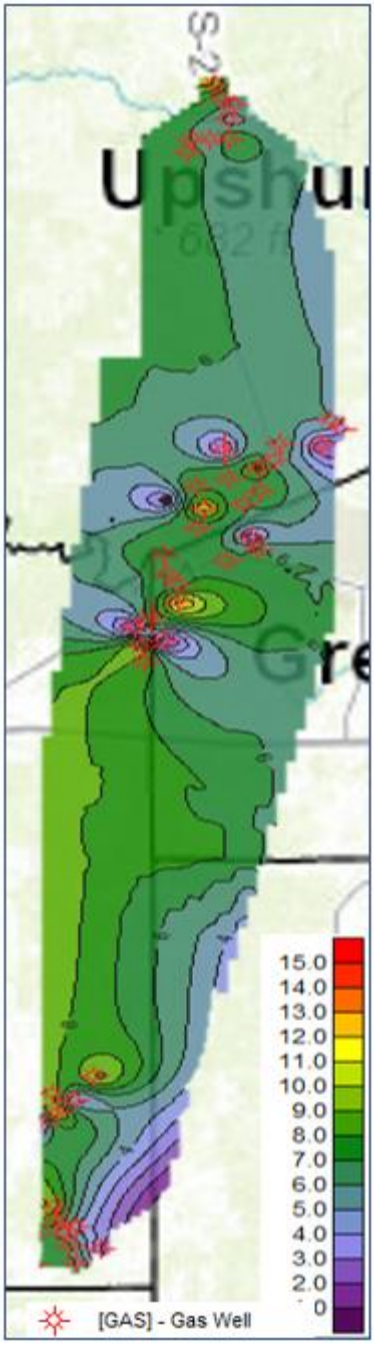


Figure 6.18 Connectivity Areal Map of the Haynesville Shale.

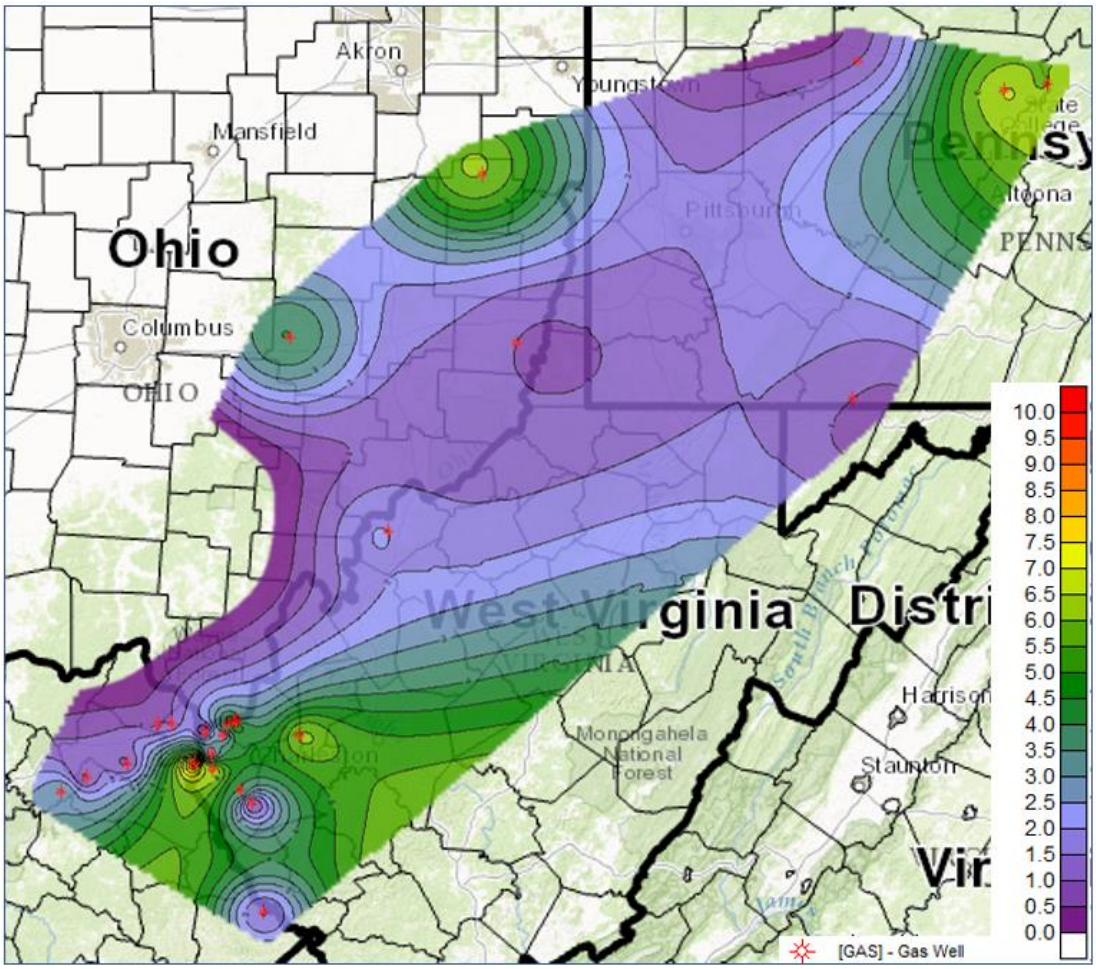


Figure 6.19 Connectivity Areal Map of the Marcellus Shale.

The wells in the region encompassed by the Barnett shale areal map in Figure 6.17 are located in an area split between the Tarrant, Wise, and Denton counties in Texas. In this region, the evaluated reservoir-scale connectivity appears to be higher in the eastern section. The wells of the Haynesville shale encompass a much narrower area in Figure 6.18. There appears to also be a trend of evaluated connectivity increasing laterally however it appears to be increasing westwards. The Marcellus shale wells in Figure 6.19 encompass an area which takes up a significant section of West Virginia and regions of Ohio and Pennsylvania. The evaluated pore connectivity in this area

appears to decrease towards its center and increase as one moves outwards. Because there is a significantly lower number of Marcellus wells, the map created using its data has a lower density of wells in it and therefore lacks a great deal of certainty compared to the maps of the other two reservoirs. Areal maps of sustainability are also made using the distribution of well data into Regions 1, 2, 3, and 4. These maps are shown in Figure 6.20, Figure 6.21, and Figure 6.22.

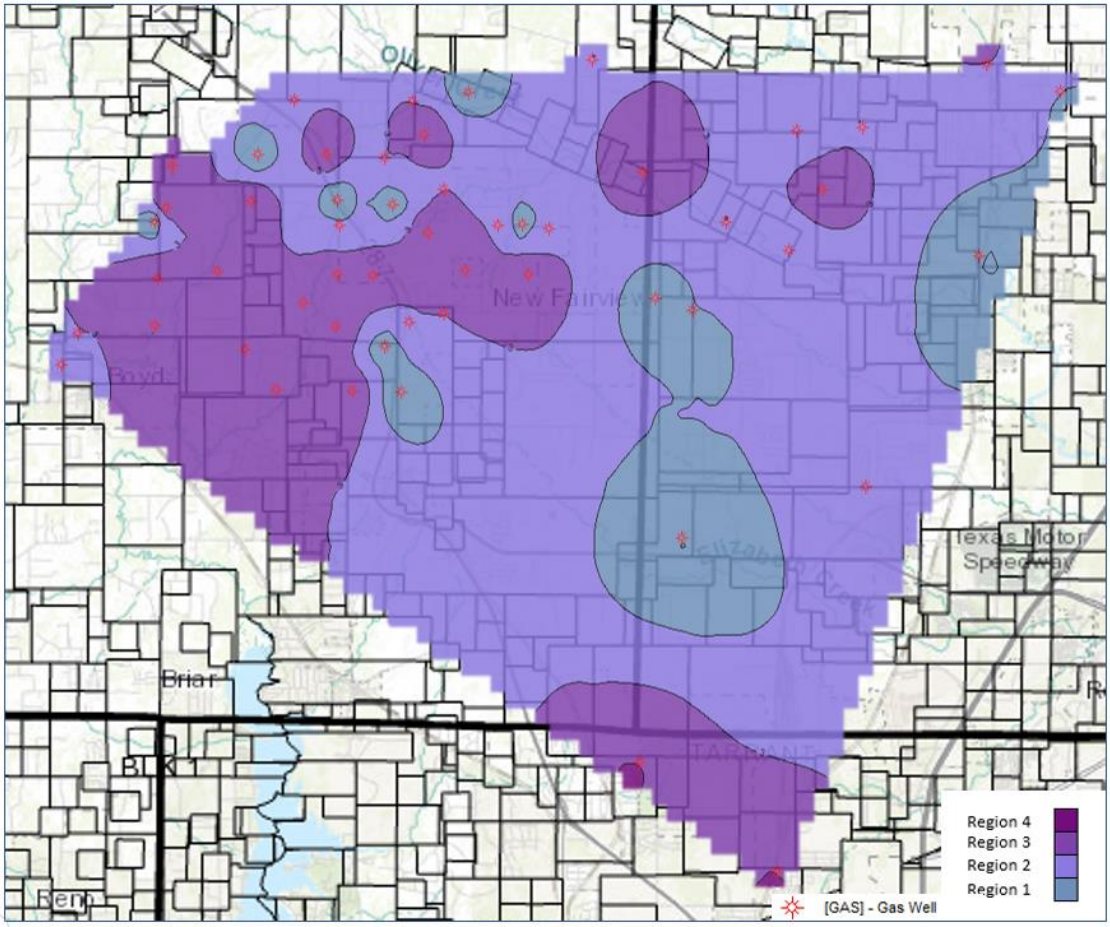


Figure 6.20 Sustainability Areal Map of the Barnett Shale.

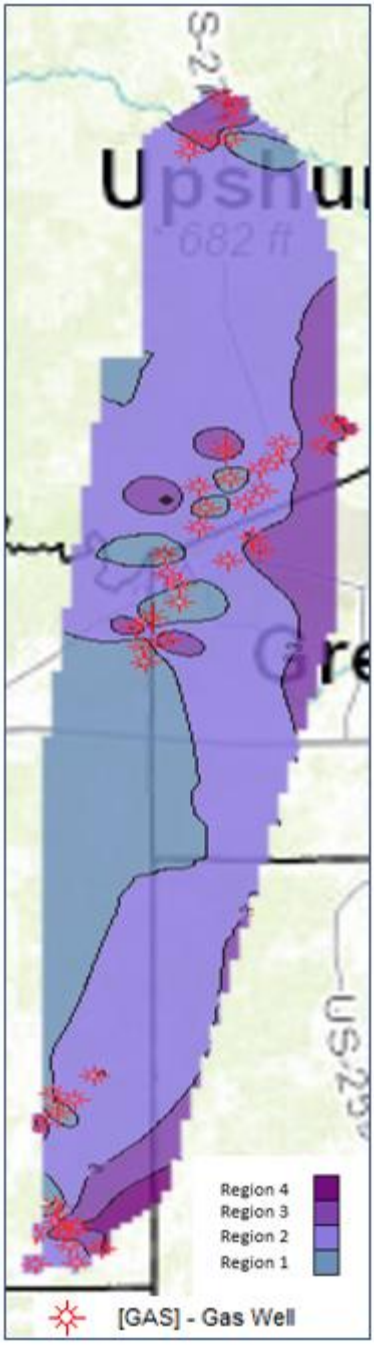


Figure 6.21 Sustainability Areal Map of the Haynesville Shale.

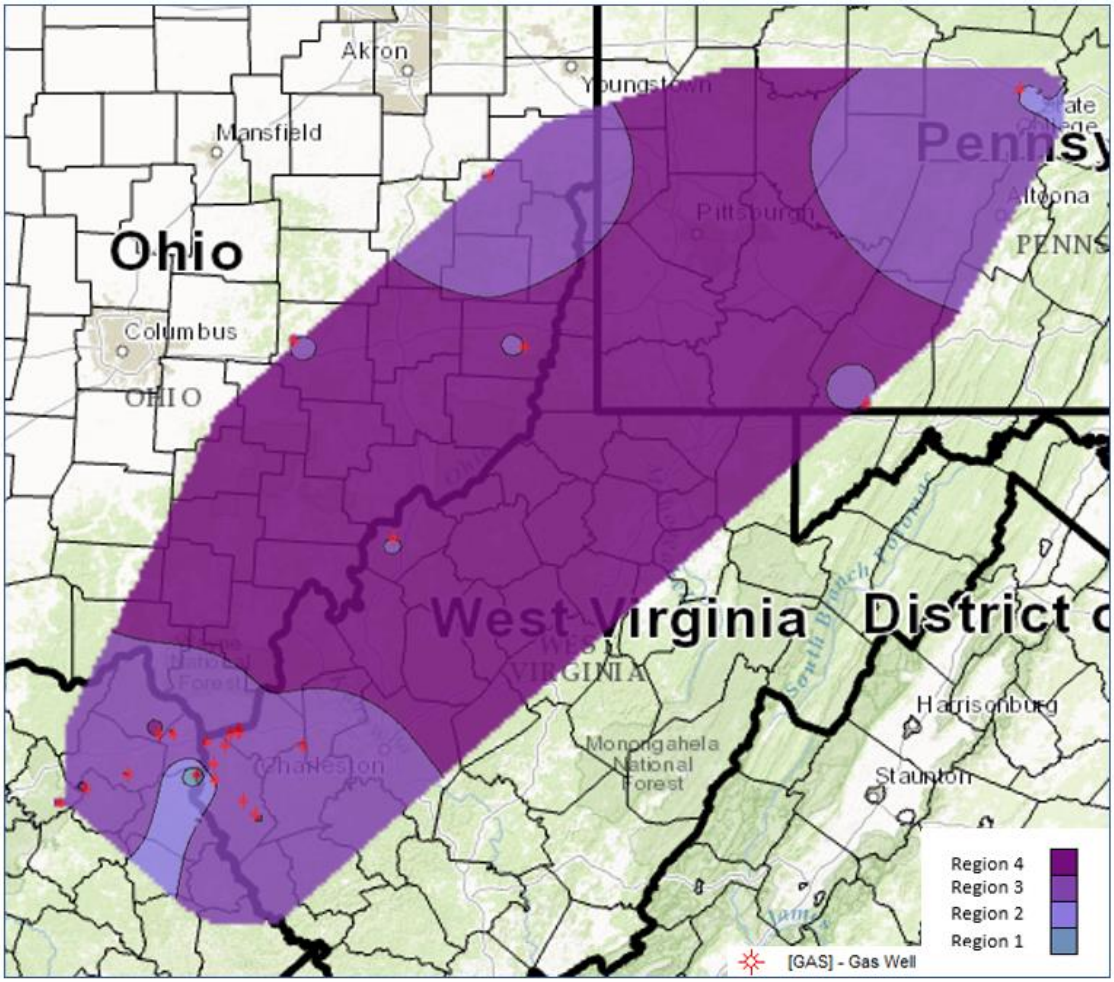


Figure 6.22 Sustainability Areal Map of the Marcellus Shale.

Interestingly, the connectivity and sustainability maps for each reservoir are very similar. The regions of high connectivity in the connectivity maps correspond to the regions of high sustainability in the sustainability maps. This suggests that the connectivity is proportional to the sustainability.

6.4 Discussion

The sustainability was fairly confidently determined for the Marcellus shale to be the lowest of the three reservoirs analyzed. The sustainability for the Barnett and the

Haynesville were much closer and more difficult to distinguish. However, by analyzing the slopes of their $\frac{q}{qmax}$ versus $\frac{Gp}{EUR}$ curves, the Barnett was evaluated to have the highest sustainability of the two. From the sustainability distributions for Regions 1, 2, 3, and 4 and the similarities in the generated areal maps, it was determined that the sustainability had a positive relationship with reservoir-scale connectivity. This is conceivable because a higher connectivity allows for a higher dispersive flux in the matrix and therefore a less steep decline in production rates. The ability of a reservoir to maintain reasonable rates for significant periods of time is enhanced by increases in its matrix connectivity. This relationship of sustainability with connectivity can be utilized in conjunction with the generated areal maps to locate regions in which there would high connectivity and the production rates would, therefore, decline at a lower rate.

The values of the evaluated connectivity may appear to be slightly lower than some that have been made on the same reservoirs in previously carried out studies. They mainly range from 1% to 15% with a small number of these estimates being in excess of 10%. The low connectivity estimates are expected because these are shales. However, it may also be as a result of the pore connectivity decreasing as more hydrocarbons are produced from the reservoir. As hydrocarbons are extracted from a reservoir at a certain depth, the reservoir pressure declines and there is less resistance towards the overburden pressure being applied to the reservoir. Based on the amount of decline the pore pressure experiences due to hydrocarbon extraction and the compressibility of the reservoir, the connectivity is reduced to various degrees. In this

study, only the boundary dominated data was analyzed. As a result of this, the connectivity values estimated may not have been values of connectivity at initial conditions but rather connectivity values that had decreased by various degrees compared to their initial values. Connectivity values obtained from measurements performed on the lab scale, on the other hand, are equal to values of the initial connectivity of the reservoirs.

In the plot shown in Figure 6.5, there were a few wells that had their data start from one region and end in another. Changes from a region of low sustainability to one corresponding to high sustainability may have been as a result of the development of an adsorbed gas phase that was unaccounted for. Changes in the other direction (high sustainability to low sustainability) may have been due to a possible reduction in connectivity with time due to the depletion and compaction of the reservoirs from overburden pressure. Irrespective of the direction, these changes in sustainability region highlight another limitation of the methodology used in this study. The study is limited not only in the sense that it is unable to provide initial connectivity estimates but also in the sense that specific mechanisms, such as the development of an adsorbed gas phase, are not taken into account in carrying out its evaluation.

Chapter 7: Conclusion

In this study, sustainability was introduced as a notion to describe the production rate declines and the performance of reservoirs. It was assessed by taking the slopes of $\frac{q}{qmax}$ versus $\frac{G_p}{EUR}$ curves derived from actual well production data for the

Barnett, Haynesville, and Marcellus shales. A general view of all the $\frac{q}{qmax}$ versus $\frac{G_p}{EUR}$ data for the three reservoirs resulted in the straightforward conclusion that Marcellus had the lowest sustainability. For the Barnett and Haynesville shales, distributions of the $\frac{q}{qmax}$ versus $\frac{G_p}{EUR}$ curve slopes needed to be made to distinguish their sustainabilities. With an average slope value of -11.11 for the Barnett and -13.35 for the Haynesville, the Barnett was determined to have the highest sustainability amongst the two.

Reservoir-scale connectivity was also evaluated for the three shale reservoirs in this study. This was done by comparing their well production data to reservoir simulation-generated data on plots of recovery and $\frac{G_p}{EUR}$ versus normalized time. With a few connectivity estimates exceeding 10%, the values in this study appeared to be fairly low compared to the results of other studies. However, it was reasoned that this study, unlike the other works, evaluates pore connectivity at periods occurring after initial conditions in which the connectivity may have declined due to the extraction of hydrocarbons from the reservoirs and subsequent depletion of the reservoir pressures. Areal maps of the pore connectivities in each reservoir were created in order to view how they varied in different regions within those reservoirs. The sustainability and connectivity were observed to generally increase eastwards in the Barnett and westwards in the Haynesville while it formed a fairly radial pattern, increasing outwards in the Marcellus.

The well data were separated into four regions, Regions 1, 2, 3, and 4, corresponding to their sustainability. The reservoir-scale connectivity for the data in these separate regions was utilized to create connectivity histograms for each region. The connectivity was observed to be higher in regions corresponding to higher sustainability. It was also observed that the generated areal maps of sustainability and connectivity were fairly similar. This suggested that the connectivity impacted the sustainability and therefore the production rate declines in these reservoirs. This was consistent with the findings made in other studies.

This study enhances our knowledge of connectivity by not only evaluating it on a large scale which is more generally representative of the reservoirs but also linking it to the production performance of the shale reservoirs through the evaluation of sustainability. It improves our knowledge and understanding of these shale reservoirs and identifies a strategy that could be used in the later stages of developing them. By establishing the term, sustainability, as a means of evaluating the production rate declines in reservoirs, and linking this term to connectivity, areas within the regions of the wells in this study could be identified in which wells could potentially be placed to produce at more sustainable rates from these reservoirs.

Future Work

This study represents the establishment of novel means of production performance evaluation of shales as well as a significant contribution to the knowledge on the Barnett, Haynesville, and Marcellus. To boost the range and representation of

these shale reservoirs in this study, this analysis could be expanded upon to encompass a larger area of the reservoirs studied. The analysis could also be applied to some of the other key shale reservoirs in the United States such as the Fayetteville or Woodford shales. To enhance the accuracy and effectiveness of the study, the simulation models and plots used could also be further enhanced by taking into account specific properties and mechanisms of the reservoirs studied such as the presence of sorption processes as in Barnett and Marcellus, and the enhanced connectivity reduction that could occur in the Haynesville due to the slit-like shape of its pores. It could also be made more robust by increasing the number of created reservoir model configurations for each connectivity modelled.

References

Al Khamees, A. M. 2015. *Simultaneous Solution for Recovery Factor and Permeability from Production Data Analysis for Liquid Rich Shales and Demonstration of this Methodology in the Oil and Gas Condensate Windows of the Eagle Ford*. M. S. Thesis, University of Oklahoma, Norman Oklahoma.

Amann-Hildenbrand, A., Ghanizadeh, A., and Krooss, B. M. 2012. Transport properties of unconventional gas systems. *Marine and Petroleum Geology* **31**: 90-99. https://doi.org/10.1016/j.marpetgeo. 2011.11.009.

Ambrose, R. I., Hartman, R. C., Campos, M. D. et al. 2010. New Pore Scale Considerations for Shale Gas in Place Calculations. Presented at the SPE Unconventional Gas Conference, Pittsburgh, Pennsylvania, 23-25 February. SPE-131772-MS. https://doi.org/10.2118/131772-MS.

Arps. J. J. Analysis of Decline Curves. 1945. *Transactions of the AIME*. **160** (1): 228-247. SPE-9452280-G. https://doi.org/10.2118/945228-G

Bear, J. 1972. *Dynamics of Fluid in Porous Media*, Revised Edition. New York: Dover Publications.

Bello, R. O., Wattenbarger, R. A., 2010. Multi-stage Hydraulically Fractured Shale Gas Rate Transient Analysis. Presented at the SPE North Africa Technical Conference and Exhibition, Cairo, Eygpt, 14-17 February. SPE 126754-MS. https://doi.org/10.2118/126754-MS.

Belvalkar, R. and Oyewole, S. 2010. Development of Marcellus Shale in Pennsylvania. Presented at the SPE Annual Technical Conference and Exhibition, Florence, Italy, 19-22 September. SPE-134852-MS. https://doi.org/10.2118/134852-MS.

Chalmers, R. G., Bustin, M. R., and Power, I. M. 2012. Characterization of gas shale pore systems by porosimetry, pycnometry, surface area, and field emission scanning electron microscopy/transmission electron microscopy image analyses: Examples from the Barnett, Woodford, Haynesville, Marcellus, and Doig units. *AAPG Bulletin* **96** (6): 1099-1119. http://dx.doi.org/10.1306/08171111052.

Chapra, S. C., and Canale, R. P. 2010. *Numerical Methods for Engineers*, Sixth Edition. New York: McGraw Hill Higher Education.

Computer Modelling Group Ltd. 2015. *GEM USER GUIDE COMPOSITIONAL & UNCONVENTIONAL RESERVOIR SIMULATOR*, Version 2015. Alberta: Computer Modelling Group Ltd.

Cordazzo, J. Maliska, C. R., and Carvalho da Silva, A. F. 2002. Interblock Transmissibility Calculation Analysis for Petroleum Reservoir Simulation. Presented at the Federal University of Santa Catarina Meeting on Reservoir Simulation, Buenos Aires, Argentina, 5-6 November.

Curtis, J. B. 2002. Fractured shale-gas systems. *AAPG Bulletin* **86** (11): 1921–1938. https://doi.org/10.1306/61EEDDBE-173E-11D7-8645000102C1865D.

Curtis, M. E., Ambrose, R. J., and Sondergeld, C. H. Investigating the Microstructure of Gas Shales by FIB/SEM Tomography & STEM Imaging.

Davudov, D. and Moghanloo, R. G. 2016. Upscaling of Pore Connectivity Results from Lab-scale to Well-scale for Barnett and Haynesville Plays. Presented at the SPE Annual Technical Conference and Exhibition, Dubai, UAE. 26-28 September. SPE-181433-MS. https://doi.org/10.2118/181433-MS.

Davudov, D., Moghanloo, R. G., and Yuan. B. 2016. Impact of Pore Connectivity and Topology on Gas Productivity in Barnett and Haynesville Shale Plays. Presented at the Unconventional Resources Technology Conference, San Antonio, Texas, 1-3 August. URTEC-2461331-MS. https://doi.org/10.15530/URTEC-2016-2461331.

Dewers, T. A., Heath, J., Ewy, R. et al. 2012. Three-dimensional pore networks and transport properties of a shale gas formation determined from focused ion beam serial imaging. *Int. J. Oil, Gas and Coal Technology*. **5** (2/3): 229-248.

Dullien, F.A.L., 1992. *Porous Media: Fluid Transport and Pore Structure*. Second Edition. San Diego: Academic Press.

Economides, M. J., Hill, A. D., Ehlig-Economides, C. et al. 2013. *Petroleum Production Systems*, Second Edition. Massachusetts: Prentice Hall

EIA. 2016a. Annual Energy Outlook 2016. 15 September 2016, https://www.eia.gov/outlooks/archive/aeo16/MT_naturalgas.cfm#natgasprod_exp (accessed 18 April 2017).

EIA. 2016b. US Crude Oil and Natural Gas Proved Reserves, Year-end 2015. 14 December 2016, https://www.eia.gov/naturalgas/crudeoilreserves/ (accessed 18 April 2017).

EIA. 2016c. U.S. Shale Production. 14 December 2016, https://www.eia.gov/dnav/ng/hist/res_epg0_r5302_nus_bcfa.htm (accessed 18 April 2018).

EIA. 2017. Drilling Productivity Report. 17 April 2017, https://www.eia.gov/petroleum/drilling/#tabs-summary-2 (accessed 18 April 2017).

Erbach, A. 2014. Unconventional gas and oil in North America. European Parliamentary Research Service.

Fu, Q., Horvath, S. C. 2015. Log-derived thickness and porosity of the Barnett Shale, Fort Worth basin: Texas Implications for assessment of gas shale resources. *AAPG Bulletin* **99** (1): 119-141. http://dx.doi.org/10.1306/07171413018.

Gilbert, L. 2009. Geology of the Louisiana Haynesville Shale Play. *Annual Institute of Mineral Law*. **56 (1):** 6.

Gutierrez, M., Øino, L.E., and Nyga˚rd, R. 2000. Stress-dependent permeability of a de-mineralised fracture in shale. *Marine and Petroleum Geology* **17** (8): 895–907. http://dx.doi.org/10.1016/S0264-8172(00)00027-1

Goral, J., Miskovic, L., Gelb, K. et al. 2015. Pore Network Investigation in Marcellus Shale Rock Matrix. Presented at the SPE Asia Pacific Unconventional Resources Conference and Exhibition, Brisbane, Australia, 9-11 November. SPE-176988-MS. https://doi.org/10.2118/176988-MS.

Hammes, U., Hamlin, H. S., and Ewing, T. E. 2011. Geologic analysis of the Upper Jurassic Haynesville shale in east Texas and west Louisiana. *AAPG bulletin* **95** (10):1643-1666. https://doi.org/10.1306/02141110128.

Heller, R. and Zoback, M. 2013. Laboratory Measurements of Matrix Permeability and Slippage Enhanced Permeability in Gas Shales. Presented at the Unconventional Resources Technology Conference, Denver, Colorado, 12-14 August. URTEC-1582659-MS.

Heller, R., Vermylen, J., and Zoback, M. 2014. Experimental investigation of matrix permeability of gas shales. *AAPG Bulletin* **98** (5): 975-995. https://doi.org/10.1306/09231313023.

Hill, R. J., Zhang, E., Katz, B. J. et al. 2007. Modeling of gas generation from the Barnett Shale, Fort Worth Basin, Texas. *AAPG Bulletin* **91** (4): 501–521. https://doi.org/10.1306/12060606063.

Hu, Q., Ewing, R. P., and Dultz, Stefan. 2012. Low pore connectivity in natural rock. *Journal of Contaminant Hydrology* **133**: 76-83. http://dx.doi.org/10.1016/j.jconhyd.2012.03.006.

Hu, Q., Ewing, R. P., and Rowe, H. D. 2015. Low nanopore connectivity limits gas production in Barnett formation. *Journal of Geophysical Research: Solid Earth* **120**: 8073-8087. http://dx.doi.org/10.1002/2015JB012103.

Hu. Q., Gao, X., Gao, Z. et al. 2014. Pore Accessibility and Connectivity of Mineral and Kerogen Phases in Shales. Presented at the Unconventional Resources Technology Conference, Denver Colorado. 25-27 August. URTEC-1922943-MS. https://doi.org/10.15530/URTEC-2014-1922943.

Hunt, A. G., Ewing, R. P., and Ghanbarian, B. 2014. *Percolation Theory for Flow in Porous Media*. Third Edition. Heidelberg: Springer.

Kale, S. V., Rai, C. S., and Sondergeld, C. H. 2010. Petrophysical Characterization of the Barnett Shale. Presented at the SPE Unconventional Gas Conference, Pittsburgh, Pennsylvania. 23-25 February. SPE-131770-MS. https://doi.org/10.2118/131770-MS.

King, G. E. 2012. Hydraulic fracturing 10: What Every Representative, Environmentalist, Regulator, Reporter, Investor, University Researcher, Neighbor, and Engineer Should Know About Hydraulic Fracturing Risk. Presented at the SPE Hydraulic Fracturing Technology Conference, Woodlands, Texas, 6-8 February. SPE-152596-MS. https://doi.org/10.2118/152596-MS.

Kulia, U. 2013. *Measurement and Interpretation of Porosity and Pore-size Distribution in Mudrocks: The Hole History of Shales*. PhD Dissertation, Colorado School of Mines, Golden, Colorado.

Loucks, R. G. and Ruppel, S. C. 2007. Mississippian Barnett Shale: Lithofacies and depositional setting of a deep-water shale-gas succession in the Fort Worth Basin, Texas. *AAPG Bulletin* **91** (4): 579–601. https://doi.org/10.1306/11020606059.

Loucks, R. G., Reed, R. M., Ruppel, S. C. et al. 2009. Morphology, Genesis and Distribution of Nanometer-scale Pores in Siliceous Mudstones of the Mississippian Barnett Shale. *Journal of Sedimentary Research* **79**: 848-861. http://dx.doi.org/10.2110/jsr.2009.092.

Loucks, R. G., Reed, R. M., Ruppel, S. C. et al. 2010. Preliminary Classification of Matrix Pores in Mudrocks. *Gulf Coast Association of Geological Societies Transactions* **60**: 435-441.

Loucks, R. G., Reed, R. M., Ruppel, S. C. et al. 2012. Spectrum of pore types and networks in mudrocks and a descriptive classification for matrix-related mudrock pores. *AAPG Bulletin* **96** (6): 1071-1098. http://dx.doi.org/10.1306/08171111061.

Misra, S. and Han, Y. 2016. Petrophysical Interpretation of Multi-Frequency Electromagnetic Measurements in Clay-and Conductive-Mineral-Rich Mudrocks. In *Unconventional Resources Technology Conference, San Antonio, Texas, 1-3 August 2016* (pp. 543-556). Society of Exploration Geophysicists, American Association of Petroleum Geologists, Society of Petroleum Engineers.

Moghanloo, R. G. 2012. *Modeling the Fluid Flow of Carbon Dioxide through Permeable Media*. PhD Dissertation, The University of Texas at Austin, Austin, Texas (May 2012).

Moghanloo, R. G., Yuan, B., Ingrahamam, N. et al. 2015. Applying macroscopic material balance to evaluate interplay between dynamic drainage volume and well performance in tight formations. *Journal of Natural Gas Science and Engineering*. 1-13. http://dx.doi.org/10.1016/j.jngse.2015.07.047.

Montgomery, S. L., Jarvie, D. M., Bowker, K. A. et al. 2005. Mississippian Barnett Shale, Fort Worth Basin, north central Texas: Gas-shale play with multi-trillion cubic foot potential. *AAPG Bulletin* **89** (2): 155–175. https://doi.org/10.1306/2F09170404042.

Ojha, S. P., Misra, S., Tinni, A. O., Sondergeld, C. H., and Rai, C. S. 2016. Estimation of Saturation-Dependent Relative Permeability in Shales based on Adsorption-Desorption Isotherm. In *AAPG Eastern Section Meeting*.

Parker, M. A., Buller, D., Petre, J. E. et al. 2009. Haynesville Shale-Petrophysical Evaluation. Presented at the SPE Rocky Mountain Petroleum Technology Conference, Denver, Colorado, 14-16 April. SPE-122937-MS. https://doi.org/10.2118/122937-MS.

Polito, P., Bhandari, A., and Flemings, P. 2014. Characterizing Matrix Permeability and Porosity in Barnett Shale. Presented at the Challenge of Studying Low Permeability Materials Workshop at the University of Cergy-Pontoise, Ile de France, 2-3 December.

Pollastro, R. M., Jarvie, D. M., Hill R. J. et al. 2007. Geologic framework of the Mississippian Barnett Shale, Barnett-Paleozoic total petroleum system, Bend Arch– Fort Worth Basin, Texas. *AAPG Bulletin* **91 (**4): 405-436. https://doi.org/10.1306/2F10300606008.

Rodriguez-Herrera, A. E., Suarez-Rivera, R., Handwerger, D. et al. 2013. Field-scale Geomechanical characterization of the Haynesville Shale. Presented at the 47th U.S. Rock Mechanics/Geomechanics Symposium, San Francisco, California, 23-26 June. ARMA-2013-678.

Sigal, R. F. 2013. Mercury Capillary Pressure Measurements on Barnett Core. *SPE Reservoir Evaluation & Engineering* **16** (4): 432-442. SPE-167607-PA. https://doi.org/10.2118/167607-PA.

Thompson, J. W., Fan. L., Grant. D. et al. 2011. An Overview of Horizontal-Well Completions in the Haynesville Shale. *Journal of Canadian Petroleum Technology* **50** (6): 22-35. https://doi.org/10.2118/136875-PA.

U.S Department of Energy (DOE). 2013. Modern Shale Gas Development in the United States: An Update. September 2013.

Union of Concerned Scientists. 2013. Shale Gas and Other Unconventional Sources of Natural Gas, http://www.ucsusa.org/clean-energy/coal-and-other-fossil-fuels/shale-gas-unconventional-sources-natural-gas#.WPgxB2krKUl (accessed 18 April 2017).

Verba, C., Crandall, D., and Moore, J. 2016. Multiscale Shale Pore Characterization. Presented at the Unconventional Resources Technology Conference, San Antonio, Texas, 1-3 August. URTEC-2448192-MS. https://doi.org/10.15530/URTEC-2016-2448192.

Williams, R. H., Khatri, D. K., Keese, R. F. et al. 2011. Flexible, Expanding Cement System (FECS) Successfully Provides Zonal Isolation Across Marcellus Shale Gas Trends. Presented at the Canadian Unconventional Resources Conference,

Calgary, Alberta, 15-17 November. SPE-149440-MS. https://doi.org/10.2118/149440-MS.

Yu, W., Sepehrnoori, K. and Patzek, T. W. 2014. Evaluation of Gas Adsorption in Marcellus Shale. Presented at the SPE Annual Technical Conference and Exhibition, Amsterdam, The Netherlands, 27-29 October. SPE-170801-MS. https://doi.org/10.2118/170801-MS.

Zamirian, M., Aminian, K., and Ameri, S. 2016. Measuring Marcellus Shale Petrophysical Properties. Presented at the SPE Western Regional Meeting, Anchorage, Alaska, 23-26 May. SPE-180366-MS. https://doi.org/10.2118/180366-MS.

Zhang, T., Krooss, B.M. 2001. Experimental Investigation on the carbon isotope fractionation of methane during gas migration by diffusion through sedimentary rocks at elevated temperature and pressure. *Geochim Cosmochim Acta* **65** (16): 2723-2742.

Zhang, P., Hu, L., Meegoda, J. N. et al. 2015. Micro-pore and Nano-pore Network Analysis of Gas Flow in Shale Matrix. *Scientific Reports*. **5:** 13501. https://doi.org/10.1038/srep13501.